UNIVERSITÀ
DEGLI STUDI
DI PADOVA

Sede Amministrativa: Università degli Studi di Padova

Dipartimento di Ingegneria Industriale

SCUOLA DI DOTTORATO DI RICERCA IN: INGEGNERIA INDUSTRIALE

INDIRIZZO: INGEGNERIA ELETTROTECNICA

CICLO: XXIV

PROCESSES AND TECHNOLGIES FOR CRYSTALLINE SILICON PRODUCTION FOR PHOTOVOLTAIC APPLICATIONS

Direttore della Scuola: Ch.mo Prof. Paolo Colombo

Coordinatore d'indirizzo: Ch.mo Prof. Giovanni Martinelli

Supervisore: Ch.mo Prof. Fabrizio Dughiero

Dottorando: Angelo Doni

ABSTRACT

Photovoltaic solar energy is considered one of the most versatile and promising renewable energy technology. It is based on the use of an infinite source of energy: the sun. The photovoltaic energy conversion process is emission free and the total environmental footprint of photovoltaic energy is very low.

Crystalline silicon is the most widely diffused technology among all the photovoltaic for its high efficiency, a well-established manufacturing process that permit the adoption of scale economies and an overall low levelized cost of energy.

Along the PV production chain research activities can be conducted on the development of novel cells, as well as on the optimization of process steps with the aim of obtaining better products at low cost and with reduced environmental impact.

Following these objectives the knowledge acquired on the development of electrothermal processes of materials allowed the development of two applications of electro-heating for improving the PV production chain. In particular an induction heating directional solidification furnace for growing multi-crystalline silicon ingots had been developed and a lab-scale prototype had been built for making experimental tests aimed at the improvement of the silicon ingots production process; an electrothermal process for the treatment of end-of-life PV modules based on radio frequency heating has also been developed and constructed.

Both the applications developed can be considered a technological breakthrough that could have a benefic impact on the multi-crystalline silicon production chain.

Abstract

L’energia solare fotovoltaica è considerata al giorno d’oggi una tra le più promettenti e versatili fonti energetiche rinnovabili. La conversione dell’energia solare in energia elettrica mediante l’uso di celle fotovoltaiche consente di utilizzare una fonte energetica inesauribile come il sole ed è caratterizzata dall’assenza di emissioni legate al processo di conversione e da un impatto ambientale complessivo ridotto.

La tecnologia basata sulle celle fotovoltaiche al silicio cristallino è la più diffusa nel mercato per l’alto rendimento di conversione, una catena produttiva industrialmente sviluppata che permette di adottare economie di scala e un costo finale relativamente ridotto che permette di ottenere valori competitivi per il costo dell’energia prodotta.

Gli ambiti di ricerca nel settore del fotovoltaico possono andare dallo sviluppo di nuove tecnologie o nuove celle al miglioramento dei sistemi produttivi attuali al fine di ridurre i costi e migliorare la qualità dei prodotti.

Le conoscenze acquisite in ambito elettrotermico hanno permesso di sviluppare dei processi innovativi che avranno un impatto interessante sulla catena di produzione di moduli fotovoltaici al silicio cristallino. In particolare sono state sviluppate due applicazioni: la prima è lo sviluppo e la realizzazione di un forno ad induzione per la solidificazione di lingotti di silicio multi cristallino per applicazioni fotovoltaiche, attività conclusasi con la realizzazione di un forno da laboratorio per l’effettuazione di test per il miglioramento dei processi produttivi della catena a monte della produzione di moduli; la seconda applicazione è stata finalizzata allo sviluppo di un sistema per il trattamento di moduli fotovoltaici a fine vita, attività conclusasi con lo sviluppo di un sistema a radio frequenza per la separazione dei materiali dei moduli fotovoltaici ai fini del riciclo.

Entrambe le applicazioni possono essere considerate delle importanti innovazioni tecnologiche che possono fornire all’industria fotovoltaica operante nel campo dei moduli al silicio cristallino interessanti opportunità di crescita.

TABLE OF CONTENTS

LIST OF FIGURES

List of figures

LIST OF TABLES

1 INTRODUCTION

In a world in which the energy intensity of human activities is at its highest the objectives that researchers working on energy policies and energy technologies should follow are the reduction of the energy intensity through the application of energy saving policies and technologies, the development of smart electric grids for enhancing the performance of the electric system, and the adoption of electric energy in substitution of traditional fossil fuels for all the possible activities for reducing the local emissions in residential areas.

The electrification of the vast majority of the energy intensive human activities is not sufficient for a sustainable growth, since the impact of electricity generation depends on the primary source used for its production. Electricity, in fact, is not an energy source, but an energy vector and therefore the social and environmental impact of human activities depends on the source of energy used for electricity production.

Renewable energies are based on the use of renewable energy sources which environmental impact is reduced in comparison to traditional fossil fuels and are therefore the optimal choice for a sustainable growth.

Although renewable energies don't depend on fossil fuels which combustion produces emissions that are hazardous for the environmental equilibrium, their environmental impact is never zero for the changes they cause in the surrounding environment following the installation process and for the indirect emissions related to the consumption of electricity, produced using a fossil fuel based energy mix, during the manufacturing process and for the use of chemical products which misuse could be hazardous for the ecosystem.

Solar energy is one of the most interesting sources of energy both for electricity and heat generation. Electricity is usually generated from solar energy by means of photovoltaic solar cells and nowadays photovoltaic electricity has gained a relevant share within most countries energy mix.

Crystalline silicon is the most widely used technology in photovoltaic solar panels and multi-crystalline silicon solar cells compete with mono-crystalline solar cells for the biggest market share. The manufacturing process for

multi-crystalline silicon solar cells is a complex mix of industrial steps that requires the knowledge of many technical subjects for their improvement. Some steps of the production chain are well-established and don't leave much room to research for the development of technological breakthrough ideas; on the other hand some critical steps with improvable technologies and characterized by high energy consumption are still in place and the PV research community has to focus its efforts on developing innovative solutions for the definition of new production standards and innovative equipment.

Manufacturing multi-crystalline silicon ingots from silicon feedstock is one of the most energy intensive activities along the whole crystalline silicon production chain, and multi-crystalline silicon ingots are manufactured using resistive heating directional solidification furnaces. The knowledge on electrothermal processes acquired by the research group working at the Laboratory of Electroheat at the Department of Industrial Engineering at Padova University made it possible to design an innovative directional solidification furnace for the production of multi-crystalline silicon ingots, based on induction heating (iDSS). The adoption of induction heating not only allows a better control of the manufacturing process, but also allows to limit the energy consumptions of this critical step, drastically reducing therefore the overall environmental impact of multi-crystalline solar cells production.

The research activity aimed at the development of the iDSS furnace led to the design, using finite element simulations, and construction of a 120 kg lab-scale induction heating directional solidification furnace, which is one of the very few lab scale furnaces which dimensions allow to take into account all the physical phenomena that are present in industrial scale furnaces. The furnace has also been designed for conducting tests on innovative silicon crystal growing processes, such as, for example, mono-like casting, which development could lead to the definition of new standards for crystalline silicon solar cells.

An electrothermal heating process could also be used for treating end-of-life PV modules for recycling. The management of all the decommissioning activities, in fact, will become essential within the next two decades for further reducing the environmental impact of photovoltaic, for recovering valuable materials and for fulfilling the normative requests on the reduction of wastes, especially wastes from electric and electronic equipment (WEEE).

An innovative approach for the separation of materials from end-of-life PV modules had been developed during the research activities at the Department of Electroheat before the publication of new EU directives on recycling of WEEE, which consider PV as electric equipment. The process developed allows to fulfill

the legislative requests for materials recycling volumes six years in advance. The waste treatment system is based on a radio-frequency electrothermal heating process that allows the separation, without combustion and emissions, of clean glass that can be sent to recycling; the remaining part of the PV module could also be further treated for recovering valuable materials. The innovative application of radio frequency dielectric heating to the treatment of end-of-life PV modules had been tested on a custom made radio frequency heating prototype and a patent application had been deposited.

In the present work the analysis of the PV market, a technical and economical comparison between the different PV technologies and the description of the two innovative applications of electrothermal heating processes will be presented.

2 PV MARKET AND TECHNOLOGIES

Photovoltaic (PV) solar energy is nowadays one of the most diffused technologies for the production of electricity from renewable sources. The possibility to use an unlimited amount of primary energy, together with the relatively low environmental impact of this technology in comparison to traditional fossil fueled power plants or other renewable energy technologies, makes PV one of the most promising technologies for guarantee a clean future for the energy sector.

The photovoltaic technology has seen an important improvement of its efficiency and a sharp cost drop since its introduction in the electrical energy market in the late 70s, thanks to technological innovations and process optimizations that made it competitive not only with other renewable energy sources, but also with traditional electric energy production systems.

Photovoltaic solar energy is not only affordable, but it is also clean since it doesn't need any fuel for the energy production process, whereas the carbon footprint and environmental impact of the photovoltaic energy production systems are limited to the use of chemical products and to the energy needs related to the manufacturing processes.

2.1 GLOBAL PV MARKET

The development of photovoltaic solar cells for the production of electricity using the photoelectric effect of doped semiconductor materials started more than 40 years ago with the aim of developing a power supply system for space applications. Since the first development of photovoltaic solar cells for space applications, the global PV market changed drastically in volumes and type of application and now solar energy is considered among the most important energy sources.

After the first phase in which photovoltaic solar cells where expensive equipment developed for technologically advanced applications, the

development of crystalline silicon solar cells in substitution to expensive high-efficiency GaAs solar cells made it possible to use photovoltaic energy as a power supply for stand-alone applications in which the connection to the electric grid, or the use of diesel generators, would have been too expensive or not practical, for example in remote installations for security communications, high mountains huts or off-shore navigation buoys.

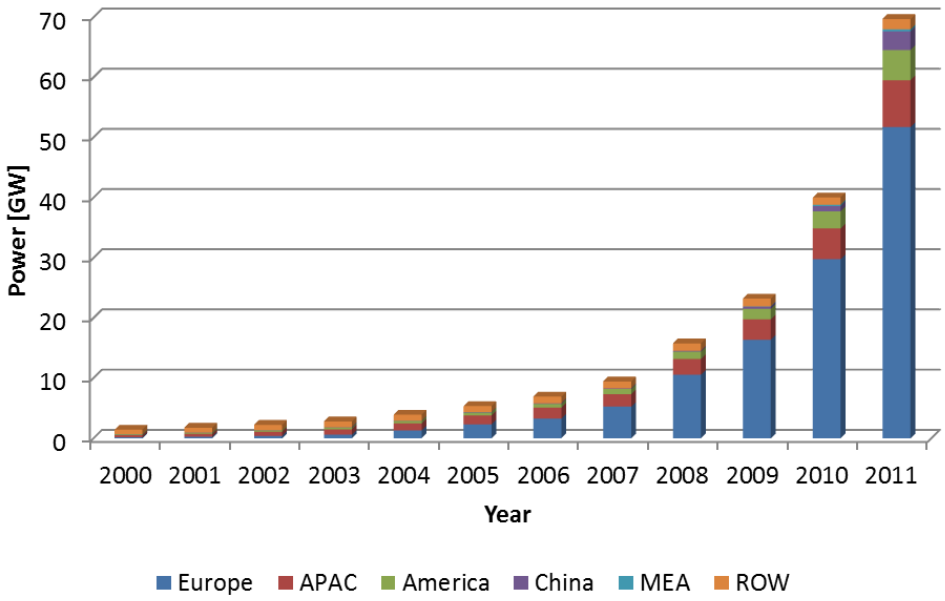

Figure 2.1 – Global installed PV power capacity from 2000 to 2011 (source: EPIA)

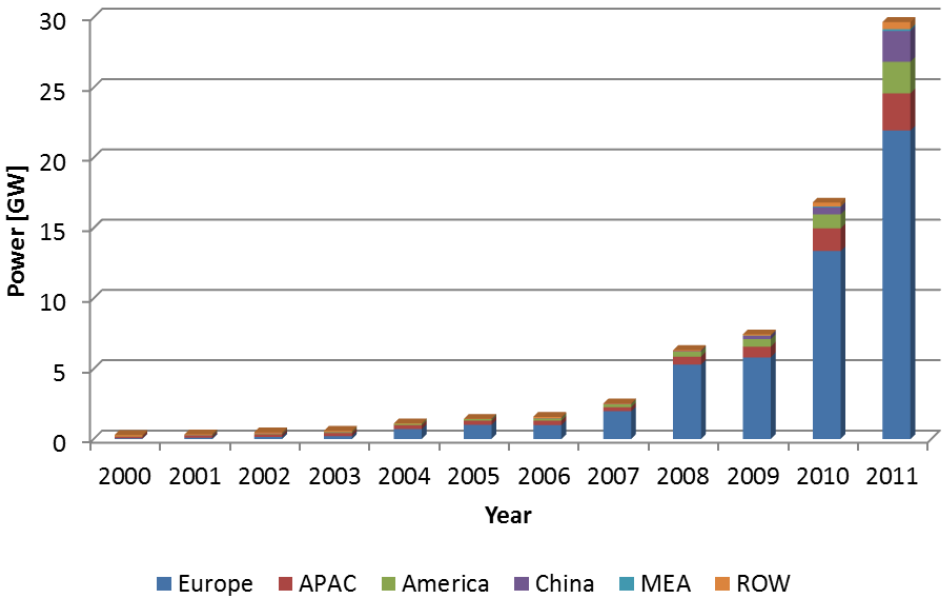

Figure 2.2 – Global annual installed PV capacity from 2000 to 2011 (source: EPIA)

The further decrease of the modules' cost in the last decade, together with financial aids given by some governmental authorities for the development of a sustainable energy production system, made the PV market growing at global level and grid connected applications ranging from small kW size residential distributed plants, to big multi-megawatt photovoltaic power plants are nowadays playing an important role on the electrical energy production market.

In Figure 2.1 and Figure 2.2 the global cumulative installed photovoltaic power and the annual photovoltaic installed power at global level, are represented [1]. It can be seen that the PV market grew at rate higher than 70% per year between 2009 and 2011, and the global cumulative installed capacity reached the 40 GW level at the end of 2010, and almost reached the 70 GW level by the end of 2011.

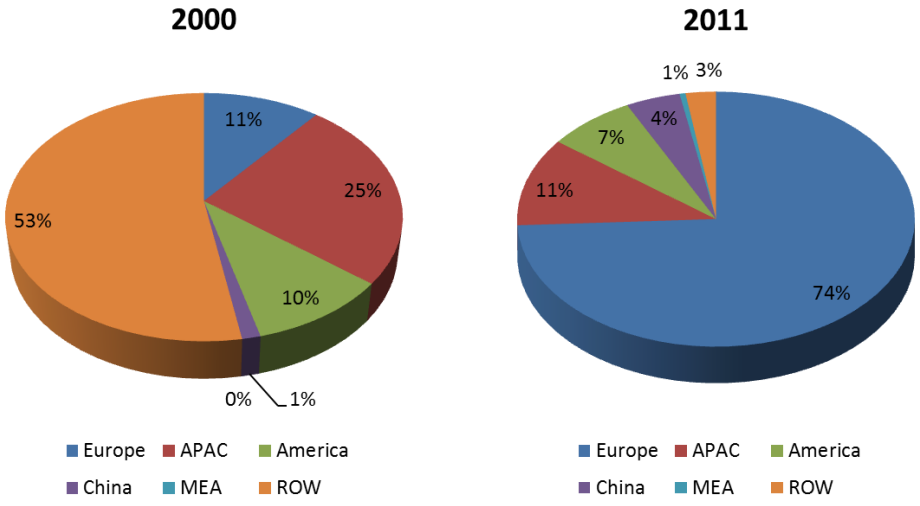

Figure 2.3 – Country distribution for cumulative PV capacity in 2000 and 2011 (source: EPIA)

Analyzing the technology distribution by countries allows to highlight the fact that the global distribution of the photovoltaic installations in the world changed drastically during the last 10 years. In fact, while the PV market was driven by the Japanese market for technological reasons at the start of the 2000s, with North America and Europe playing a secondary, the increased awareness over environmental impact of human activities in Europe and big investments at country level for the development of PV, which will be described in 2.2, made Europe becoming the biggest global market for photovoltaic, with a market share for newly installed PV plants in 2011 of almost 74%. China and the United States, together with Japan after the Fukushima accident could play an important role in the future global PV market for their big installations potential and a realistic scenario of strong support policies; north Africa and

middle east Asia could also be new markets in which the investment in PV could be profitable for their sun exposure, especially for non-conventional technologies such as, for example, CdTe thin films. The different global distribution of PV in 2000 and 2011 is shown in Figure 2.3.

2.2 EUROPEAN PV MARKET

The European market, as described in 2.1, is the biggest global PV market with a cumulative installed PV capacity of more than 51 GW at the end of 2011 and almost 22 GW of new installations during the last year (2011). Considering that in 2000 the European PV market accounted for 53 MW of newly installed power and 154 MW of cumulative installed capacity, it is easy to see how the support scheme policies aimed at the development of renewable energy technologies had a strong impact on the overall energy market with the big growth of PV.

Germany, thanks to its long-lasting and well-designed support schemes had been for years the European country with the biggest cumulative installed capacity and has been the technological center for European based photovoltaic companies. In 2008, for the first time, Germany lost its leadership as the country with the biggest annual PV installation, with Spain installing a total PV power of more than double the German one. This fact was due to an attractive feed in tariff support scheme developed by the Spanish government that pushed many European companies to invest on PV installations, mainly big multi-megawatt PV power plants. The feed in tariff system, though, was based on expensive premiums that led to the non-self-sustainability of the support program, requiring the definition of a cap for new installations.

The Spanish feed in tariff system failure, together with the economic crisis, had a severe impact on the Spanish photovoltaic market and industry due to the stop of investments in a technology that was no longer considered economically viable and due to the mistrust on government support schemes. Following the installation halt in Spain, the German market re-gained its market leadership until 2011 when Italy became the biggest PV market in Europe for annual installations, thanks to the favorable installation conditions and to the most generous support scheme for PV in Europe. The analysis of the current Italian PV market will be conducted in 2.3, whereas the graphs showing the annual and cumulative installations in Europe between 2000 and 2011 and the distribution

of PV between the European countries are shown in Figure 2.4 and Figure 2.5 [1].

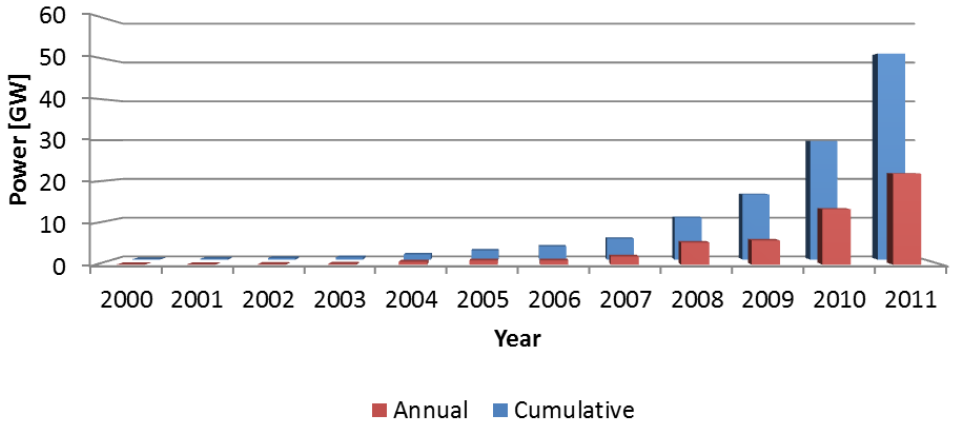

Figure 2.4 – Annual installations and cumulative PV installed capacity in Europe from 2000 to 2011 (source: EPIA)

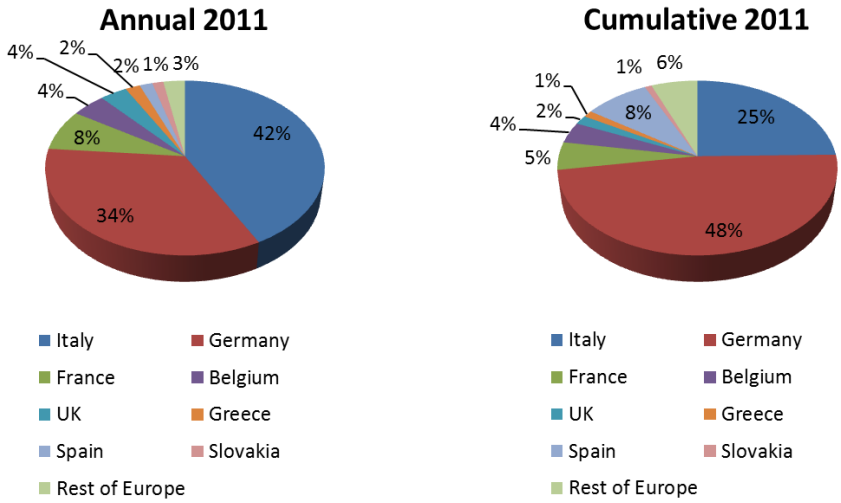

Figure 2.5 – PV installations distribution between Member States in 2011 (source: EPIA)

Considering the segmentation of the type of installations in Europe, in Figure 2.6 and Figure 2.7 it is possible to see that the distribution of different types of installation is country dependent and it is very heterogeneous. For example it can be noted that in the mature German market the majority of PV systems had been installed in commercial or industrial buildings, showing that small investors are generally not keen on investing in a barely known technology and may be suspicious about the real advantages of new technologies and may not fully trust on support scheme systems. On the other hand, support scheme

systems that don't take into account the different cost of PV for big power plants and small household installations encourage big investors on the realization of big multi-megawatt power plants with high return of investment, reducing, though, the spread of the beneficial effect among the whole community, making PV essentially a business based on speculation activities.

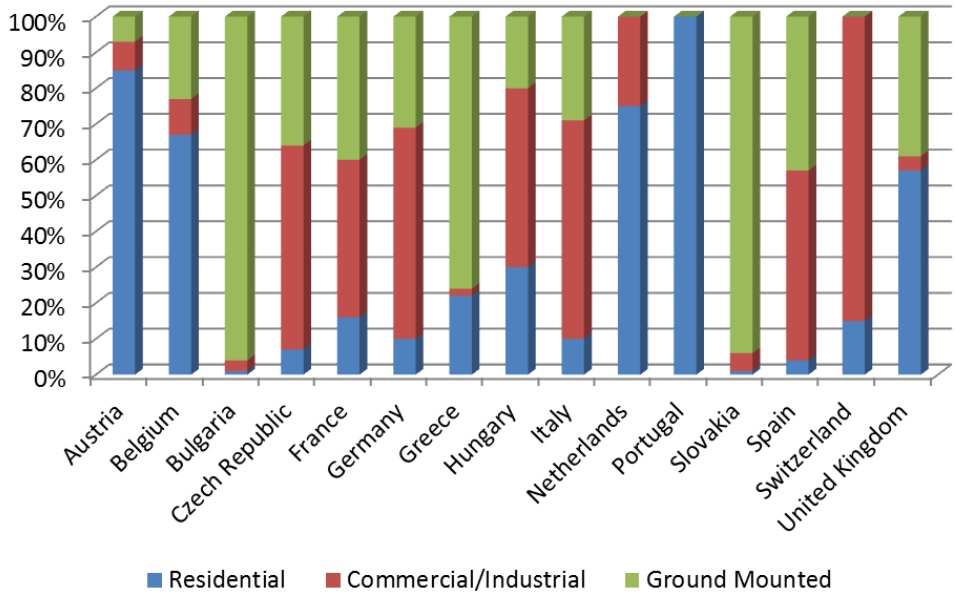

Figure 2.6 – Market segmentation for newly installed PV plants in Europe in 2011 (source: EPIA)

Following a roadmap aimed at the self-sustainability of the PV market without public support schemes, the governments should plan a gradual reduction of the incentives given to the PV technology, starting from big power plants for which the grid-parity had already been reached in some regions.

Considering the importance of PV in the European energy market, it is worth noting that PV nowadays cover a relevant part of the European energy mix, covering 2% of the total energy demand and roughly 4% of the peak demand, with higher shares in the biggest PV market; the Italian energy mix, for example, had been covered by PV for more than 5% starting from the end of 2011. Photovoltaic power plants in Europe also showed the 3rd highest growing rate among all the energy sources between 2000 and 2011, being the second faster growing renewable energy market after wind energy (see Figure 2.8) [2].

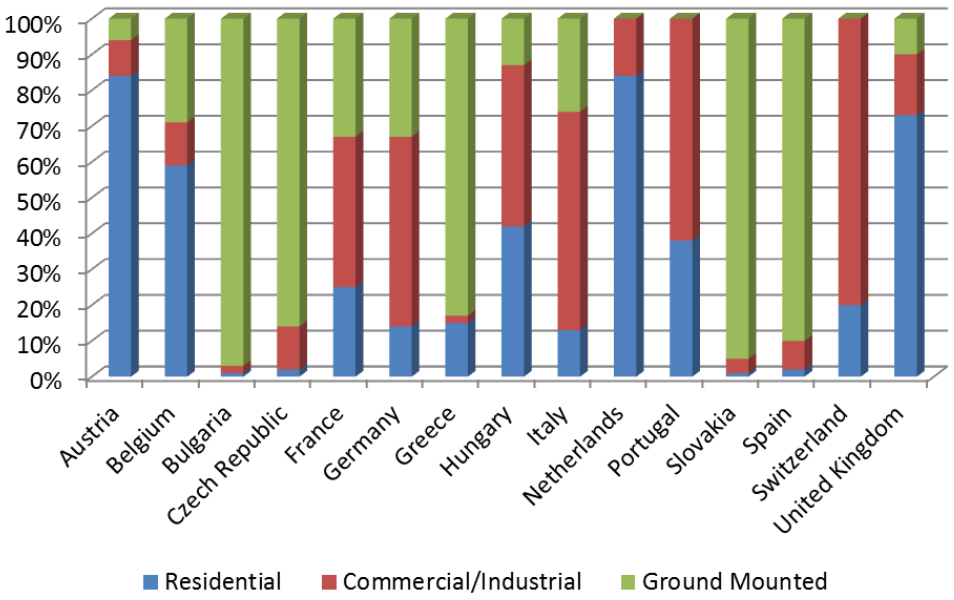

Figure 2.7 – Market segmentation for cumulative installed PV capacity until 2011 (source: EPIA)

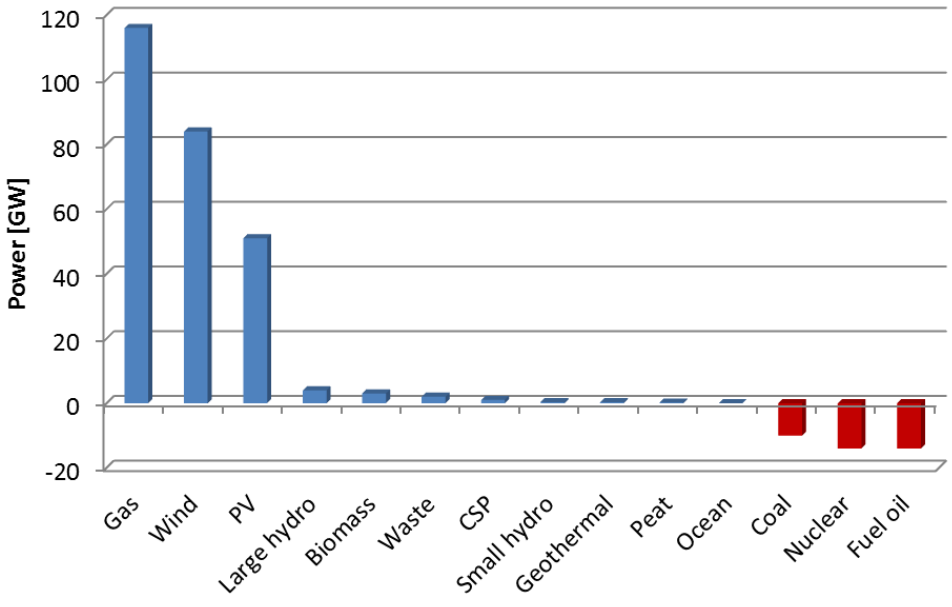

Figure 2.8 – Net installed capacity in Europe 2000-2012 (source: EPIA)

2.3 ITALIAN PV MARKET

Italy, together with Spain and Greece, represents one of the European countries with the biggest potential for PV installations in term of relative energy productivity. In fact, as it can be seen in Figure 2.9 [3], [4], Italy, especially in the south of the country accounts for the highest values for the specific yearly energy production due to the high global irradiation levels.

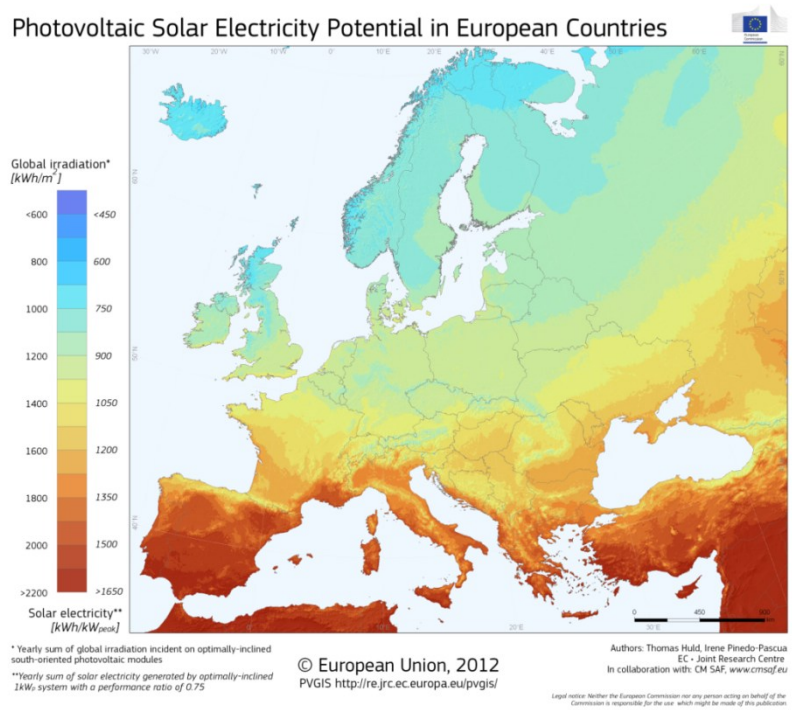

Figure 2.9 – PV electricity potential in Europe (source: PVGIS)

The most favorable installation conditions in comparison to Germany, though, hadn't been considered interesting enough by investors during the first years of development of the PV technology; their interest on this renewable energy technology grew only after the definition of the first support scheme law in 2006, called "primo conto energia".

The lack of interest on renewable energy in Italy started to fade only when generous feed in tariffs had been proposed, making the PV technology an interesting way for investing capital with the highest rate of return in the economic market. PV had become an economical issue in Italy before being an affordable and clean technology for the production of electricity. Five different support schemes for PV, based on feed in tariffs and premium tariffs had been designed, with the last, called "quinto conto energia" [5], published on the Italian official journal on July 2012.

While the beneficial effect of the Italian support schemes for PV has been the growing of the market and the development of a PV generation system that account for more than 5% of the Italian electricity mix starting from the end of 2011, the highest feed in tariffs in Europe caused speculation effects and sharp market growth followed by growth rate decrease which effect is detrimental on the PV workforce.

The Italian PV industry also pushed on keeping high feed in tariffs at every law revision, without considering the possibility to grow a self-sustainable PV market based on manufacturing cost reductions achievable with process and technology innovations; the reduced investments on R&D and process innovation, together with the common decision of the PV industry to invest only on the development of an "installation" sector with a low add value, had been one of the contributory cause for the crisis that the Italian PV sector is currently facing.

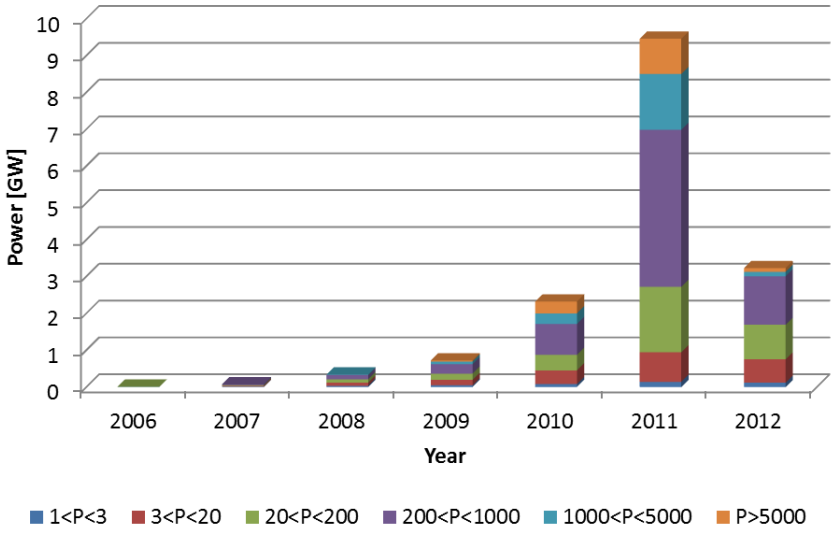

Figure 2.10 – Annual PV installations in Italy from 2006 to 2012 (source: GSE)

During the first year of application of the Italian feed in tariffs (2006) 1 402 PV power plants had been installed, for a total annual installed power of 9.4 MW, with the 50% of this value composed by plants with a power ranging between 3 and 20 kW. The market grew steadily, reaching a maximum of 175 425 PV power plants installed in 2011 for a total additional power of 9.4 GW with a growth rate for annual installations of 1 000% in 5 years. After the market speculations in 2011 the market growth decreased and in 2012 139 201 PV power plants had been installed, contributing for an additional power capacity of 3.2 GW. The cumulative PV power capacity at the end of 2012 had been of 16.1 GW with 470 358 PV power plants installed [6]. The electrical

energy generated by the Italian PV power plants also grew from 10.7 TWh in 2011 to 18.3 TWh, 6.3% of the total electrical energy production, in 2012 [7].

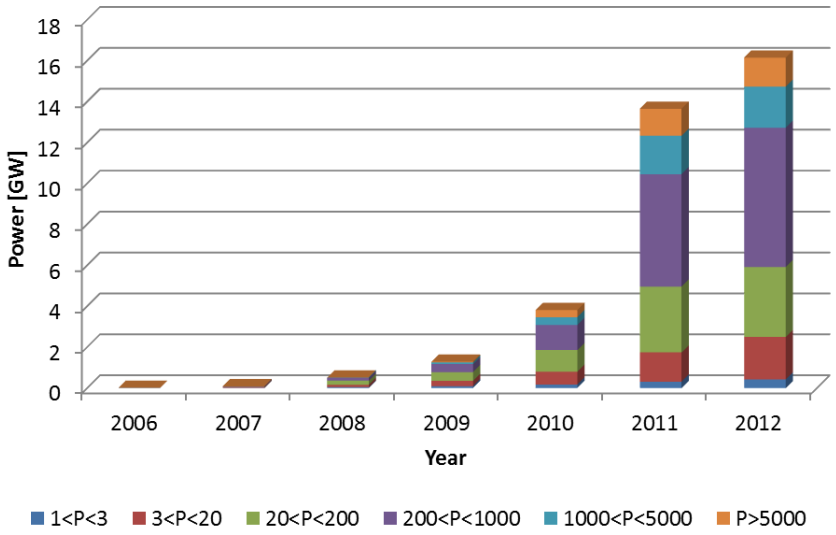

Figure 2.11 – Cumulative PV capacity in Italy from 2006 to 2012 (source: GSE)

The annual PV installations in Italy, the cumulative PV power from 2006 to 2012 divided per power range and the PV energy monthly production for 2011 and 2012 are presented in Figure 2.10, Figure 2.11, and Figure 2.12; the percentage of the electrical energy produced with different technologies in Italy in 2012 is shown in Figure 2.13.

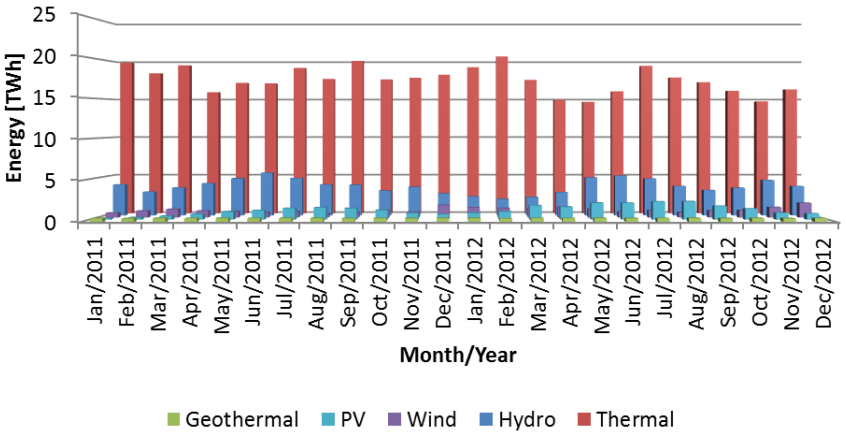

Figure 2.12 – Monthly energy production of PV and other energy sources in Italy in 2011 and 2012 (source: Terna)

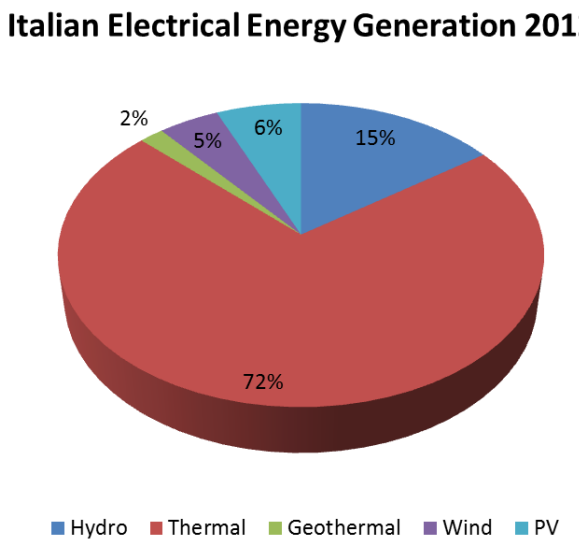

Figure 2.13 – Contribution of the different technologies to the total electrical energy production in Italy in 2012 (source: Terna)

2.4 PV MARKET FUTURE OUTLOOK

Making forecasts of the future of the PV market is considered one of the most important activities for assessing the growth potential for the PV technology among the competing energy production ones, and for developing energy policies for guarantee the reliability of the energy system and a sustainable growth.

Forecasts are always based on historical data and on assumptions over the possible political, economic and social scenarios. Making forecasts is therefore a complex activity that requires a strong knowledge of the market dynamics and the conduction of a multi-parameter analysis that considers also the effects of possible technological breakthrough in competing markets. The future market volumes, thus, cannot be forecasted by simply interpolating the historical data.

Making a dedicate analysis on the future of the PV market is not the objective of this work and will require a dedicate study; the fast dynamics of the PV market, also, make it difficult to conduct reliable studies over the possible future scenarios, especially now that the PV market, after a strong growth period, is slowly reaching its maturity and stability.

In the last years strong policy driven market growth had been registered, but these growth rates cannot be used for assessing the future volumes of the PV

market since they will lead to over-estimations and not sustainable market volumes; on the other hand market volumes drop signals cannot be considered as the end of the PV market growth era, since they are usually temporary social based reactions, often related to speculation phenomena, to support policies changes. Making forecasts and scenarios is then not a simple matter of market volumes, technologies and costs, but requires considering a vast amount of specific data and assumptions.

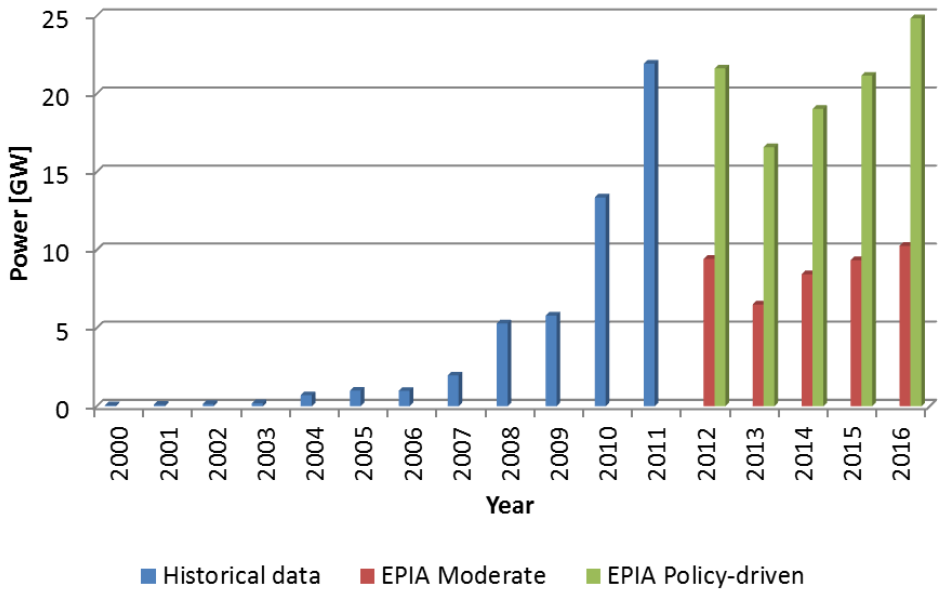

Figure 2.14 – European annual market scenarios until 2016 (source: EPIA)

Considerations about the future of the PV market will thus be conducted simply considering the scenarios evaluated by the European Photovoltaic Industry Association (EPIA) for the short term, until 2016 [1]. The "moderate" and "policy driven" scenarios and their impact on annual installations and cumulative capacity are presented in Figure 2.14 and Figure 2.15; the moderate scenario considers the possible growth of the PV market with strongly reduced financial aids, whereas the policy driven scenario shows the possible impact of energy policy directed towards the development of a strong PV market on the annual growth rate.

Whereas the future of the PV market is uncertain and crisis periods like the one faced by the PV industry in 2012 could happen again in the future, PV will soon reach its market maturity and will probably confirm its long-term importance in the energy production market.

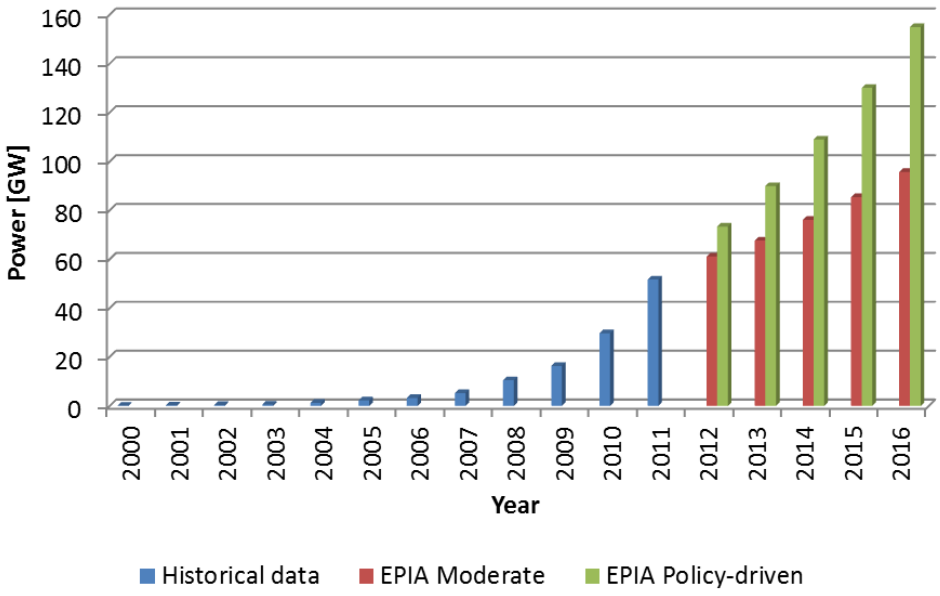

Figure 2.15 – European cumulative scenarios until 2016 (source: EPIA)

2.5 PV TECHNOLOGIES

Whereas the photoelectric effect had been discovered in 1839 by Edmond Becquerel, the start of the modern photovoltaic era is considered to be in 1954 when Person, Fuller and Chaplin, working at the Bell laboratories, discovered the possibility to obtain a voltage from a p-n junction exposed to solar light. After this discovery, the first solar cells had been developed at lab scale and in the very first years they were based on silicon, gallium arsenide (GaAs) or Cadmium Telluride (CdTe) with the higher cell efficiency in the order of 6%.

The high material cost for manufacturing solar cells, though, limited the diffusion of the PV technology only to highly technological applications and the development of new high efficiency solar cells had been driven by the aerospace industry that was aiming at the development of solar panels for applications in aerospace satellites.

In the second half of the '70s the growing of the electronic industry and the availability of CZ silicon used for the production of the first integrated circuits, made it possible to test new solar cells and cell efficiency of up to 13% for mono-crystalline silicon solar cells and 22% for GaAs had been reached.

Starting from the '80s the first commercial silicon solar cells started to be produced in USA, Japan and Europe, mostly by universities or government funded laboratories that had been able to set up the first production pilot lines thanks to governments' financial support. Meanwhile the big growing of the electronic and semiconductor industry pushed the development of the new photovoltaic technology allowing the first commercial solar modules or solar applications in consumers' appliances, mainly pocket calculators, to enter the market.

Starting from the '80s the PV industry developed many technological and process improvements that made it possible to obtain the high efficiency solar modules that are nowadays installed in small stand-alone applications, building integration and big multi-megawatt power plants. The maximum cell efficiencies obtained in lab-scale solar cells using different technologies, from the mid-1970s to 2012 are presented in Figure 2.16.

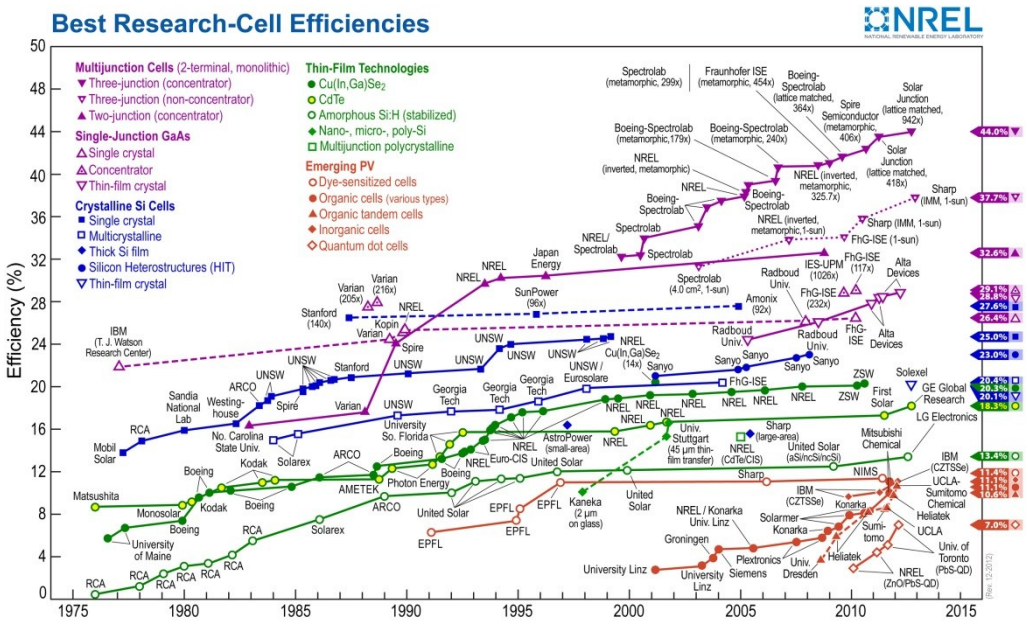

Figure 2.16 – Historical view of the best recorded lab-scale cell efficiency for different technologies (source: NREL)

The most diffused technology at commercial level for stand-alone and grid connected applications is based on crystalline silicon (c-Si) solar cells; this technology showed its suitability for general applications and the cost reduction during the last decades, together with small but steady increases in efficiency made it the undisputed market leader.

Other technologies had been developed, but their lower efficiency, together with a manufacturing cost comparable to c-Si ones, reduces their potential growth. Some technologies, though, can play an important role in market niches; thin films applied to build integration are an interesting demonstration of this fact.

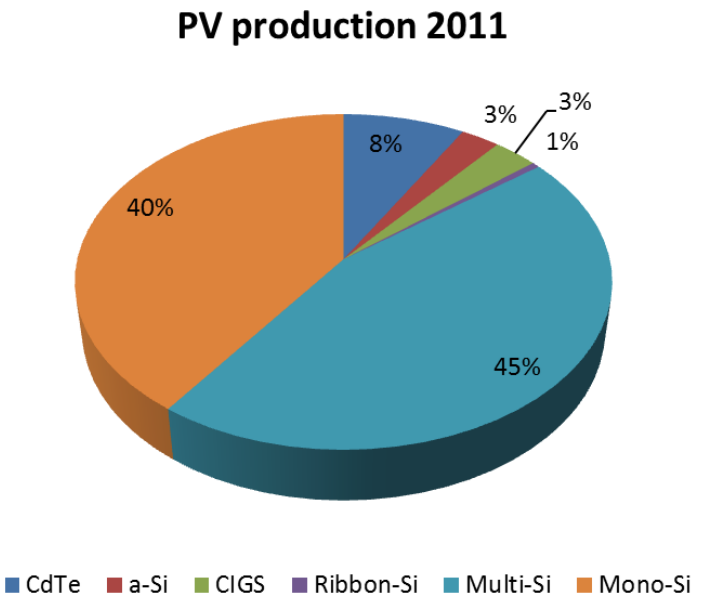

Figure 2.17 – Technology shares for PV production in 2011 (source: Fraunhofer ISE / Navigant consulting)

The main technologies used for manufacturing solar cells will be described in the following paragraphs and are:

- Crystalline silicon solar cells (c-Si)
  - Mono-crystalline solar cells
  - Multi-crystalline solar cells
- Thin film solar modules
  - Amorphous silicon solar modules (a-Si)
  - Cadmium telluride (CdTe)
  - Copper Indium (Gallium) diselenide (CIS/CIGS)
- Multi-junction solar cells
- Dye sensitized solar cells, and polymeric and organic solar cells.

The market share for the different technologies in 2011 is shown in Figure 2.17 [8].

2.5.1 CRYSTALLINE SILICON PV

The majority of solar cells and modules available on the PV market is based on crystalline silicon technology for historical and technological reasons; being silicon one of the first doped semiconductor materials used for studying the photoelectric effect of p-n junctions, it received the biggest attention and interest by the industrial research community.

Crystalline silicon solar cells are manufactured using either mono-crystalline or multi-crystalline silicon wafers, with the first technology characterized by the highest efficiency and the second one that compete with mono-crystalline solar cells for the biggest share in the PV market, thanks to the reduced manufacturing cost. The record lab-scale cell efficiency for mono-crystalline solar cells is 25%, obtained by the University of New South Wales in 1999, whereas the record efficiency for multi-crystalline solar cells is 20.4%, obtained by Fraunhofer ISE in 2004.

The industrial steps needed for the production of crystalline silicon solar cells, together with the innovative process for the production of multi-crystalline silicon ingots for photovoltaic applications developed at the Laboratory of Electroheat at Padova University, will be described in 4 and 5 .

2.5.2 THIN FILM PV

Thin film solar cells, also called second generation solar cells, are based on semiconductor materials like amorphous silicon, cadmium telluride or copper indium diselenide, deposited in micrometric layers over a foreign substrate that could be rigid or flexible.

Thin film technologies had been developed starting from the mid '70s with the aim of obtaining an inexpensive substitute for crystalline silicon solar cells. The high material costs, and the consequent high modules' cost, in fact, had been for years the biggest hurdle to the global diffusion of the photovoltaic technology for electrical energy production applications.

While thin films, from a theoretical point of view, should have better electrical performance in comparison to crystalline silicon solar cells, thanks to the reduction of the active material thickness that limits the recombination effects, increasing therefore the open circuit voltage V_{OC} and filling factor FF, the low absorption coefficient for semiconductors like silicon poses some limits on the minimum thickness of the active layer. Developing light trapping methods and surface texturization could make it possible to obtaining higher efficiency

thin film solar cells; the manufacturing cost of these nano-scale treatments, though, makes them not feasible and limits therefore the maximum achievable efficiency for thin film solar cells.

2.5.2.1 AMORPHOUS SILICON

Developed starting from 1973, when Spears and Les Comber discovered the electrical properties of amorphous silicon deposited by means of a SiH_4 glow discharge on a foreign substrate, amorphous silicon solar cells are based on the same active material used in crystalline silicon solar cells, but, the deposition method used in substitution to the crystalline silicon growing process allows a strong reduction for material costs in these types of solar cells.

Whereas silicon is the same chemical element used in crystalline silicon solar cells, the deposition method used for the fabrication of amorphous silicon solar cells doesn't allow the formation of an oriented crystalline structure and the silicon atoms are therefore connected one to the other in a non-ordinated way.

The feedstock material used for the deposition of an amorphous layer on a foreign substrate, usually made of glass or stainless steel, is silane (SiH_4). The use of a different feedstock material in comparison to crystalline silicon solar cells made amorphous silicon solar cells independent from the cost volatility of polysilicon that affected the crystalline silicon industry during the polysilicon shortage period.

The deposition of the active layer is done using the Plasma Enhanced Chemical Vapor Deposition technique (PE-CVD). The deposition is conducted inside a vacuum chamber in which a radio frequency (RF) or high frequency (HF) plasma (13.56 MHz or 400 MHz) is sustained between an electrodes grid and the substrate heated at 160-200°C. The gas injected inside the plasma torch is SiH_4, which allows the deposition of a 0.1 μm layer of a-Si:H (amorphous silicon with hydrogen bonding that increases the electrical performance) and a 0.3 μm thick layer of micro-crystalline silicon (multi-crystalline silicon at microscopic level) on the substrate.

The typical cell structure is the so-called p-i-n structure, in which the two p- and n-doped layers are separated by an intrinsic semiconductor layer. This structure allows increasing the carrier lifetime that otherwise would be too short within the doped parts of the cells.

The active layer needs to be separated and interconnected to form a series of cells. Laser techniques are used for allowing a monolithic cells interconnection,

while transparent oxides, usually ZnO, are used for the creation of the electric contacts. The transparency of the contacts is essential since they are deposited not only below the active layer, but also on top of it.

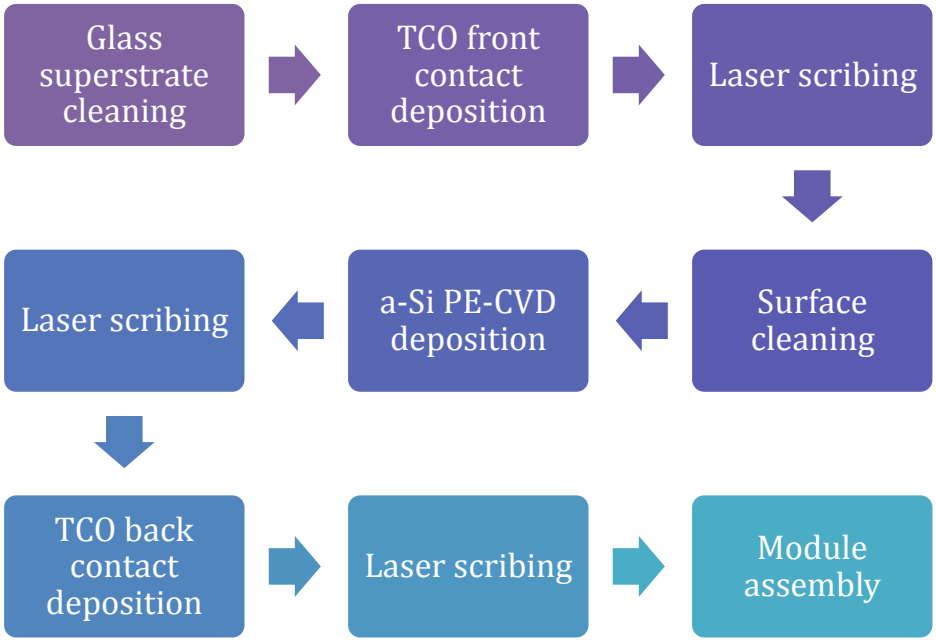

Figure 2.18 – Industrial steps for the production of a-Si solar cells using PE-CVD

The schematic description of the industrial process for the production of glass-glass micro-crystalline-amorphous tandem cells using 400 MHz PE-CVD is shown in Figure 2.18 and the schematic representation of a PE-CVD vacuum chamber is shown in Figure 2.19; whereas the typical structure of an amorphous silicon solar module with the laser cuts necessary for the electric series interconnection of solar cells is shown in Figure 2.20.

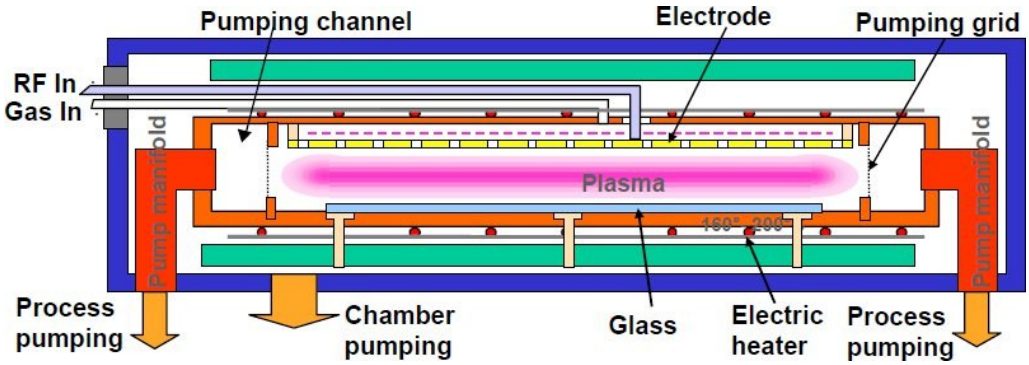

Figure 2.19 – Schematic representation of the PE-CVD equipment for amorphous micro-crystalline silicon deposition

The typical band-gap of amorphous silicon solar cells is in the order of 1.75 eV; whereas the highest lab-scale recorded stabilized efficiency is 13.4%,

obtained by LG electronics in 2012. It's worth noting that a-Si:H efficiency is affected by the Staebler-Wronski effect; which is a light induced degradation during the first 200 hours of sun exposure that could reduce the initial efficiency of up to 30%. The degradation effect hasn't been completely described yet, but is related to the a-Si:H compound that changes its physical structure with sun exposure. The process is reversible and the initial efficiency could be obtained after a thermal annealing process.

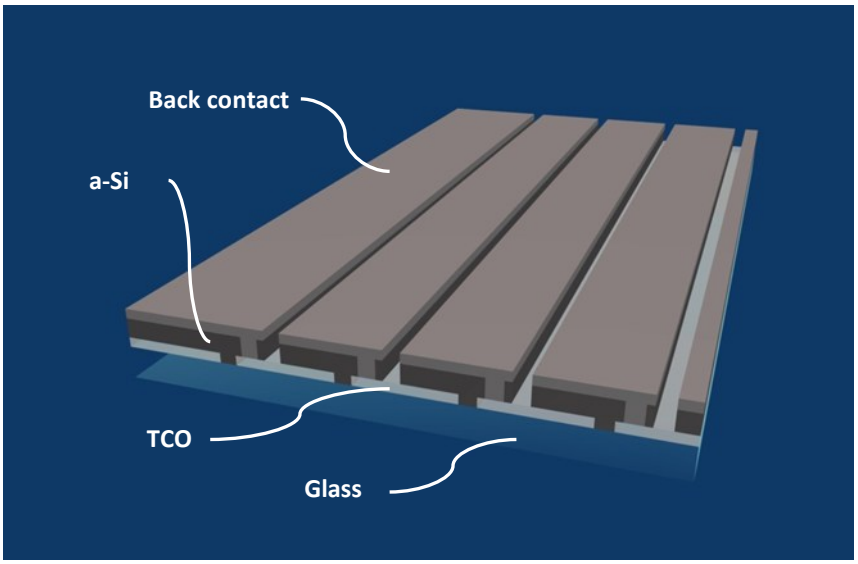

Figure 2.20 – 3D representation of the cross section of an a-Si thin film solar module. The glass superstrate, the back contact layer (white), the a-Si layer (dark grey), the transparent contact oxide (light grey), and the laser cuts are represented.

Amorphous silicon technology was expected to reach commercial efficiencies higher than 10% and manufacturing cost much lower than c-Si ones that could make it interesting for general use PV applications; the reduction of c-Si cost, together with a non-sufficient efficiency improvement for a-Si limited its application to the building integration PV market or to installations with particular climate that make this technology preferable in comparison to c-Si.

2.5.2.2 CADMIUM TELLURIDE

Cadmium telluride had been chemically synthetized for the first time by Margottet in 1879 using the chemical elements cadmium and tellurium; the first experimental tests on the semiconductor properties of the chemical compound date back to 1954 when Jenny and Bube discovered the possibility to dope n-type or p-type CdTe, and the first CdTe/CdS cells, with a cell efficiency of 6%, had been realized by Bonnet in 1976.

Although CdTe solar cells had been among the first ones to be developed at the start of the modern PV era, more than 20 years separated the realization of the first solar cells to the development of the first market-mature cadmium telluride solar module.

Cadmium Telluride, as shown in Figure 2.17, has nowadays the biggest market share among thin films and had been the only technology able to gain a relevant market share in the multi-megawatt size PV market.

Cadmium telluride is a chemical compound made of cadmium, a chemical element belonging to the II-B group and tellurium, a chemical element belonging to the VI-A group.

Cadmium is a by-product of the extraction and refining of Zinc and Lead ores. Cadmium is a Toxic and environmental hazardous element and is therefore considered a waste by the mining industries. Its use in a closed loop system with a well-designed recycling system could lead to beneficial environmental effects since cadmium use and disposal could then be controlled, avoiding its possible dissolution into water.

Tellurium on the other hand is a non-toxic element, a by-product of the extraction and refining of Copper ores, characterized by a limited availability that limits the production of CdTe PV modules to some tenths of GW per year. The possible price volatility of Tellurium related to its scarcity requires the development of a recycling system for end of life PV modules for the recovery of the expensive and rare materials. An industrial scale pre-funded recycling system for CdTe thin film solar modules had been developed by the US based company First Solar and guarantee the minimization of the potential environmental hazards related to the use of Cadmium; it also guarantee cost stability making the PV production independent on the raw materials price volatility and scarcity.

CdTe is considered a stable compound, not soluble in water and solvents and stable at room temperature and up to 1000°C. The potential environmental and health hazards related to events of fire had been demonstrated to be negligible, thanks to the encapsulation of the active materials between two layers of soda lime glass that incorporate the active materials within the molten mass, avoiding any fume emission or cadmium leakage [9].

CdTe is a direct band-gap semiconductor with an energy gap of 1.5 eV and a light absorption spectrum that allows the conversion of a broad band of wavelengths from UV to the energy band-gap, making it one of the most suitable semiconductor for PV applications.

CdTe modules are produced as a CdTe/CdS heterojunction; they are not affected by light induced degradation, and have good performance in hot climates due to the reduced temperature coefficient in comparison to crystalline silicon solar cells. The best efficiency recorded for CdTe/CdS PV cells is 18.3% obtained by GE Global Research in 2012; whereas typical module efficiency is in the order of 12.5%.

CdTe solar cells are usually encapsulated between two soda lime glass plates, using EVA (Ethyl Vinyl Acetate) as encapsulant; whereas the active layers deposited are a transparent contact oxide (TCO) layer, the CdTe/CdS layer and a back contact reflecting layer.

The deposition steps start from the front glass and the process is therefore based on the deposition over a superstrate. The TCO layer, usually made of indium-tin-oxide (ITO), or tin-oxide (SnO_2) for reducing the cost volatility effects related to the indium scarcity, is deposited over an EVA layer through DC-sputtering. An 80 nm multi-crystalline layer of CdS is then deposited and forms the n-type part of the p-n junction, whereas CdTe is subsequently deposited using closed space sublimation.

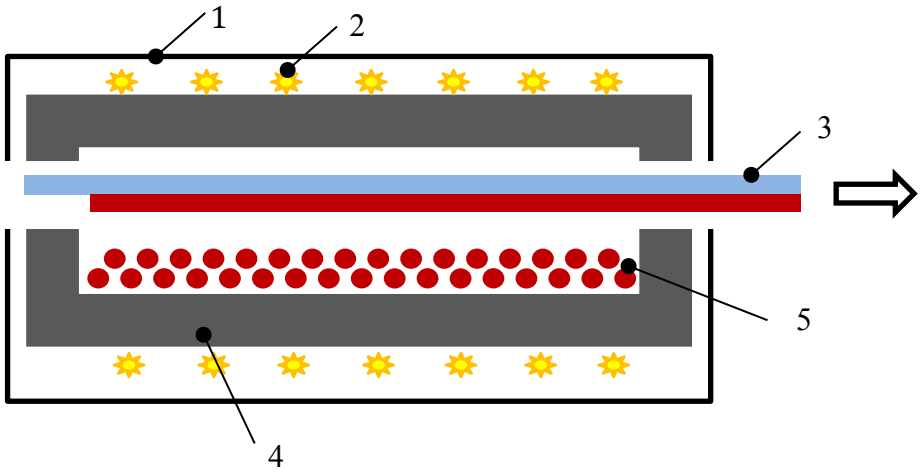

1: Radiation shield
2: Heating lamps
3: Moving substrate (500°C)
4: Graphite crucible
5: CdTe granulate

Figure 2.21 – CdTe film closed space sublimation equipment

Many technologies are available for the deposition of thin films of multi-crystalline CdTe on foreign substrates or superstrates. The closed space sublimation technique is based on the CdTe property of sublimating congruently in vacuum at temperature higher than 600°C and condensing

stoichiometrically onto the substrate surface heated at 400°C. The schematic description of the closed space sublimation deposition method is shown in Figure 2.21.

After the active layer had been deposited the back contact, usually ZnO layer, needs to be deposited. This layer is not transparent and has reflective properties that make it possible to let the solar cell capture the reflected photons. The module undergoes after each deposition step a laser scribing process that allows the realization of a monolithically series connected solar module. A schematic representation of the cross section of a CdTe solar module is shown in Figure 2.22 with the representation of the series connection and current flow. After the back contact deposition and the laser scribing processes, an EVA layer is finally deposited before the bottom glass plate is put into place, completing the module structure after the lamination process.

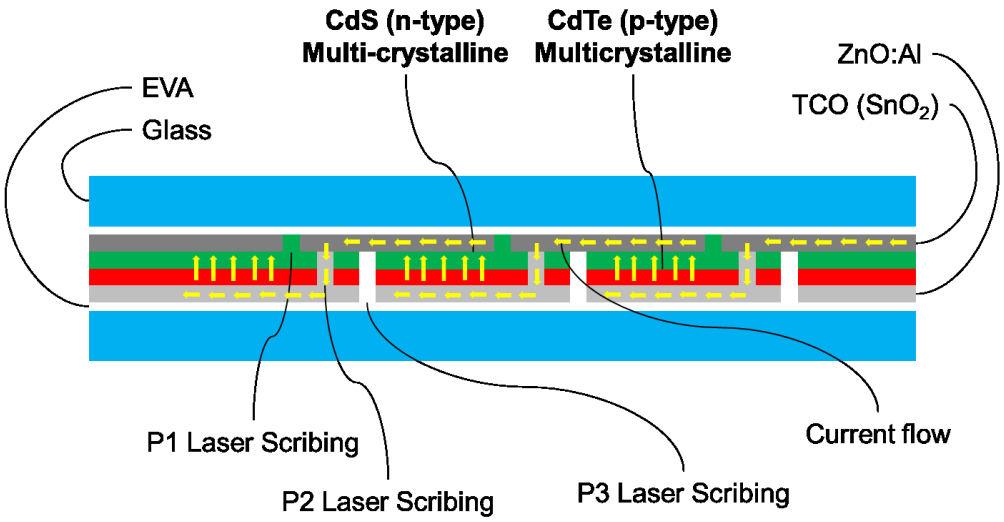

Figure 2.22 – Schematic representation of a CdTe solar module cross section

CdTe solar panels could be a valid alternative to c-Si PV modules for their relatively high efficiency and low cost due to the realization of a standardized production process conducted by First Solar; CdTe will never be able to reach the PV market leadership due to material availability issues, but it could have been an interesting competitor to c-Si in multi-megawatt size applications, and applications in high temperature climate. The unjustified limitations on the use of Cadmium that will enter into force in a few years in many countries, including European Union, though, will limit the growing of this interesting technology, eventually relegating CdTe to applications in emerging countries.

2.5.2.3 CIS-CIGS PV

CIGS solar cells are the most innovative thin film cells available in the PV market. They are usually made by a compound of copper, indium, gallium and selenium, deposited on a glass or flexible substrate through in-line co-evaporation.

CIS ($CuInSe_2$) solar cells are characterized by their peculiar property of 99% absorption of the solar light within a few micron of photoelectric material, making it possible to obtain solar cells with one of the highest efficiency available on the market. Using small doses of gallium, realizing then CIGS solar cells ($Cu(In_{1-x}Ga_x)Se2$) highly increases the cell efficiency along the whole solar spectrum, making CIGS solar cells among the most versatile ones.

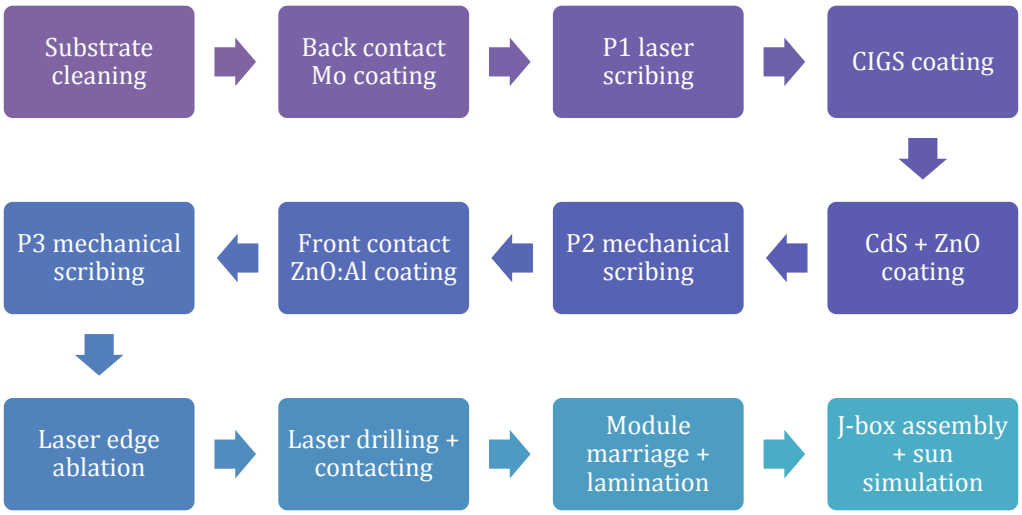

Figure 2.23 – Industrial steps for the manufacturing of CIGS thin film PV modules

CIGS commercial PV modules are manufactured following the process steps described in Figure 2.23. In particular the active part of the cell is composed by a 0.5 µm thick back contact layer made of Molybdenum, deposited through DC-sputtering, a 2 µm $Cu(InGa)Se_2$ multi-crystalline layer deposited through co-evaporation, a 0.05 µm thick buffer layer of CdS deposited by means of a chemical bath, and a 1 µm thick ZnO:Al transparent conductor oxide, deposited through DC-sputtering; the lamination and laser scribing steps necessary for the manufacturing of the modules, are similar to the one described for the other thin film technologies.

Commercial CIGS modules with a module efficiency of almost 13% are currently available in the PV market and the CIGS technology is accounted for the best cell efficiency among the PV modules: ZSW obtained 20.3% efficiency in 2010; this value is comparable to multi-crystalline silicon highest efficiency.

Whereas the CIGS technology can be considered among the most promising technology for the future PV market for its extremely stable high efficiency, its high manufacturing costs in comparison to crystalline silicon PV modules reduce its attractiveness within the PV market. The CIGS industry has also to face the material availability issues related to the use of indium which price and market is dominated by the LCD industry and the possible technology bans related to the use of the CdS buffer layer. Researchers working on the development of the CIGS PV technology have already developed solar cells with substitutive materials for indium and cadmium; their optimization, though, together with an important cost reduction, are already far to be reached.

2.5.3 MULTI-JUNCTION SOLAR CELLS

The thermodynamic limit for the efficiency of single junction solar cells had been demonstrated to be 40.7% [10]. Obtaining higher efficiencies is a challenge that the PV industry had followed for years and obtaining efficiencies higher than the theoretical limit for single junction solar cells had been demonstrated to be possible with multi-junction solar cells.

The base principle that leads to the high efficiency of multi-junction solar cells is the possibility to absorb the whole solar light spectrum. Multi junction solar cells are in fact manufactured as a stack of solar cells with different characteristics and with different band-gap. The top cell act as a sort of filter for the bottom cells, absorbing high energy photons and letting lower energy ones reach the bottom cells. For a triple junction solar cell, which spectral splitting is shown in Figure 2.24, being the top solar cell characterized by an energy band-gap E_{G1}, it will absorb high energy photons, $h\nu > E_{G1}$; the middle solar cell will absorb photons with energy $E_{G2} < h\nu < E_{G1}$, with E_{G2} the value of its energy band-gap, and the bottom cell will absorb photons with energy between $E_{G3} < h\nu < E_{G2}$.

Multi-junction solar cells can be manufactured as a stack of solar cells transparent to low energy photons, depositing the bottom solar cell over a substrate and consequently depositing the solar cells one on top of the other. Multi-junction solar cells are usually manufactured using GaAs, GaInP, InP, GaInAs, and Ge, and the multi-junction technology has also been adopted by the

thin film silicon PV industry in tandem amorphous-microcrystalline silicon solar cells.

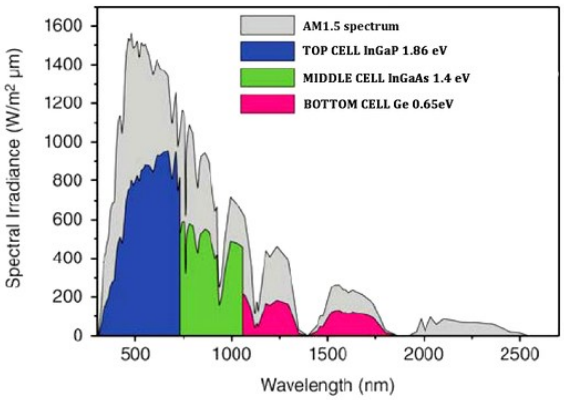

Figure 2.24 – Solar cell splitting for a multi-junction solar cell (source: Fraunhofer ISE)

The electric connections of the solar cells can be separate with each sub-cell electrically independent to the others, making therefore an optimal multi-junction solar cell, or monolithically series connected with each cell affecting the other cell performance.

Record multi-junction solar cells had been manufactured, for solar concentration applications, with a maximum efficiency of 44%. Their high cost and a concentration technology not enough reliable and developed, made them struggle to gain relevant market share.

2.5.4 DSSC SOLAR CELLS

Following the objectives of obtaining high efficiency solar cells from inexpensive materials, the PV industry, together with the chemical industry, started to develop solar cells based on inorganic, organic, or polymeric materials which show photoelectric properties.

Dye sensitized solar cells (DSSC) are an example of these newly developed solar PV technologies. DSSC solar cells are made of a conductive glass (anode) sputtered with a thin semiconductor layer of titanium oxide (TiO_2) nano-particles. The semiconductor layer is soaked with a photosensitive organic dye, which molecules are arranged on the semiconductor grain boundaries. When the dye is illuminated, the photons energize the dye that transfer an electron to the TiO_2 layer connected to the conductive glass that acts as an electrical connection between the cell and the electric circuit. The electric circuit

is closed through a second electrode (cathode) made of a conductive glass plate with a porous micro-crystalline catalyst layer made of platinum or carbon and an electrolyte that effectively closes the electric circuit. The schematic representation of a DSSC solar cell is shown in Figure 2.25.

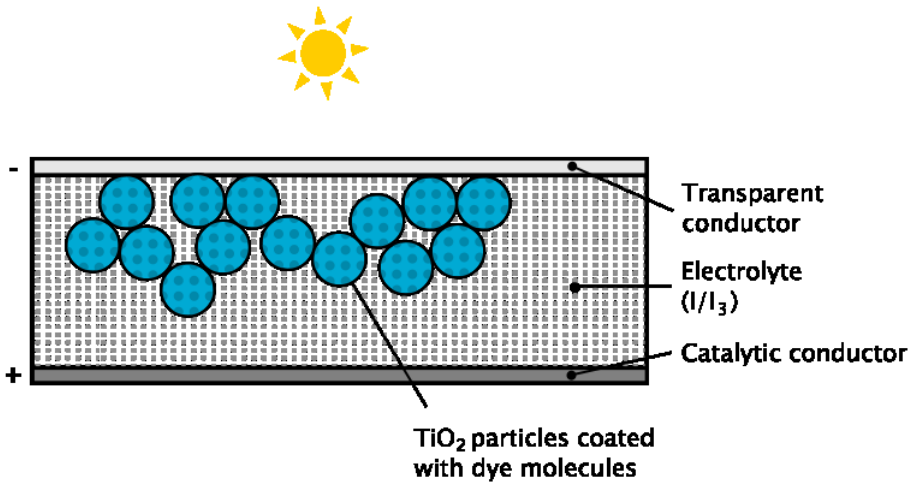

Figure 2.25 – Schematic representation of a Grätzel dye sensitized solar cell.

DSSC solar cells, as well as other organic or inorganic based newly developed solar cells had been able to reach maximum cell efficiencies in the order of 11.4%; their manufacturing process is inexpensive and not energy intensive, but they are still at lab-scale level and they are far from their industrialization. It is therefore reasonable to predict that they will not be able to gain a relevant market share within the next two decades.

3 ECONOMICAL COMPARISON BETWEEN C-SI AND THIN FILM PV TECHNOLOGIES

Since the first studies on amorphous silicon solar cells conducted in the mid-1970s, the main goal for the thin film PV industry has been to develop modules that could be low-cost alternatives to traditional PV modules based on crystalline silicon.

Thin film PV modules have been used for years mainly in consumer products (e.g. calculators), or in special applications for which c-Si modules could be unsuitable, such as, for example, building integration.

Thin film modules have never been a real competitor for the c-Si PV industry, especially in the range of MW size applications in which the lower cost of thin film modules have never been enough to compensate a lower efficiency, nevertheless starting from the mid-2000s the PV market has changed rapidly; the thin film share has grown steadily, lots of thin film producers entered the market with their products and several thin film based multi-MW PV power plants, mainly based on CdTe technology, have been installed worldwide. The reason for the thin film market share growth in those years can be found in the introduction in the market of more efficient thin film PV modules that were cost effective in a period when the polysilicon shortage affected the price of c-Si modules.

After the polysilicon shortage problem has been solved, the c-Si industry invested on developing low-cost high efficiency multi-crystalline solar cells that could be more cost effective than thin films, strengthening its leadership in the PV market.

For a correct evaluation of the real cost effectiveness of different technologies in an actual PV plant, module manufacturing cost or selling price for different technologies shouldn't be used as the sole term of comparison, since this can lead to incorrect considerations that don't take into account other cost drivers unrelated to manufacturing cost such as, for example, balance of system costs.

During the first part of the PhD research activity an economical comparison has been made on an energy cost basis, calculating the levelized cost of the

energy produced by the different power plants considering the energy production and all the cost drivers for building, operating and maintaining the plant for a 20 years lifetime.

In the following sections the main characteristics of the technologies chosen for the comparison are briefly presented.

3.1 MULTI-CRYSTALLINE SILICON

Between the crystalline silicon based PV technologies, multi-crystalline was considered, at the moment of conducting the study, the most cost competitive one. In fact, in comparison with mono-crystalline silicon, it had the advantage of a much lower manufacturing cost, owed mainly to the crystallization process that is less energy intensive (e.g. it doesn't need the Czochralski growth process), and a relatively low efficiency gap from the highest efficiency of mono-Si solar cells.

The efficiency declared by the manufacturers for multi-crystalline silicon PV modules at Standard Testing Conditions ranged, at the time of conduction of the study, from 13 to 16%, while the efficiency of mono-crystalline silicon PV modules was in the order of 14-16% and up to 19.5% for high efficiency modules. Nowadays the efficiency had increased to 14-16% for multi-crystalline PV modules, and 15-17% for mono-crystalline PV modules, with a record efficiency of 20% for high efficiency mono-crystalline PV modules.

Combining the data of modules production cost (€/m^2) with the efficiency information, one can easily obtain the manufacturing cost of modules in €/W_p. This value, though, cannot be used for a direct comparison of the two c-Si technologies for the presence of other cost source, either power related or surface related, which contributes on the total system cost. In particular, balance of system costs and maintenance costs are usually surface related, i.e. they increase with the increasing of the surface needed for the same installed power, and are therefore directly related to efficiency, making it not reliable a comparison in terms of manufacturing power related cost. Since these costs are a relevant part of total system costs they must be taken into account for a correct comparison between different technologies. A comparison based only on manufacturing costs can be considered sufficiently accurate only if the efficiency gap is small enough to make the difference in surface related costs negligible and if the behavior of the different technologies in different environmental conditions is similar.

3.1.1 MULTI-SI COMMERCIAL STATUS AND MARKET

The market share for multi-crystalline silicon technology at the time of conducting the research could be evaluated in 46% of the global PV market.

In Italy there were several companies producing multi-Si solar cells and modules. The Italian annual production capacity of multi-Si solar modules could not be easily estimated for the presence of several companies that produced modules using cells imported from other countries. Just to give an idea of the production capacity of the Italian c-Si industry at the time of conducting the study, it can be noted that in 2007 the 9 main producers of c-Si modules (mono-Si and multi-Si) had been accounted for a total production capacity of 280 MW_p [11].

3.1.2 MULTI-SI MANUFACTURING COST

The lowest module manufacturing cost for multi-crystalline silicon can be estimated in less than 1.2 €/W_p at the time of the study. The manufacturing cost had then been furthermore reduced with manufacturing equipment standardization and technology innovations that allowed using less active material volumes. One of the challenges for the c-Si industry is still the reduction of wafer thickness without a reduction of yield, and kerf loss reduction during wafer sawing, for a reduction of the specific consumption of silicon in the final module. It's worth noting, though, that whereas at the time of publishing this study the manufacturing cost were strongly related to polysilicon cost, nowadays the drop of polysilicon cost due to the building of a dedicated supply chain made the manufacturing cost less dependent to materials' cost. It is expected that the polysilicon cost will fluctuate due to changes in the polysilicon market framework; new shortage periods and price volatility, though, are not expected for the overcapacity of the raw materials supply chain.

It's worth noting that a reduction of the manufacturing cost for PV modules doesn't always lead directly to a reduction of the module price. Module prices, in fact, are often driven by the market and it may happen that they can increase, even if manufacturing costs are steadily decreasing, when there is an increase of demand not readily followed by an increase of module production.

This market situation, together with changes on economic support laws, can also lead to rapid changes on the convenience of a particular PV technology in comparison with the others.

This doesn't mean, though, that the PV industry doesn't have to follow a roadmap for manufacturing cost reduction. In fact, even if this cost reduction doesn't lead directly to a reduction of module prices, this will be necessary in the long term for confirming the competitiveness of the PV industry in the energy market when PV generated electricity will reach the grid parity, economic supports from governments will be not necessary and there will be a stronger correlation between cost of energy, module prices and module manufacturing costs.

3.2 AMORPHOUS SILICON

Amorphous silicon is the first thin film PV technology that entered commercial production in the early 1990s. One of the main advantages of a-Si is that it requires a very small quantity of active material in comparison with c-Si and it can be deposited on rigid (e.g. glass) or flexible (e.g. stainless steel) substrates. While flexible solar cells are useful for building integration applications, in the high power range applications only glass-glass encapsulated a-Si modules had been considered in the study. Nowadays a-Si modules are not used in large scale power plants and have their own market niche in building integration applications.

3.2.1 A-SI COMMERCIAL STATUS AND MARKET

Silicon thin film PV modules have reached the commercial maturity and are on the market in the form of single junction amorphous silicon, double and multi-junction tandem and microcrystalline-amorphous modules. Amorphous silicon technology could be accounted at the time of publication of the study for more than a third of the global thin film module production.

Regarding the production of a-Si modules in Italy it must be noted that there were no production plant at the time of publication, but the European market offered the opportunity to easily buy turn-key solutions for building facilities for the production of a-Si modules. Nowadays three a-Si Italian firms are present in the PV market; the actual production of the three plants, though, is unknown.

3.2.2 A-SI MANUFACTURING COST

Manufacturing cost for thin film silicon solar modules is dominated by non-active material costs (e.g. glass for substrate and encapsulation) and other

investment costs. A typical cost breakdown for a-Si shows that only few percent of the total module manufacturing cost are due to active material cost [12]. This means that the manufacturing cost is not strongly related to the silicon cost. It's worth noting that the silicon feedstock used for a-Si modules is normally monosilane (SiH_4), a product whose cost is independent and less volatile than polysilicon used for the production of c-Si solar cells.

The total manufacturing cost for a-Si technology was in the order of 1 €/W_p in 2010. High standardization of the manufacturing process, and the possibility to buy turn-key solutions for a-Si production plants and equipment could have led to big manufacturing cost reductions. Some thin film production equipment manufacturers stated that with the introduction of new optimized processes and equipment, a manufacturing cost reduction of 30% in the short term could have been achieved. Nowadays the two biggest companies working on the development of turn-key solutions for producing a-Si PV modules retired from the market, highlighting the difficulties of competing in the PV market with traditional c-Si technology.

3.2.3 EFFICIENCY

The main disadvantage of thin film silicon based PV modules is low efficiency. Stabilized efficiency declared by manufacturers is in the order of 5-6%. This value increased with the adoption of technology solutions that allow absorbing solar energy in a wider light spectrum, such as tandem or multi-junctions and micro-crystalline/amorphous technology. These solutions allowed an increase of stabilized efficiency to values in the order of 7-9.5% in 2010; nowadays the stabilized efficiency of micro-crystalline/amorphous PV modules is in the order of 10%.

The efficiency values considered in the analysis are the so called stabilized efficiency values, i.e. the efficiency of the modules after the initial light induced degradation owed to the Staebler-Wronski effect [10].

It's worth noting that amorphous silicon modules are characterized by a good efficiency at low solar radiation levels and diffuse radiation. The power of the module is also less affected from variations of the cell temperature in comparison with c-Si modules. This characteristic can in some applications lead to an annual specific energy production higher than c-Si. Normally a-Si modules are installed in tilt fixed support structure for their lower efficiency and cost in comparison with c-Si modules that make the use of solar trackers not cost competitive.

3.3 CADMIUM TELLURIDE

The second thin film PV technology that has been compared to multi-crystalline silicon is Cadmium Telluride. Although this technology had been developed for years without being able to gain considerable market shares, starting from the last years of 2000s it had shown an enormous growth and gained the market leadership between thin film technologies with more than a half of the global thin film module production since 2010. The reason of this success can be addressed to its low cost in comparison with c-Si, mainly due to the high standardization of the manufacturing system developed by First Solar, and, considering the possible thin film competitors, to the higher efficiency in comparison to a-Si.

CdTe modules have been used in several multi-MW power plants around the world and had been sometimes considered as a real competitor for c-Si in large scale power plant applications.

3.3.1 CDTE COMMERCIAL STATUS AND MARKET

The CdTe PV modules market is dominated by the US based company First Solar, the world biggest producer in 2010 with modules production facilities in Europe and a global yearly production capacity of more than 1 GW_p in 2010. In Italy there is no current production of CdTe modules even if a company started the building of a facility for the yearly production of 18 MW_p of CdTe modules that never started modules' production.

3.3.2 CDTE MANUFACTURING COST

A complete cost model has been made by First Solar for NREL in the late 1990s [13] - [14], but no more recent data are available. First Solar in many conferences and public speaking declared a module manufacturing cost below 1 $\$/W_p$ at time of publication of the study; this cost level had been considered possible by analysts, thanks to the adoption of economies of scale and deposition processes that don't need great material consumption and can assure high production yield.

3.3.3 CDTE EFFICIENCY

The efficiency of CdTe modules is in the range of 7-11% in standard testing conditions (STC). This value is lower than c-Si, but much higher than single

junction a-Si. CdTe performances also don't show initial degradation as it happens for a-Si. In lower irradiation levels manufacturers declare a higher efficiency than in standard testing condition and the module power is less affected from temperature variations in comparison with silicon based technologies. CdTe behave much better than c-Si in hot climate.

3.3.4 CdTe material issues

Since Cadmium is a toxic element, some issues may arise on its use in PV panels. Several studies had been conducted to evaluate the potential toxicity of CdTe PV modules during their lifetime and in case of fire. These studies generally agree on the fact that CdTe modules in a glass-glass encapsulation are not hazardous for the environment and neither for people or animals [15].

CdTe PV modules must be disposed of properly at the end of their lifetime, but this isn't an issue since modules are voluntary collected by the producer and recycled. Recycling is also necessary to solve the future possible problem of availability of Tellurium. Even with the developing of a full recycling process with high raw material yield, the Tellurium scarcity will limit the global annual production of CdTe modules to only a few GW_p [16] and an increase of Tellurium cost is therefore predictable. Another obstacle to the growth of this technology is the ban of Cd compounds from the EU that made the US based company deciding to stop production in EU in 2012.

3.4 Cost analysis for a 1 MW power plant

In this paragraph the power plant characteristics and the parameters used for the evaluation of the energy yield and energy cost of a mega-Watt size PV power plant will be described.

3.4.1 Overview on plant and site characteristic

For the evaluation of the energy yield of different PV technologies operating in the same environmental conditions, a PV power plant with 1 MW of installed DC power have been considered. Modules are considered to be installed on a two-axis solar tracking system. This type of installation had been chosen because it was considered the one with the best energy yield at the time of starting the study. It must be noted that thin film modules have never been installed yet on 2-axis trackers for commercial purposes and that the solar

tracker market in Italy had rapidly changed within few months starting from the end of 2009, with an increase of the number of installations for single-axis systems and a drop of the number of installations for 2-Axis systems. Nowadays 2-Axis trackers are almost never used for their high cost; the new PV market situation make the results of the study not representative of future installations, but the approach for evaluating the competitiveness of a technology in comparison to competing technologies is still valid and replicable to different installation types. These considerations don't affect the results of the study since the objective of the study was to build a model for making comparisons of different PV technologies in the same installation and environmental conditions. The study can then be easily updated to the current Italian situation characterized by the majority of PV modules been installed on fixed tilt installations, with the possible further extension of the analysis to different technologies which market share grew in the last year, such as, for example, CIGS thin films.

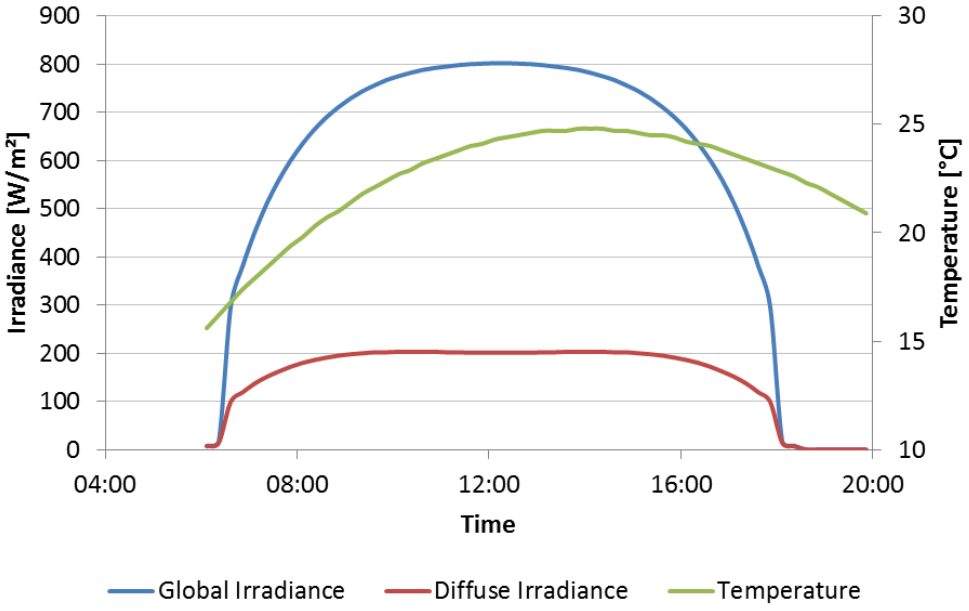

Figure 3.1 – Example of the temperature and irradiance data for the reference day in September

The installation site considered for the PV power plant was in southern Italy at 41°06'43" latitude north. This site had been chosen for the big interest on installing MW size solar plants in southern Italy at time of publication; the site is accounted for an average yearly global irradiation level for modules installed at optimal inclination of 1 818 kWh/m². This value has not been used for the calculation of the total energy production of the power plants because it doesn't permit to take into consideration the actual behavior of different technologies at

different irradiance levels (i.e. it doesn't allow to take into account the better energy yield of thin films at low irradiance or high temperature). Real data on solar irradiance levels, together with information on the daytime temperature profile have been used instead. In particular the global and diffuse irradiance data for a flat panel installed on a 2-Axis tracking system, together with the air temperature data, have been found using the Photovoltaic Geographic Information System (PVGIS) developed by the European Commission Joint Research Center (JRC) and available online for public use [17]. The irradiance and meteorological data used in this study are synthesized in Table 3.1 and an example of a monthly average daily profile for irradiance and temperature is shown in Figure 3.1.

Table 3.1 - Solar irradiance and temperature data available through the PVGIS system.

Type of Data	Unit	Frequency
Solar irradiance on a flat panel installed on a 2-Axis tracking system	W/m^2 (Global and Diffuse)	One data every 15 minutes for one reference day per month
Daytime temperature profile	°C	

Table 3.2 - Power plant and components technical data

	c-Si	a-Si	CdTe
Module data			
Power @ STC [W_p]	220.0	135.0	77.5
V_{OC} @ STC [V]	36.5	60.8	90.5
I_{SC} @ STC [A]	8.20	3.45	1.22
Efficiency @ STC [%]	13.4	9.5	10.8
Efficiency @ 200 W/m^2 [%]	11.1	8.4	11.0
NOCT [°C]	47.5	44.0	45.0
P_{MPP} Temp. coeff. [%/°C]	-0.485	-0.240	-0.250
Surface [m^2]	1.64	1.42	0.72
PV Plant Data			
Number of Modules	4 520	7 392	12 880
Number of Trackers	226	308	322
PV Power [kW_p]	994.4	997.9	998.2
PV Surface [m^2]	7 413	10 497	9 274
Ground cover ratio	0.15	0.15	0.15
Plant surface [ha]	4.94	7.00	6.18

The main technical data of the components chosen for the power plant design and the characteristics of the three PV power plants are presented in Table 3.2

Differences in the plant total PV energy between the three technologies are due to the necessity of approximating the total number of PV panels to a number compatible with the division of the plant in arrays. The fact that the total power of the plants is different from one to the other and from the selected size of 1 MW has a negligible influence on the final cost of energy.

3.4.2 ENERGY YIELD FOR THE PV POWER PLANT

For evaluating the energy yield of a PV power plant in real installation conditions, a model based on the use of solar irradiance data has been made. Knowing the irradiance and temperature values with time intervals of 15 minutes for every monthly reference day, the instantaneous PV power had been calculated for every interval using technical data declared by module manufacturers. When data were not available estimates of them have been done. The interpolation of the PV power between every instantaneous data calculated within the model allowed the tracing of a profile for the daily power theoretically producible by the PV plant. The integration of this power during a day results on the daily PV energy produced and therefore to the monthly and yearly DC electrical energy.

For obtaining a realistic value for the energy yield of the three power plants, a series of de-rating factors for instantaneous power or energy, some of them independent on the PV technology, other strictly related to the characteristics of each technology, have been taken into account. Some of the de-rating factors are due, for example, to shading, module aging, low inverter load factor at low irradiance level, and conversion and electric losses.

De-rating factors needs to be used with caution because a misuse of them could lead to unrealistic results. Realizing a full simulator based on a complete model for different technologies PV cells will definitely lead to more realistic results. Unfortunately the majority of the data needed for building this type of model are not disclosed by manufacturers, especially for thin films, therefore building a complete and reliable model is almost impossible without the collaboration of manufacturers; the use of a simplified model based also on de-rating factors is therefore needed.

The results for the net annual AC energy produced by the three power plants, calculated for the first year are synthesized in Table 3.3.

Table 3.3 – Net annual energy production

	c-Si	a-Si	CdTe
Energy [kWh/yr]	1 820 066	1 894 763	2 010 033
Specific energy [kWh/kW$_p$/yr]	1 830	1 899	2 014

3.4.3 POWER PLANT COSTS

The power plant costs had been calculated considering all the main figures for building the plant and the yearly costs for maintenance, plant operation and for spare parts.

The model is based on real market prices for components, where available, or on educated estimates for those components whose selling price is considered strategically relevant and communicated by manufacturers or distributors to third parties or customers only under non-disclosure agreements.

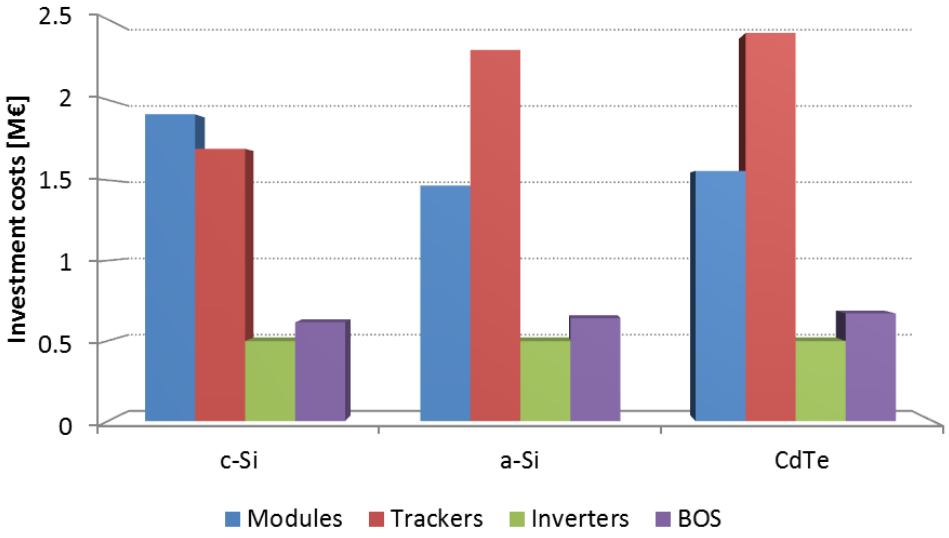

Figure 3.2 – Main investment costs for a MW size PV power plant

In Table 3.4 some of the main cost drivers that have to be taken into account for building the PV power plant, together with their estimated cost for the three PV plants analyzed in the study, are described, and in Figure 3.2 the impact of various components of investment cost on total cost is shown.

Table 3.4 – Main costs for a 1 MW power plant

	c-Si	a-Si	CdTe
Modules investment cost [€]	1 909 248	1 466 942	1 557 192
Trackers investment cost [€]	1 582 000	2 156 000	2 254 000
Inverters investment cost [€]	498 735	498 735	498 735
Other costs [€]	319 199	329 734	344 794
Total investment cost [€]	4 309 182	4 451 411	4 654 721
O&M cost [€/yr]	41 942	45 498	47 050
Land use cost [€/yr]	24 709	34 989	30 912

3.4.4 COST OF ENERGY

For a direct comparison of the three different technologies under an economic point of view the levelized cost of energy had been calculated.

The levelized cost of energy cost (LCoE) is an index representing the unitary cost for the electricity produced by a power plant. This takes in consideration all the costs for building and operating a power plant, as well as additional costs, such as fuel costs for non-renewable energy fueled power plants.

The LCoE, expressed in €/kWh had been calculated for the three PV power plants using the following equation that allows to consider the present value for the building and operation cost and for energy production as well.

$$LCoE = \frac{\sum_{n=1}^{L} \frac{I_n + O_n}{(1+r)^n}}{\sum_{n=1}^{L} \frac{E_n}{(1+r)^n}}$$

In which:
I_n = investment cost at year n (€)
O_n = operation and maintenance cost at year n (€)
E_n = energy produced at year n (kWh)
r = discount rate
L = power plant lifetime.

The value of the LCoE calculated for a 20 years lifetime for the three plants analyzed in the study is shown in Figure 3.3.

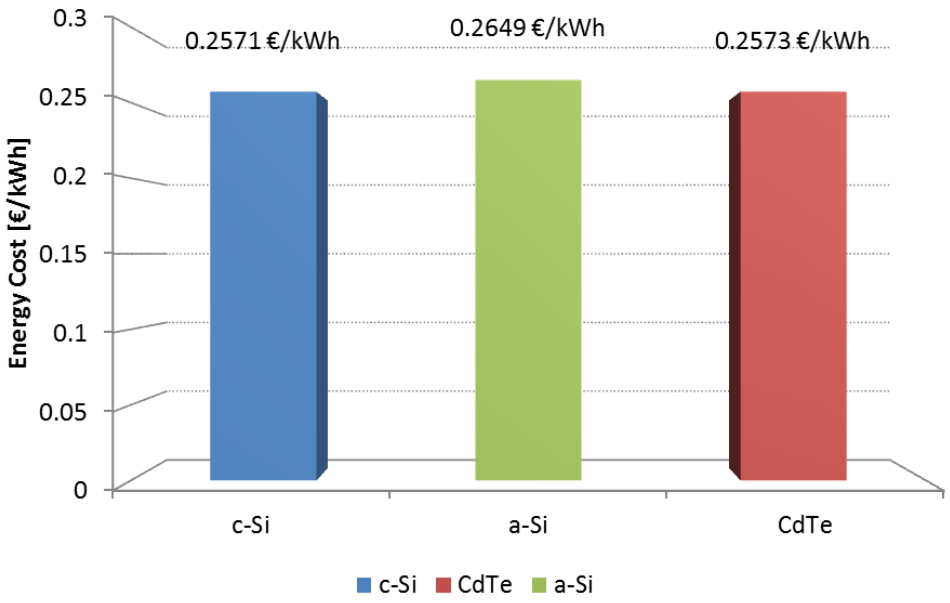

Figure 3.3 – Levelized cost of energy for 1 MW PV power plant for different technologies

3.5 FINAL REMARKS

The PV market in Italy has shown in the last years a big growth either in grid connected home applications or in power plants applications. The high irradiance levels and the high feed-in tariffs made the investment in MW size PV power plants very attractive for Italian and European investors and the majority of PV power plants installed were based on the traditional c-Si PV technology.

The introduction in the market of thin film solar modules characterized by efficiency higher than 10% and a manufacturing cost lower than c-Si posed some questions on whether these technologies could be an affordable alternative to traditional c-Si modules.

The building of a cost model made it possible to compare the traditional multi-crystalline silicon PV technology and two thin film technologies (micro-crystalline/amorphous silicon and cadmium telluride) considering both the technological and economic perspective. In particular an economic analysis aimed at evaluating the cost of the energy produced by a 1 MW PV power plant based on the three technologies has been done.

The results show that in the particular application considered for the study there is a little difference between the cost of energy for c-Si and CdTe based

plants. In fact the two technologies are accredited for a cost of energy of 0.2571 and 0.2573 €/kWh respectively for c-Si and CdTe. The differences were so small that even a small change in component prices or other costs could have led to an advantage of one technology in comparison with the other. The micro-crystalline/amorphous silicon technology, though, was accredited for an higher cost of energy: 0.2649 €/kWh, still close to its competitors, but high enough to make the technology unsuitable for MW size grid connected on field applications.

A point in favor of c-Si technology is investment cost. In fact, as it can be seen in Table 3.4, building a 1 MW PV power plant based on c-Si modules required a smaller capital investment for obtaining a similar cost of energy considering a 20 year plant lifetime. This is due to the higher cost for BOS components (including high costly tracking systems) for thin films.

After completing the research, the market leadership of c-Si strengthened thanks to the cost reduction of c-Si mainly caused by changes in the framework of raw materials supply and to the technology improvements for thin films, especially a-Si below the expected roadmap.

In Table 3.5 and Figure 3.4 a qualitative comparison of the main characteristics of the different technologies considered in the study for the application in 1 MW power plants is presented. A mark between 1 and 10 for each of the main features required for the application had been given for the different technologies. The total score can be used as an index of the overall suitability of different PV technologies for the same application.

Table 3.5 – Characteristics of different PV technologies for the application in 1 MW size PV power plant

	c-Si	a-Si	CdTe
Module cost	7	8	8
Efficiency @ STC	9	6	7
Efficiency @ 200 W/m^2	5	8	9
Temperature coeff.	6	7	8
Energy production	8	8	9
Material availability	7	9	6
BOS cost	9	5	6
Land Use	8	5	6

The biggest weaknesses of each technology are where the PV industry has to work for enhancing its shares in the energy market. In particular, c-Si technology had the main weakness of a lower energy yield and high energy

needs for wafer production; during the last few years the technology development allowed to increase the efficiency and to reduce the energy needs, reducing therefore the carbon footprint. Micro-crystalline/amorphous silicon technology won't be a tough competitor for c-Si and CdTe for its efficiency limits even with multi-junction solar cells. The impact of an efficiency increase for this technology would lead to a bigger increase in competitiveness than the one related to module cost reduction because it would lead to a big decrease of BOS cost. CdTe is now the only thin film technology that can be competitive in the MW size PV market, but unfortunately have to face the problem of the, somehow unjustified, ban of components using Cd based compound from many countries.

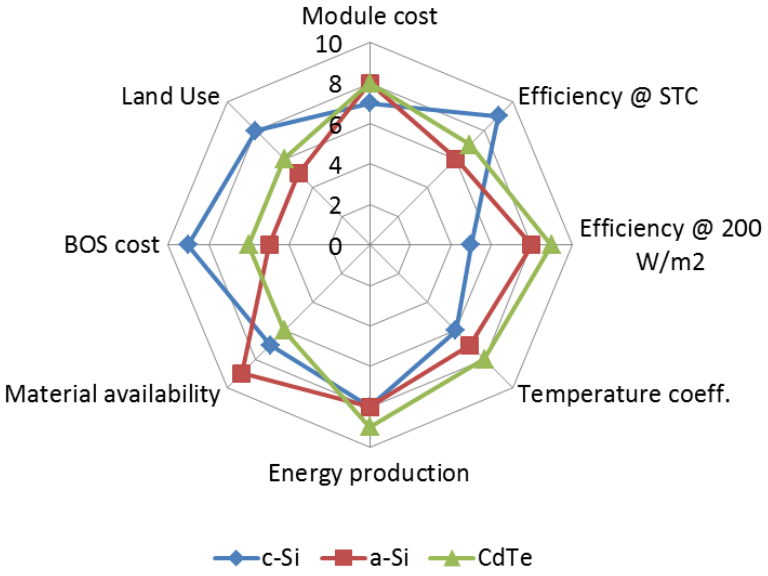

Figure 3.4 – Strengthens and weaknesses of different PV technologies in MW size PV power plants

It's worth noting that this study, conducted for a specific location in southern Italy, is not aimed at assessing which technology is in general the best choice, since many technological, economic and legislative factors that affect the results can change widely from one location to another, leading to different results. The model and the analysis, though, can be extended with ease to other technologies such as, for example, the well-established mono-crystalline silicon technology that regained big market share in the last years or CIGS and other emerging technologies as soon as they reach their market maturity.

4 CRYSTALLINE SILICON PV PRODUCTION CHAIN

Crystalline silicon photovoltaic modules are nowadays the most diffused and installed solar energy conversion equipment for their relatively high efficiency in comparison with competing technologies and for their reliability and well-established production chain.

Whereas crystalline silicon PV modules may seem technologically simple products, made only of glass, electric connections and solar cells, the production chain that lead to the manufacturing of PV modules is very complex and requires some critical steps that are energy intensive and need effective process control.

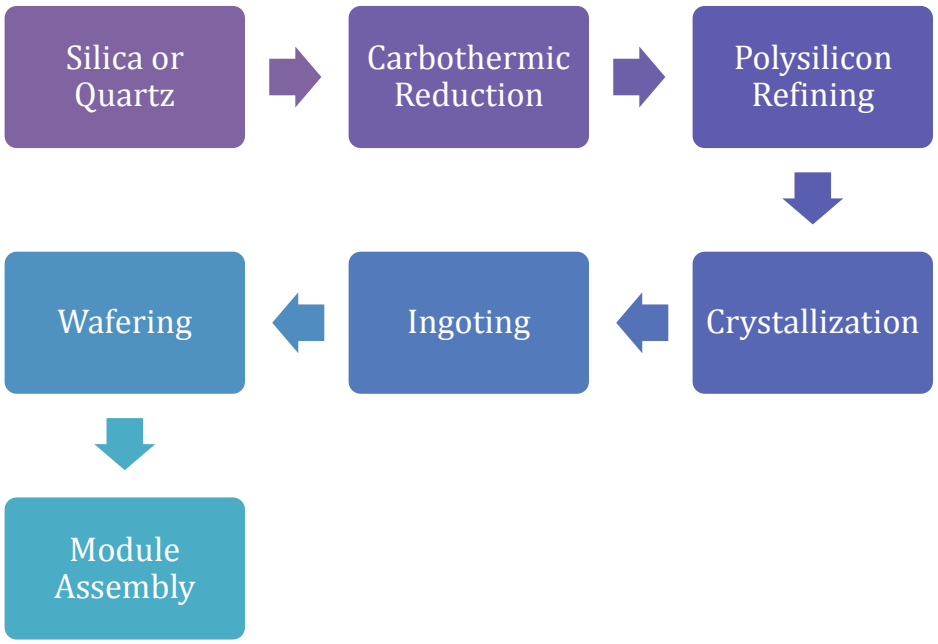

Figure 4.1 – Principal process steps for the production of PV modules starting from silica ores

The production of crystalline silicon PV modules, either mono-crystalline or multi-crystalline, starts from the refining of raw materials needed for solar cells, and ends with the final assembly of solar modules. The manufacturing chain is characterized by some complex and energy intensive steps and the complete description of every step of the production chain requires knowledge of many

different subjects related to chemical science, electrical, materials, mechanical and automation engineering, as well as thermal processes of materials.

A brief description of the main steps of the production chain is shown in Figure 4.1 and the detailed analysis of the most important industrial processes needed for the production of crystalline silicon PV modules will be conducted in the following paragraphs.

4.1 POLYSILICON PRODUCTION

Silicon is the raw material used for the production of crystalline silicon wafers for photovoltaic applications, but, even if silicon is the second most abundant element on earth's crust (27%) it is not available as a pure element in nature since it is often found as silica or silicates.

The refining processes needed for the extraction of Si from silica or quartzite ores are numerous and many of them are very energy intensive and time consuming. Whereas the silicon source material supply chain for photovoltaic applications was, from the start of the PV market growth until the mid-2000s, part of the supply chain for the electronic integrated circuit (IC) industry [18], nowadays the PV industry can rely on a dedicated supply chain for solar silicon.

The reasons that pushed the PV industry to invest on the development of a dedicate supply chain for solar grade silicon have not been directly related to a real shortage of pure silicon, but the big growth of PV made the supply of rejected material from the electronic industry not sufficient for following this growth rate. The PV industry could have then used highly purified raw materials (99.999999%) prepared for the IC electronic industry that wasn't facing any shortage problems; the high cost of the so produced materials, though, together with the need of less expensive less pure material (99.999%) and a realistic scenario of electronic grade silicon shortage due to PV use of silicon, made the PV industry investing on the development of the current polysilicon supply chain.

In the following paragraphs metallurgical grade silicon production and polysilicon refining, the two industrial steps needed for the production of purified silicon for PV applications are described.

4.1.1 METALLURGICAL GRADE SILICON

The first industrial step needed for the purification of silicon, either for photovoltaic and semiconductor applications, is the carbothermic reduction of silica for producing metallurgical grade silicon with silicon purity between 98 and 99.5%. This process is based on the carbothermic reaction of silica (quartz) and carbon materials in a submerged electric arc furnace and is described by the following simplified equation [10]:

$$SiO_{2(s)} + 2C_{(s)} = Si_{(l)} + 2CO_{(g)}$$

The process stream for obtaining metallurgical silicon from silica or quartz and coal is shown in Figure 4.2.

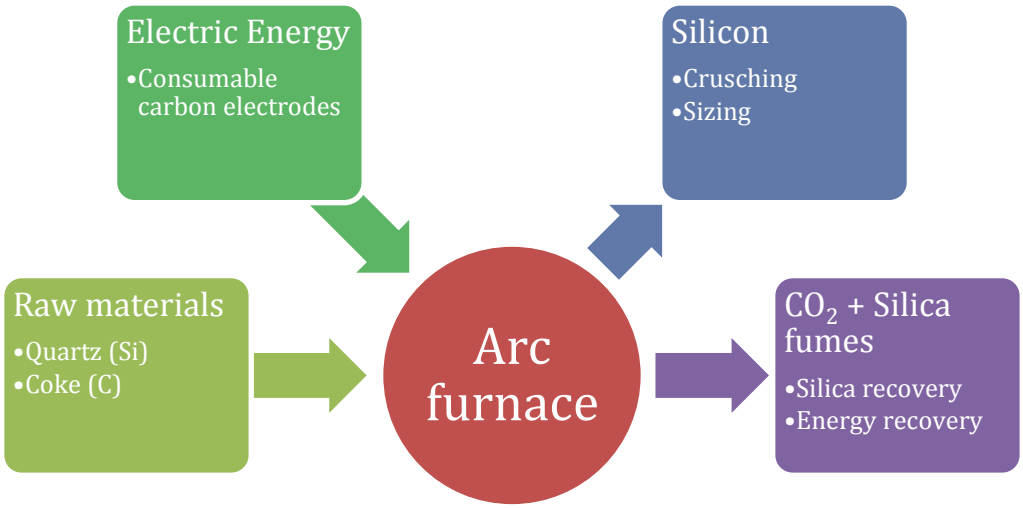

Figure 4.2 – Simplified process flow for the production of metallic silicon from quartz

The materials used in the reacting furnace are usually quartz, metallurgical grade coal, woodchips and coke. The raw material charge is heated by the effect of the arc sustained between three submerged carbon electrodes, connected to a three-phase multi-megawatt power supply, and the grounded crucible at temperature between 1900 and 2100°C; liquid silicon can then be tapped from the bottom of the furnace while raw materials can be charged from the top. Carbon monoxide CO is further oxidized in carbon dioxide CO_2 and released into atmosphere. It's worth noting that, although PV technology is considered by

many as an emission-free electrical energy production technology for its no emissions during its active life, the production of PV modules requires not only vast amounts of electricity that could be obtained from renewable energy or fossil fueled power plants, but also chemical reactions that produce CO_2 emissions as secondary products. The carbon footprint of PV, though, even if it is not negligible, is relatively low in comparison to other electrical energy production technologies [19].

The purification process for obtaining metallurgical grade silicon from silica or quartz is actually more complex than the process described in this paragraph. The carbothermic reaction, in fact, is followed by some side-reactions that produce silica fumes that can be treated and recovered, making it possible to obtain materials that can be profitably sent to the concrete and refractory industry. The liquid silicon obtained from this process is then treated before being refined for semiconductors or solar applications, allowing to separate elements dissolved in silicon, such as Al, Ca and Mg, which concentration could be detrimental on the overall quality of the metallurgical grade silicon.

Liquid silicon, after the refining process, solidificate and is therefore crushed for obtaining small lumps with dimensions up to 100 mm. Small fines are separated from the product for their difficult handling process and for the ease of contamination.

4.1.2 ELECTRONIC AND PHOTOVOLTAIC GRADE SILICON PRODUCTION

Metallurgical grade silicon, also called silicon metal, cannot be used for semiconductor applications and neither for photovoltaic applications for its insufficient purity. Higher purity can be obtained through further refining of silicon metal with processes that are used both for the electronic and photovoltaic industry, or that are dedicate to the solar industry.

Further refining is possible through the purification of volatile silicon hydride, obtained from silicon metal, using fractional distillation, followed by the decomposition of the hydride to hyper-pure elemental silicon by chemical vapor deposition or pyrolysis.

The four steps of the purification process for obtaining either solar grade or electronic grade silicon from metallurgical grade silicon are:

- synthesis of the volatile silicon hydride,
- purification,
- decomposition to elemental silicon,

- recycling of by-products.

The most widely used process, commonly referred to as Siemens process for the name of the company that first developed it, will be described in this paragraph, while other processes, such as, for example, the Union Carbide process, will be briefly presented without going into details at the end of the paragraph. Some details on one of the upgraded metallurgical grade silicon (UMG-Si) refining process for PV silicon production will also be presented.

4.1.2.1 SIEMENS PROCESS

The Siemens process, developed in the late 1950s, is the most widely used process for the production of polysilicon for semiconductor and photovoltaic applications. It is based on the thermal decomposition of trichlorosilane on a heated silicon rod or filament at 1100°C inside a deposition chamber and, as original patents ran out, nowadays accounts for the vast majority of the current polysilicon production. A schematic overview of the Siemens process for refining silicon metal is shown in Figure 4.3 [10].

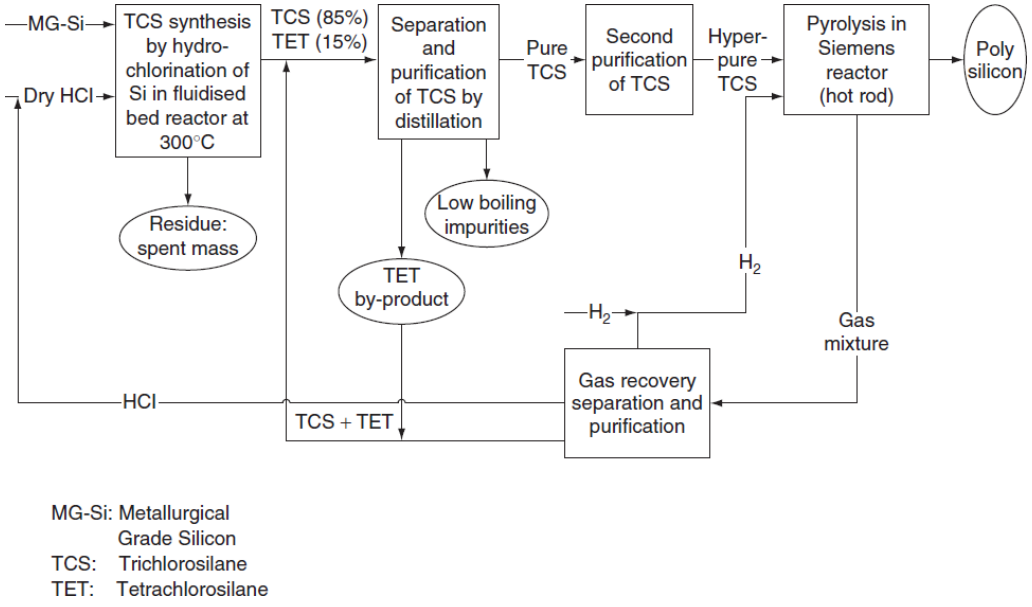

Figure 4.3 – Schematic description of the Siemens process [10].

The production of trichlorosilane from silicon metal is conducted in a fluidized bed reactor at 300-350°C without a catalyst, following the reaction:

$$Si_{(s)} + 3HCl = HSiCl_3 + H_2$$

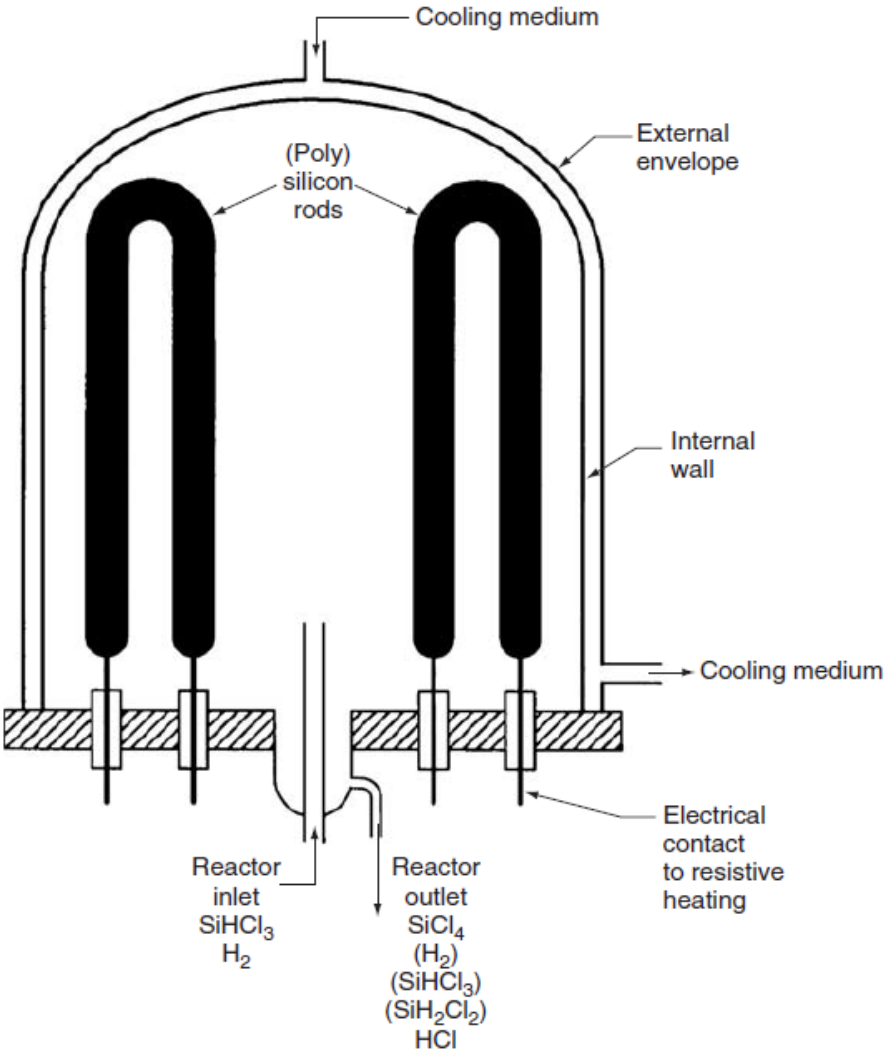

Figure 4.4 – Schematic representation of a Siemens reactor [10]

While the following competing reaction produce unsuitable tetrachlorosilane in molar proportion of 10-20%:

$$Si_{(s)} + 4HCl = SiCl_4 + 2H_2$$

High purity trichlorosilane is then vaporized, then diluted with high purity hydrogen, and introduced in the deposition reactor made of a steel bell jar and decomposed on the surface of high purity U-shaped silicon rods electrically heated at 1100°C. The schematic representation of a Siemens reactor is shown in Figure 4.4, whereas the reactions that allow the production of large hyper-pure silicon rods are the following:

$$2SiHCl_3 = SiH_2Cl_2 + SiCl_4$$

$$SiH_2Cl_2 = Si + 2HCl$$

$$H_2 + HSiCl_3 = Si + 3HCl$$

$$HCl + HSiCl_3 = SiCl_4 + H_2$$

The process is very energy intensive and the steel bell jar has to be cooled to avoid the deposition of elemental silicon on its surface. The adoption of steel bell jar in substitution of quartz bell jar, though, in spite of a slight increase of the system complexity, allows the realization of deposition chambers able to accommodate more than 30 rods, instead of a single rod for quartz bell jars, increasing drastically the process throughput and reducing the energy consumption.

The Siemens process is also affected by the production of by-products that are not used by the PV industry. The most critical by-product is tetrachlorosilane $SiCl_4$ that binds vast amounts of valuable silicon and chloride. Tetrachlorosilane is used in industrial applications for producing fumed silica. The fumed silica market growing rate, though, is much lower than the PV market growing rate, making it necessary to recycle $SiCl_4$ on site, realizing a closed loop for silicon and chloride for photovoltaic applications.

The hyper-pure silicon rods produced using the Siemens process are then crushed into chunks that can be directly used in furnaces for the production of mono-crystalline ingots and wafers for either photovoltaic and electronic applications, or multi-crystalline silicon ingots and wafers for PV.

4.1.2.2 OTHER REFINING PROCESSES

The Siemens process, as described in 4.1.2.1, is the most diffused industrial process for the treatment of metallic silicon for the production of electronic grade or solar grade polysilicon. The Siemens process, though, is affected by some technological disadvantages that can be described as:

- high energy consumption with the most energy needed for cooling the reactor's walls,
- necessity of two power supplies for the pre-heating (up to 400°C) and heating (at 1100°C) of the seed rods,
- possible contaminations due to graphite electric contacts,
- problems with process continuity following power failure,
- possible filament burn out due to hot spots,
- possible non uniform deposition,

- fine gas flow and power control needed,
- batch process,
- production of large amounts of by-products.

Many alternative processes have been developed trying to overcome the technological weaknesses of the Siemens process. None of these processes, though, had been able to gain a big share of the silicon feedstock market for PV or semiconductor applications.

The Union Carbide process, for example, is based on the pyrolysis of monosilane (SiH_4) on heated silicon seed rods inside a metal jar reactor. The reaction followed by the process for obtaining elemental silicon for the semiconductor industry is the following and the schematic description of the process is represented in Figure 4.5:

$$SiH_4 = 2H_2 + Si$$

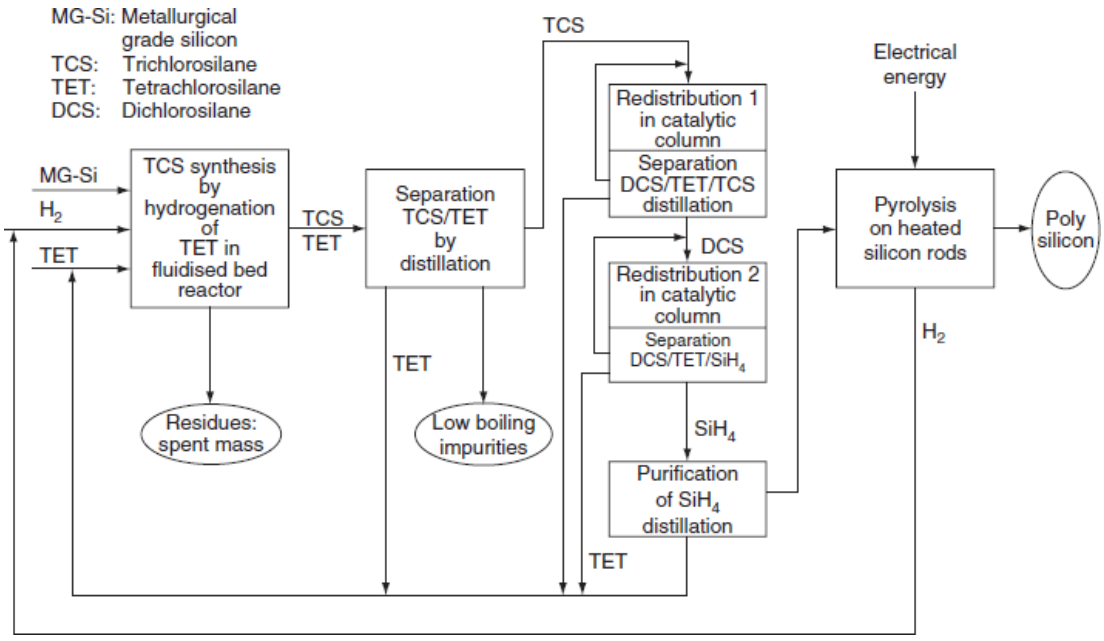

Figure 4.5 – Schematic description of the Union Carbide industrial process [10]

The process, developed since 1976, was firstly funded by the US government for the development of an inexpensive route to solar silicon and was based on silane and on the production of polysilicon with fluidized bed reactor. Following the withdraw of the US government from the project, the company decided to develop the process using pyrolysis of monosilane instead of fluidized bed reactor.

Whereas this process allows to obtain large diameter cylindrical, uniform, void free silicon rods that are suitable for the application in the Float Zone technique, the process steps required for the production of monosilane, together with a photovoltaic market rapidly changing following the big growth of multi-crystalline silicon technology, made this technology less suitable than the Siemens process for photovoltaic applications.

Another industrial process, developed at the same time of the Union Carbide process and within the same political support framework aimed at the development of PV during the oil crisis, is the Ethyl Corporation process. This process, developed firstly for the PV industry, but which ended with an application for the semiconductor industry is based, like the Union Carbide process, on the production of elemental silicon form monosilane. The production of monosilane, though, doesn't start from metallurgical grade silicon, but from alkaline fluorosilicate (M2SiF6, M being an alkaline element, usually Na or Li), a by-product of the fertilizing industry; the production of polysilicon is also done in a different way in comparison to the Union Carbide process, since it is based on the pyrolysis on a fluidized bed reactor, making it possible to make continuous production and to drastically reduce the energy needs due to the cooling of the bell jar walls in the Siemens and Union Carbide reactors.

The process is governed by the following reactions:

$$2H_2 + M + Al = AlMH_4$$

$$SiF_4 + AlMH_4 = SiH_4 + AlMF_4$$

Silicon tetrafluoride SiF4 is sublimated by heating the fluorosilicates; it is then hydrogenated to monosilane by metal hydrides such as lithium aluminum hydride or sodium aluminum hydride; the by-product AlMF4 is believed to find application in the aluminum industry, making it a valuable saleable product.

The products of the Ethyl Corporation process are small silicon grains that could be directly used by the semiconductor or solar industry without any further treatment. Granulate high specific surface, though, increase the ease of contamination for the silicon feedstock, making them not well accepted by the semiconductor industry and neither by the solar industry.

4.1.2.3 SOLAR GRADE SILICON OBTAINED WITH METALLURGICAL ROUTE

Following the growth of the PV industry in the mid-2000s, the increased interest in finding alternative routes for the production of polysilicon feedstock

made some companies invest in innovative refining processes for metallurgical silicon for photovoltaic applications.

Whereas the processes described in 4.1.2.1 and 4.1.2.2 are based on the use of gaseous raw material, silane or chlorosilane, for the production of electronic grade or solar grade silicon, a metallurgical route for refining 99% pure metallic silicon into solar grade silicon had shown to be possible.

The refining steps of the metallurgical refining process, typical of the metallurgical industry, are described schematically in Figure 4.6.

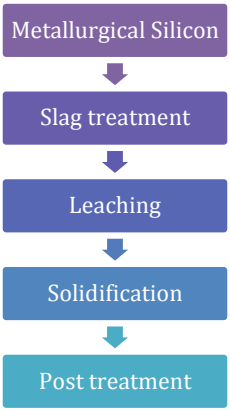

Figure 4.6 – Principal industrial steps for producing solar grade polysilicon through metallurgical treatment

In particular the refining steps are: slag treatment of metallurgical grade silicon, followed by wet chemical leaching, directional solidification of the treated silicon and ingoting for making bricks of the chosen dimensions.

The directional solidification step is important because it allows to segregate the impurities included in metallurgical grade silicon on the top part of the ingot, making it possible to obtain sufficiently pure silicon ingots for photovoltaic applications after removing the top part of the casted ingot. The removed material is then treated, recycled and used with newly produced metallurgical grade silicon for making new SoG-Si ingots.

It's worth noting that the final product is in form of bricks and is not crushed for the non-uniformity due to segregation of impurities on different parts of the bricks. The bricks needs to be used completely for guarantee the product characteristics.

The advantages of the metallurgical route for obtaining SoG-Si in comparison to traditional Siemens or chemical processes are the synergies between the metallurgical silicon production process and solar grade upgrade process,

allowing economies of scale and reducing the numbers and complexity of the refining steps needed for the production of process gasses. The energy needs for metallurgical purification of silicon metal are much lower than the ones related to the Siemens or tetrachlorosilane based processes [20], limiting therefore the carbon footprint of PV cells and modules produced using upgraded metallurgical grade (UMG) silicon. Silicon produced via metallurgical route had shown its suitability for the production of good quality multi-crystalline and mono-crystalline solar cells [21], [22], [23]; the reduction of the polysilicon cost, as low as at $20/kg, related to the current feedstock oversupply and industrial overcapacity [24], though, could drastically limit the competitiveness of UMG-Si in the photovoltaic market.

4.2 CRYSTALLIZATION AND INGOTING

Polysilicon feedstock produced from metal silicon either using the traditional Siemens process, other silane-based processes or metallurgical refining method cannot be used directly for the production of solar cells for its non-crystalline structure.

Good semiconductor and photoelectric properties, in fact, are related not only to the quality of the silicon feedstock, but also to the crystalline structure of silicon used for solar cells; it is therefore necessary to produce silicon ingots not only with silicon chunks that are not suitable for the production of solar wafers, but also for upgraded metallurgical grade silicon bricks that lack the crystal structure needed for the production of high efficiency solar cells.

Silicon ingots are produced using different techniques in correlation to the crystalline structure needed for the final solar cells. In fact, mono-crystalline or multi-crystalline silicon solar cells can be produced using the same feedstock: solar grade polysilicon.

The most diffused technologies for manufacturing crystalline silicon ingots are Czochralski (CZ) and Floating Zone (FZ) techniques for mono-crystalline silicon ingots and the Directional Solidification (DS) casting process for obtaining multi-crystalline ingots for photovoltaic applications.

4.2.1 CZ FOR MONO-CRYSTALLINE SILICON

Mono-crystalline silicon ingots for photovoltaic applications have historically been produced using equipment developed and design for the realization of semiconductor substrates for the integrated circuits electronic industry.

The Czochralski growing technique is the most diffused technology for the crystallization of silicon ingots for the production of mono-crystalline wafers and CZ pullers are widely produced using a well-established, mature and cost effective technology.

Growing mono-crystalline silicon ingots is possible using CZ pullers similar to the one represented in Figure 4.7. The pullers, working in inert atmosphere (usually Argon) for preventing contamination of the molten silicon, are constituted by a cylindrical quartz crucible filled by the feedstock. The system allows using different types of feedstock with different characteristic and geometry, making it possible to customize the material blend for controlling the mono-crystalline silicon physical characteristics.

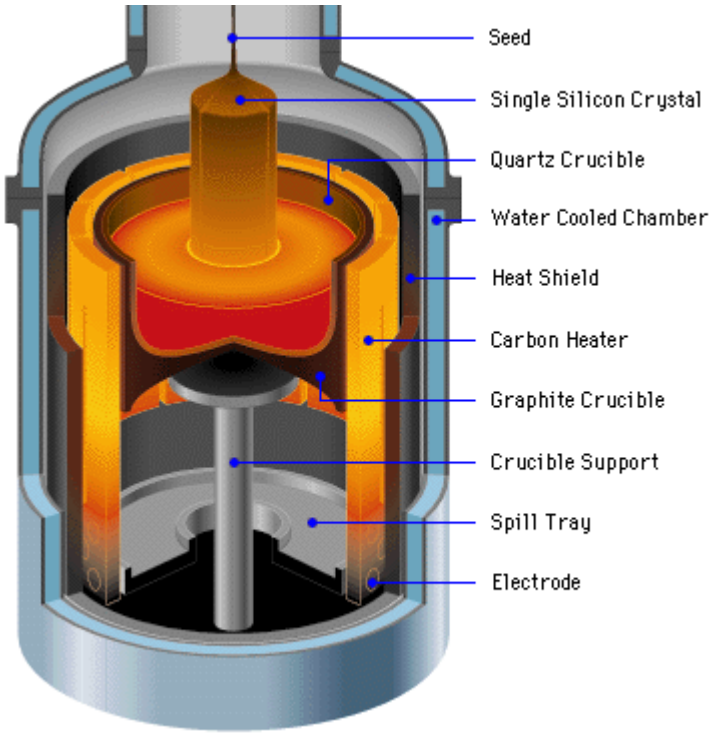

Figure 4.7 – Schematic drawing of a Czochralski puller (source: R. Victor Jones, Harvard)

The hot zone of the system is usually heated through resistive heating using a set of graphite heaters; the temperature reached inside the hot zone is the melting temperature of silicon: 1410°C.

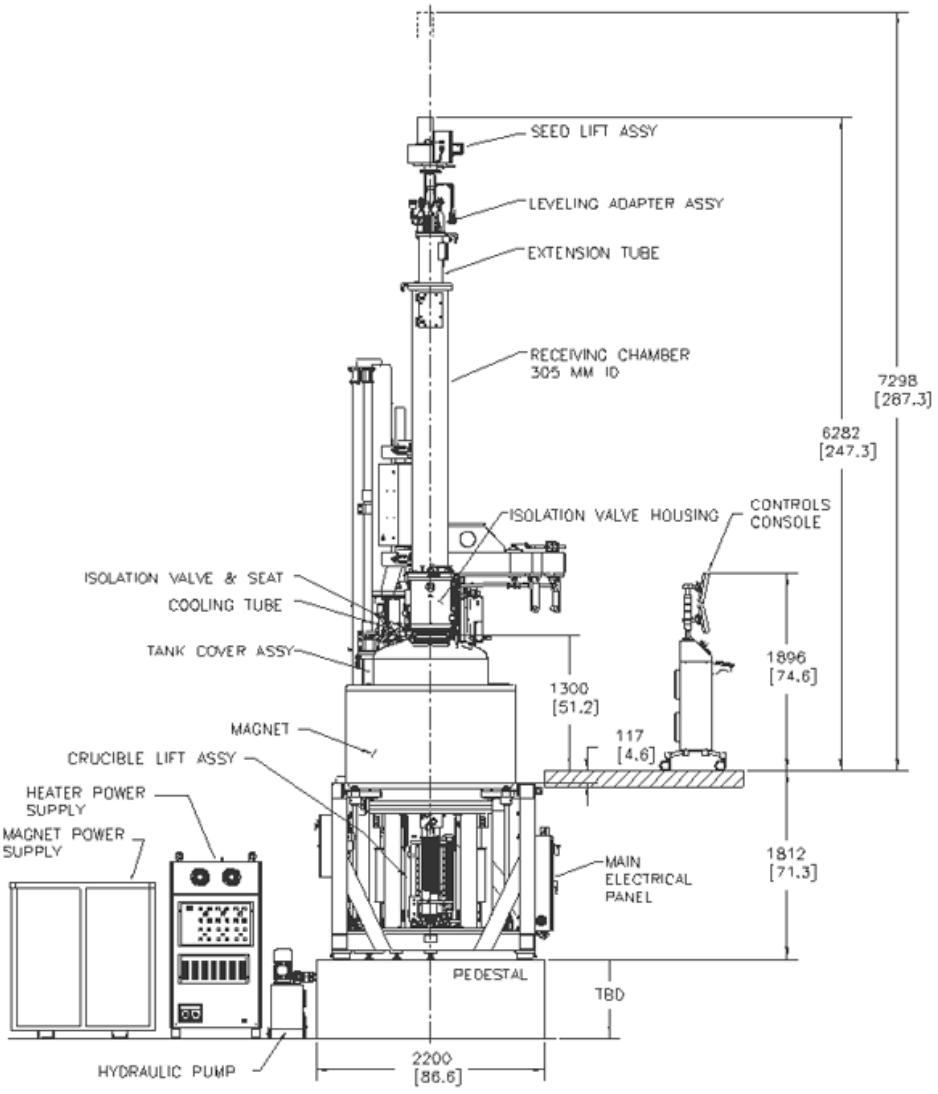

Figure 4.8 – Typical dimensions of a commercial CZ puller from a technical data-sheet (source: Kayex)

The crystallization process starts from a mono-crystalline seed that is immersed in the silicon melt from the top and is slowly pulled and rotated, making it possible to obtain a mono-crystalline dislocation free crystal. The crucible also rotates and is slowly pulled down during the solidification process. The system allows to grow <100> oriented crystals, making it possible to easily texture the surface of the so obtained solar cells.

Nowadays CZ pullers with the possibility to feed the system with feedstock during the melting process and with electro-magnetic systems for controlling the fluid flows inside the melt (EM stirring) are available in the market for making silicon ingots of 10" and up to 180 kg in weight. The hot zone dimensions, the main process parameters and the typical dimensions of a 10",

180 kg CZ puller, taken from a commercial data-sheet are shown in Table 4.1 and Figure 4.8.

Table 4.1 – Typical characteristic of a 10" CZ puller with magnetic stirring[1]

Production specifications	
Furnace chamber diameter	1040 mm
Pull chamber height	2800 mm
Pull chamber extension tube height	1000 mm
Throat diameter	305 mm
Seed lift rate	0-508 mm/h
Seed jog speed (nominal)	400 mm/min
Total crucible travel	500 mm
Crucible lift rate	0-127 mm/h
Crucible jog speed (nominal)	127 mm/min
Seed rotation (reversible)	0-30 rpm
Crucible rotation (reversible)	0-30 rpm
Silicon charge capacity	
Crucible dimensions	*Charge*
22 in × 430 mm	150 kg
24 in × 430 mm	180 kg
Process parameters	
Argon consumption	75 – 175 slpm
Electric power	260 kVA

4.2.2 FZ FOR MONO-CRYSTALLINE SILICON

Mono-crystalline silicon ingots for electronic and photovoltaic applications can be manufactured also with different technologies in comparison to the traditional CZ technique; the float-zone method is an interesting application of an electrothermal induction heating process for high quality mono-crystalline dislocation free ingots growth.

The float zone method uses a single coil medium frequency inductor for melting a layer of a silicon feedstock rod; molten silicon then solidificate as a large mono-crystalline crystal on top of a rotating seed [25], as shown in Figure 4.9.

The process, requiring no crucibles and no holding systems for the feedstock that hangs up freely above the inductor, reduces drastically the oxygen contamination of the ingot, allowing to obtain high quality mono-crystalline

[1] Kayex KX170-MCZ

silicon ingots that are used for producing the highest efficiency PV modules available in the market.

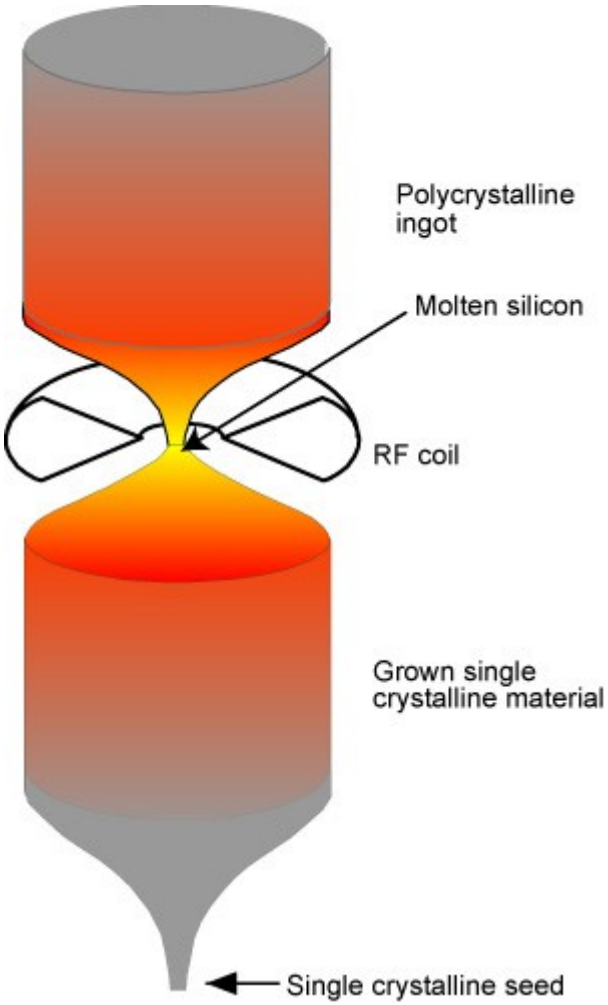

Figure 4.9 – Schematic representation of the float zone technique for growing mono-crystalline silicon ingots

The necessity to use silicon rods as feedstock instead of polysilicon chunks, together with the low throughput of the process in comparison to CZ, and the high manufacturing cost for FZ mono-crystalline silicon ingots, make the FZ technique a niche application for very high efficiency mono-crystalline solar modules that are well suited for the application in installations with reduced available surface.

4.2.3 DS CASTING FOR MULTI-CRYSTALLINE SILICON

Multi-crystalline silicon solar cells had gained a relevant share in the PV market for their low cost in comparison with mono-crystalline solar cells and an

efficiency that has increased over time thanks to process improvements. Nowadays multi-crystalline silicon solar cells compete with mono-crystalline for the leadership in the PV market.

While multi-crystalline silicon is characterized by a lower efficiency in comparison to mono-crystalline silicon, due to grain boundaries and dislocations that reduce the minority carriers lifetime, the reduced manufacturing cost and energy requirements of multi-Si in comparison with CZ growth, make this technology very interesting.

Multi-crystalline silicon ingots are nowadays mainly produced in directional solidification (DS) furnaces in which polysilicon chunks or bricks are melted and directionally solidificate starting from the bottom of the quartz crucible. The crystal orientation guarantees ideal performance for solar wafers and make it easier to texture their surface for enhancing the photoelectric performance. In Figure 4.10 a picture of a 350 kg silicon charge in a quartz crucible for directional solidification casting is shown.

Figure 4.10 – 350 kg polysilicon charge in a quartz crucible used in an induction heating directional solidification furnace

While the directional solidification process and the equipment used for growing bulk multi-crystalline silicon ingots will be described in details in 5.1, it's worth highlighting in this paragraph that directional solidification for growing multi-crystalline silicon ingots allow the use of square crucibles, reducing therefore the material waste due to squaring and wafering. Nowadays

furnaces able to handle up to 800 kg of silicon have been developed; these furnaces, known as G6[2], can produce 36 multi-crystalline standard size silicon bricks for every solidification process, reducing drastically the manufacturing cost and total process time per kg of silicon produced.

4.3 SQUARING AND WAFERING

Mono-crystalline silicon ingots produced either using the Czochralski or Float Zone methods are characterized by a circular cross section. Whereas this shape is necessary for growing dislocation free mono-crystals, the use of circular wafers in solar modules would lead to an overall reduction of the modules' efficiency due to the gap between each circular shape wafer. Although some researches have been conducted for growing square shaped mono-crystalline ingots using modified CZ pullers with travelling magnetic fields [26], and few producers experimented the cutting of ingots of hexagonal shape, mono-crystalline silicon ingots are cut into quasi-cross section ingots before the wafering process. The quasi cross-section shape, characteristic of mono-crystalline wafers, allows to reduce the gap between adjacent cells, while keeping the silicon loss as low as possible.

Multi-crystalline silicon ingots, on the other hand, need to undergo the squaring process for removing the head, tail and side of the ingots that are characterized by less pure material, and subsequently multi-crystalline silicon bricks are cut from the ingots.

Usually 156×156 mm square section bricks are cut from 10" mono-crystalline ingots and from multi-crystalline casted blocks using wire saws. The schematic representation of the squaring process for mono-crystalline and multi-crystalline silicon ingots is shown in Figure 4.11.

Following the squaring process, the bricks are cut into thin wafers (as thin as 150 μm) that will then be processed for obtaining the solar cells. The wafering process is done using two multi-wire sawing techniques: slurry sawing and diamond sawing.

Both the wafer sawing techniques are based on multi-wire sawing equipment that is schematically shown in Figure 4.12 [27]. A stainless steel or diamond wire, with a length ranging from 250 to 500 km and a thickness around 150 μm

[2] The multi-crystalline silicon industry decided to standardize the dimensions of the ingots as following: G1=1 brick; G2=2x2=4 bricks; …; G6=6x6=36 bricks.

is disposed across four drum as to form a wire web. The silicon ingot is glued to a supporting frame and pushed against the moving wire that cut it into thin wafers thanks to the abrasive effect of a SiC slurry or of the diamond wire. The dimension tolerances for the main parts of the equipment needs to be strictly controlled to guarantee the constant thickness of the as cut wafers. For example the distance of each wire from the adjacent ones is not constant along the drum length for considering the wire wear effect.

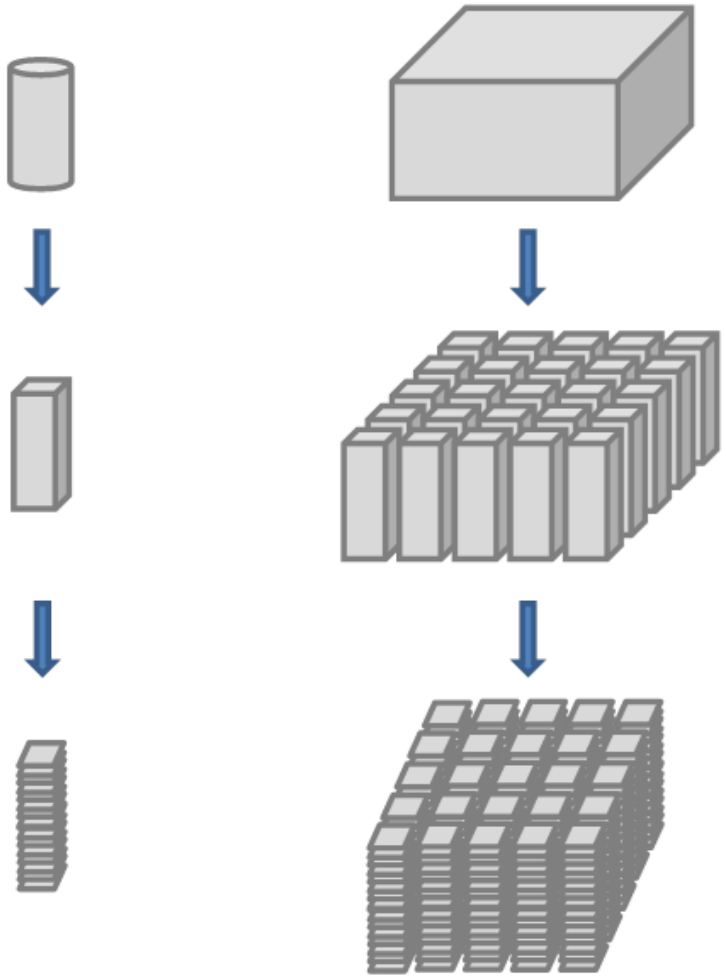

Figure 4.11 – Schematic representation of the squaring and wafering process for mono-crystalline and multi-crystalline silicon

While the stainless SiC slurry steel wire cutting process has been used for years for cutting silicon wafers for both the semiconductor and photovoltaic industry for its relatively low cost, the development of dry cutting processes

gained interest in the last years and new multi-wire sawing processes based on diamond wafer have been developed.

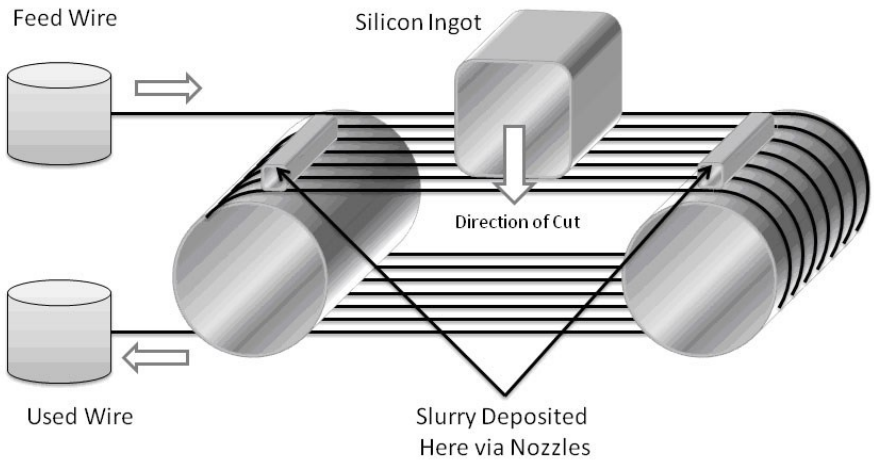

Figure 4.12 – Slurry based wire sawing technique schematic (source: CRS Reprocessing)

While the use of diamond wires increase the cutting cost, this technology allows to obtain higher surface quality wafers and reduce the amount of superficial imperfections and micro-cracks due to the abrasive effect of SiC particles of different dimensions. The use of diamond wires also allows to easily recovery and recycle the silicon kerf losses related to the sawing processes, virtually without expensive post-cut treatments; the possibility to re-melt and solidificate the kerf losses could lead to the production of relatively big amounts of feedstock materials at competitive cost. The SiC slurry, on the other hand, cannot be easily recycled since silicon particles would need to be separated from the slurry and chemically treated for removing all the contaminants dissolved in the slurry.

Following the multi-wire cutting process the silicon wafers are not ready to be used in PV solar modules. In fact they need a series of surface treatments that made it possible to have a photoelectric effect within the semiconductor material. These processes are summarized in Figure 4.13.

The first treatment that an as-cut silicon wafer needs to undergo for its preparation for becoming a solar cell is a surface chemical etching. This chemical process allows to remove the most external layer of the wafer, usually damaged by the sawing process, making it possible to obtain a smooth surface. The surface is then chemically attacked for texturization; a well-defined and oriented texture allows to increase the overall cell efficiency enhancing the optical and electric performance of the cell at microscopic level. The p-n junction is then created through phosphorous diffusion in case of p-type silicon

substrates or boron diffusion in case of less used n-type substrates. The edges of the solar cells need then to be electrically insulated through lased cutting.

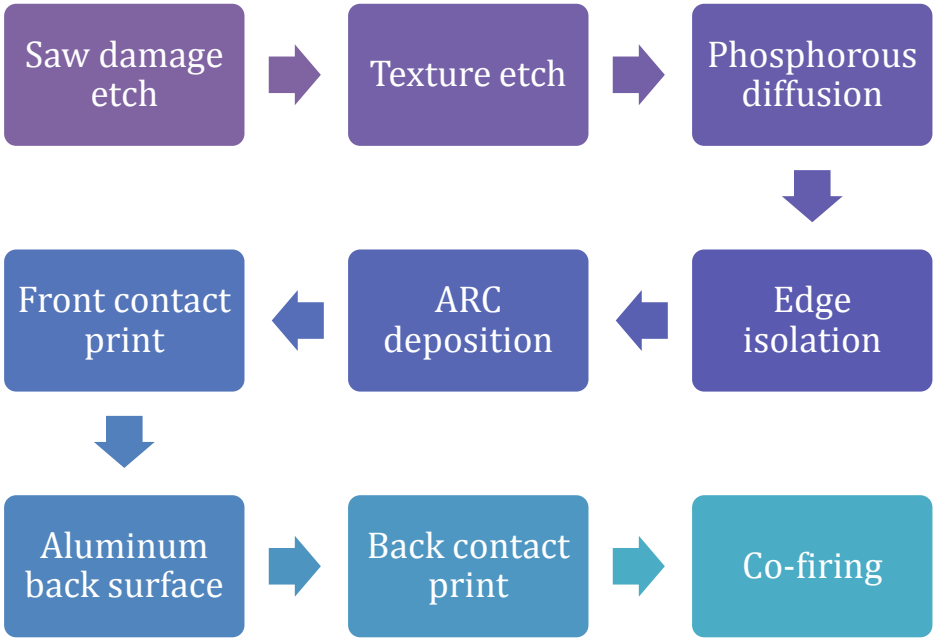

Figure 4.13 – Principal industrial steps for the realization of solar cells from silicon wafers

Following these steps the solar cell is then ready and the photoelectric effect can be achieved. Further treatments, though, are essential for guarantee optimal cell performance and for collecting the electricity generated within the cell.

The first step is the deposition of an anti-reflecting coating; a thin layer that gives the characteristic bluish color to the solar cell is deposited as to reduce drastically the light reflected by the cell surface. Subsequently the silver paste front contact grid is screen-printed and a conductive layer is deposited on the back side of the cells. After the co-firing process that make it possible to have a direct electrical contact between the semiconductor materials and the electrodes, the solar cell is completed and, following a testing and selection process, it can be sent to the final part of the PV modules manufacturing chain: module assembly, which will be described in the following paragraph.

4.4 Modules assembly

Solar cells manufactured following the industrial processes described in the previous paragraphs cannot be used directly in electrical energy production

applications, neither in small stand-alone systems or big multi-megawatt solar farms. In fact solar cells needs to be connected together for increasing the system DC voltage before their connection to a DC/AC converter or a DC electric load with or without energy storage systems. Solar cells need also to be protected from atmospheric elements such as, for example, humidity and dust, which effect could be detrimental on the overall system efficiency.

Solar photovoltaic modules with 60 to 72 solar cells are then assembled and introduced in the market as renewable energy production equipment with a 20 years energy production guarantee; the cross section of a solar module with the main materials and layers used for its assembly is shown in Figure 4.14, whereas the efficiency guarantee requirements are shown in Figure 4.15.

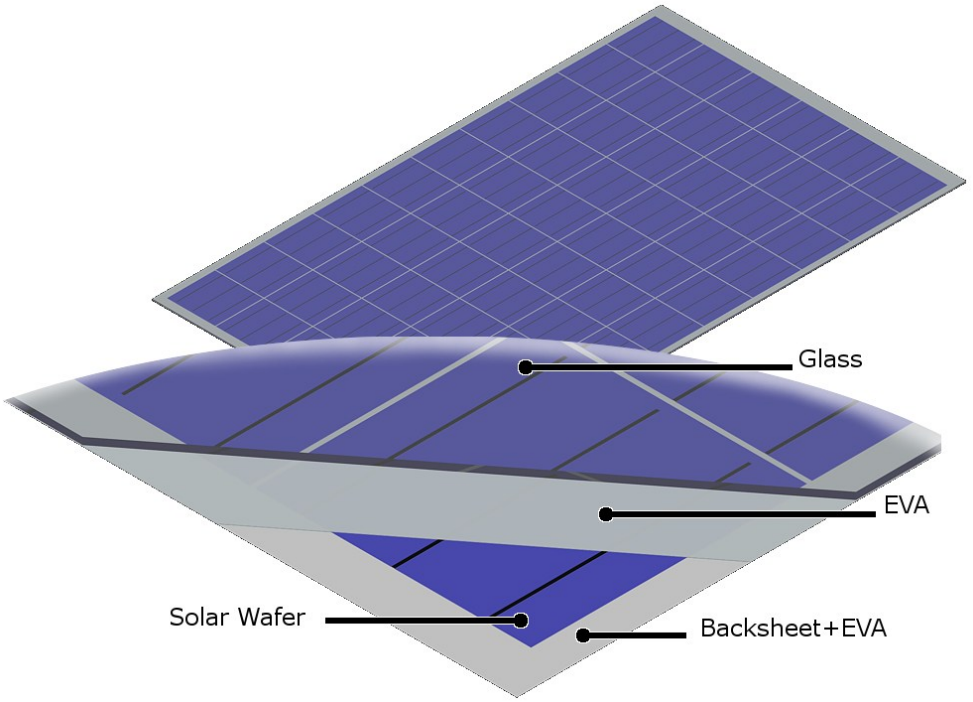

Figure 4.14 – Crystalline silicon PV panel cross section showing the principal materials used for its fabrication

While the final module assembly of a photovoltaic panel could seem an activity of secondary importance, a careless approach to these industrial steps could lead to the manufacturing of low-quality products characterized by a good starting efficiency with fast degradation that don't guarantee the forecasted energy production of the system, making the economic investment non profitable.

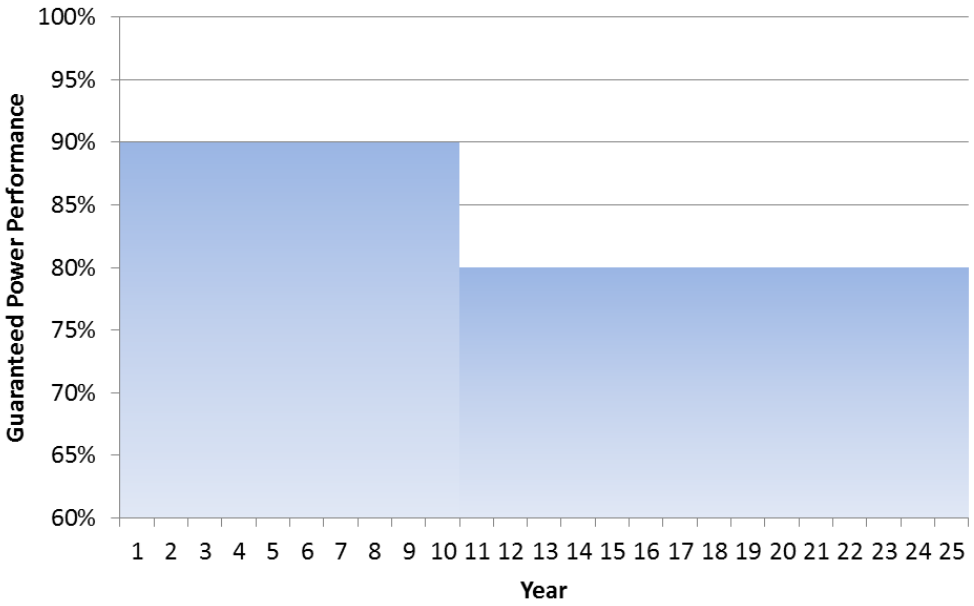

Figure 4.15 – Industry standard warranty for the performance of PV modules

The main activities that are needed for manufacturing a solar panel starting from crystalline silicon solar cells are schematically descripted in Figure 4.16 and they are: electrical connection of the cells, lamination, junction box assembly and testing.

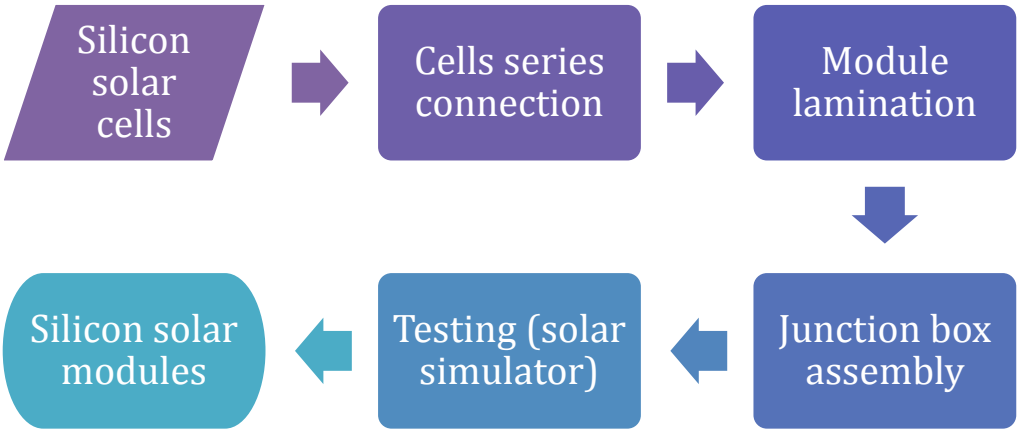

Figure 4.16 – Principal industrial steps for the assembly of silicon solar cells into silicon solar modules

Silicon solar cells are characterized by an open circuit cell voltage of 550-650 mV. This voltage is not sufficient for any electrical appliance or converting system and the electrical connection of solar cells in series is therefore necessary. Solar cells are usually disposed in arrays of 10 to 12 cells connected in series. Copper ribbons are used as electric connections and are soldered on the screen-printed contacts of the solar cells as to connect the front of a solar cell to the back of the adjacent one, making a series connection of the array. The solar cells arrays are then disposed on top of two layers of polymeric materials: a multi-layer backsheet made of PE, PET and/or PVF and a layer of EVA. Another layer of EVA is placed on top of the solar cells, under a 3.2 mm thick textured glass that gives mechanical strength and protection to the system, while guarantees optimal optical performance for the system for decades.

The PV modules after the assembly process undergo a lamination process; they are heated in vacuum at temperature between 135 and 150°C for 15 to 30 min depending on the type of EVA and curing process. During the lamination process the EVA layers melt and cross linking phenomena take place within the EVA polymeric structure. The two layers connects therefore to each other and adhere to the solar cells, glass and backsheet, allowing to remove all the air gap within the systems, acting as a strong encapsulant of the active part of the system. The EVA also acts as a strong adhesive material between each part of the solar module; whereas these characteristics are the biggest hurdles to the development of recycling systems for end-of-life PV modules, as it will be described in chapter 6 , they effectively guarantee the performance of PV modules for decades and this technology will probably be used for years before the possible introduction of encapsulation techniques designed for recycling [28].

After the lamination process a junction box with by-pass diodes is connected for allowing the easy interconnection of PV solar modules in arrays and fields for guarantee the needed voltage and current requested by the conversion system or load. An aluminum frame is then usually mounted for giving the PV modules additional mechanical strength and ease of fixing to the holding systems. Each module is finally tested in a flash sun-light simulator for checking its performance before its introduction in the market and installation in PV plants ranging from small stand-alone applications as, for example, road signs or traffic lights, to small grid connected household installations and up to big multi-megawatt PV power plants with or without solar tracking systems.

5 iDSS FOR CRYSTALLINE SILICON INGOTS CASTING

The competitiveness of solar electricity, in comparison with traditional and renewable energy sources, requires the photovoltaic (PV) industry to follow the requests of cost reduction and efficiency improvement for solar modules.

PV modules are mostly based on mono-crystalline and multi-crystalline solar cells, with the two technologies competing for the biggest market share.

Multi-crystalline silicon ingots for solar wafers are usually produced using directional solidification systems (DSS), which allow to obtain high quality crystalline silicon with high throughput and at low cost. With the aim of further cost reductions and efficiency improvements, crystal growers working with DS systems are nowadays facing the challenge of increasing the maximum ingot mass to benefit from scale economies. Whereas the advantages of increasing the maximum ingot mass are well known, a bigger DS furnace requires a better control of the solidification process.

In the following paragraphs the directional solidification process for casting multi-crystalline silicon ingots will be described and an innovative directional solidification furnace developed and built at the Laboratory of Electroheat at the Department of Industrial Engineering at University of Padova, based on induction heating instead of traditional resistive heating, will be presented. The innovative furnace, called iDSS (induction Directional Solidification System), is believed to be one of the technological breakthrough that could enhance the competitiveness of crystalline silicon PV technology in the global PV market.

5.1 DIRECTIONAL SOLIDIFICATION SYSTEMS FOR CRYSTALLINE SILICON CASTING

Multi-crystalline silicon photovoltaic cells are characterized by a lower efficiency in comparison to mono-crystalline ones. Multi-crystalline technology, though, guarantees some big advantages in comparison to mono-crystalline PV that make it competitive in the PV market. These advantages can be

summarized in lower manufacturing costs, less strict technological requests for the feedstock material and the possibility to grow square section ingots, increasing the overall material yield after the ingoting process.

The efficiency of multi-crystalline solar cells depend on the recombination effects due to the presence of impurities and defects like grain boundaries and dislocations. For obtaining high efficiency multi-crystalline solar cells it is necessary to finely control some process parameters during the crystallization process. It is essential, in fact, to have a complete control of the temperature profile in the melt and the velocity of the solidification process in order to control the amount and activity of the material's defects. Impurities nucleation, multiplication and segregation phenomena needs to be analyzed in details for their high impact on the photo-electrical characteristics of multi-crystalline solar cells; grain boundaries and metal impurities inclusions, in fact, interact with electrons and holes increasing the frequency of recombination effects, drastically reducing the diffusion length and therefore the minority carrier's lifetime. Not only controlling the solidification process is essential for obtaining high efficiency multi-crystalline solar cells, but a dedicate control of the cooling phase is essential for avoiding the increase of the dislocation density within the casted silicon ingots during the cooling process.

It is possible to obtain the reduction of the defects density within the casted material through the control of the planarity of the solid-liquid interface during the solidification process, through the control of the fluid flows within the melt and therefore with the growth of columnar shape crystals, reducing drastically the electric activity along the grain boundaries.

Producing multi-crystalline silicon ingots with the above descripted characteristics is possible using casting technologies that allow to control the crystal growth process and solidification direction. Directional solidification technology is the most used one for the production of multi-crystalline silicon ingots for photovoltaic applications.

The process steps for producing multi-crystalline silicon ingots for photovoltaic applications using a directional solidification furnace are the following and are schematically represented in Figure 5.1 and Figure 5.2:

- Heating,
- Melting,
- Thermal gradient creation in the melt,
- Directional solidification,
- Annealing,

- Controlled cooling,
- Free cooling.

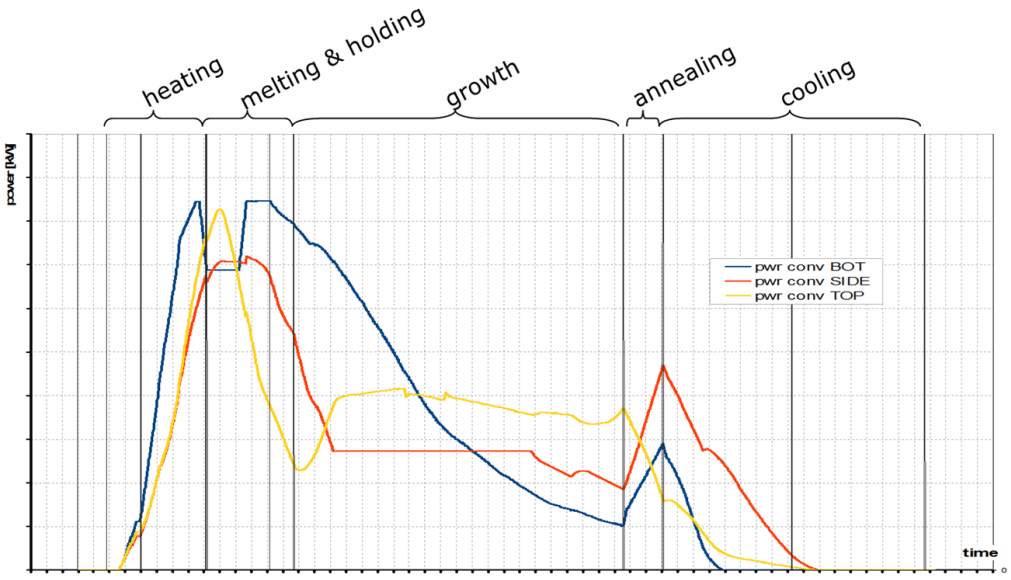

Figure 5.1 – Process power during a multi-crystalline casting process using a 3 heaters induction-heating DS furnace

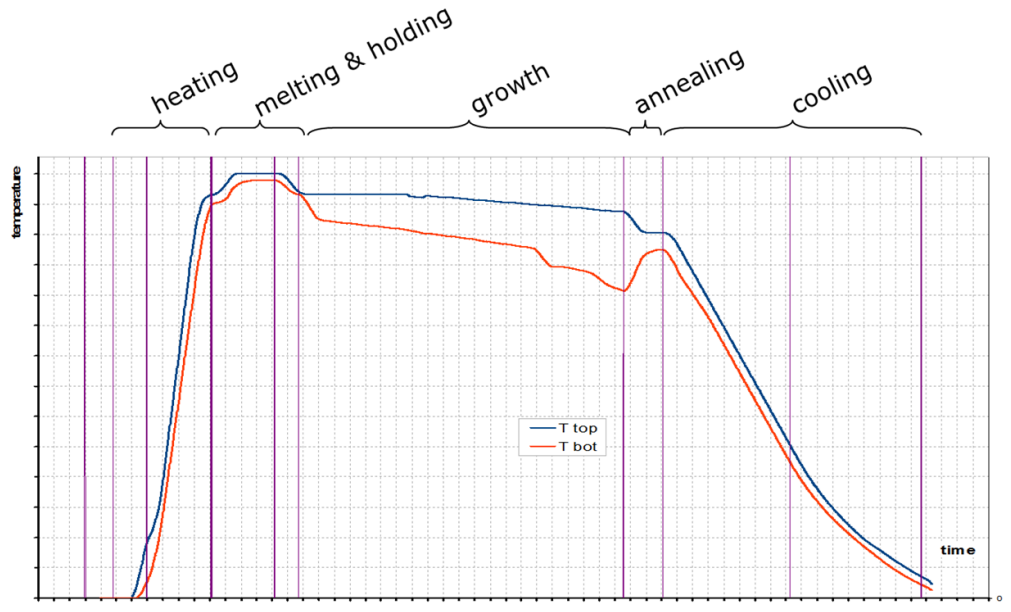

Figure 5.2 – Process temperature during a directional solidification casting process.

The heating phase is obtained through the application of the maximum furnace power for making the feedstock material reach 1410°C, silicon's melting temperature. A fast heating phase allows to drastically reduce the thermal losses associated to this process phase; the heating velocity, though, needs to be

controlled to avoid overheating of parts of the systems with detrimental effects on components' lifetime.

The first phase ends when, after the decreasing of the heating rate, at the reaching of the melting temperature the melting process starts. This process is conducted at constant temperature and all the energy is absorbed by the silicon charge as latent heat. After completing the melting process the temperature is increased; this promotes the fluid flows inside the melt, through the reduction of the material's viscosity, making it possible to have a more homogeneous melt.

After completing the melting of the silicon charge, the most critical phase of the entire process needs to be conducted. Molten silicon solidificate inside a quartz crucible and the solidification process needs to be controlled for allowing the directional crystallization of multi-crystalline silicon.

Directional solidification furnaces allow to impose a thermal gradient on the melt, making it possible to control the start of the solidification process. Multi-crystalline silicon for photovoltaic applications usually solidificate in columnar shaped crystals starting from the bottom of the crucible. The thermal gradient is realized either with a differential power application or with moving parts that allow to control the heat flows inside the furnace during the solidification process. Optimal solidification conditions can be achieved through the application of a vertical thermal gradient ranging from 2 to 5 K/cm. Higher values of the thermal gradient could improve the effectiveness of the solidification process, but could lead to the damage of some furnace components due to thermal stress.

The solidification process, after imposing the thermal gradient, starts from the bottom of the crucible and the crystallization continues following the thermal gradient direction with typical solidification velocity ranging from 1 to 36 cm/h. During the solidification process the solid liquid interface needs to be kept as planar as possible for making it possible to have vertical oriented columnar grains. A slightly convex solid liquid interface, obtained by heating the sidewalls of the crucible, has beneficial effects on the overall quality of the final ingot thanks to the reduction of the possibility of nucleation starting from the side of the quartz crucible.

Once the silicon ingot is fully solidificate, it is necessary to control the cooling process; a thermal annealing step allows the reduction of the internal stresses within the ingot and reduces the possibility of creation of cracks that could be detrimental on the process yield. The adoption of a Si_3N_4 coating on the crucible walls allows to avoid the sticking of the silicon ingot to the quartz crucible,

reducing therefore the possibility to damage the ingot due to tensile stresses of the crucible during the cooling process. After the annealing and controlled cooling phases, a non-controlled cooling phase in atmosphere is conducted until the ingot temperature reach room temperature.

5.2 iDSS – INDUCTION HEATING DIRECTIONAL SOLIDIFICATION SYSTEM

Whereas directional solidification furnaces are based on a well-established technology, innovations are still possible for improving the production yield, product quality and for reducing the production cost in a market where even high quality products needs to follow a roadmap for cost reduction.

A better control of the multi-crystalline silicon ingots casting process can be achieved using an innovative DS furnace based on an induction heating system (iDSS: induction Directional Solidification System). The furnace has been designed at Padova University and it is characterized by three independent induction heating systems; a top inductor for controlling the thermal gradient, a bottom inductor that operate both as an heating system during the melting process and as a heat exchange cooling system during the solidification process, and a multi coil lateral inductor with independent turns connection that allows the control of the solidification front shape and the reduction of the insulation board thickness, acting therefore like an “active insulation” system; the lateral inductor can also be used for developing travelling magnetic fields application and electromagnetic stirring within the melt. This design, in comparison with traditional resistance heated DSS, allows a better control on important process parameter during the melting and solidification process and reduce the operation cost related to the consumption of graphite resistors.

Whereas these characteristics make the iDSS suitable for its installation as the heating system for big DS systems for producing high-efficiency, low-cost multi-crystalline silicon ingots, the possibility to control the solid liquid interface shape, during both the melting and solidification steps, make it possible to use it also for casting high-efficiency quasi-single crystalline silicon ingots.

The study of the casting process for multi-crystalline silicon ingots has been conducted at the Department of Industrial Engineering at Padova University with multi-physics thermo-magnetic numerical simulations. A lab-scale iDSS furnace has been built in the Laboratory of Electroheat within the research project “Polo di Ricerca nel Settore del Fotovoltaico”. The furnace will allow to

process up to 120 kg of silicon for conducting experimental tests focused on the improvement of casting processes, ranging from multi crystalline silicon ingot growth, to quasi-single crystalline silicon ingots casting.

5.2.1 INDUCTION HEATING

Before describing the main features of the iDSS furnace and the innovative solutions that make it a technological breakthrough in the multi-crystalline silicon ingot production market, in this paragraph the description of the phenomena on which the induction heating process is based is conducted.

Induction heating is a method of heating electrically conductive materials through the application of a time varying magnetic field whose lines of force enter the conductive mass of the materials. In this process, the time varying magnetic field induces an electric potential (voltage) within the conductive mass, which lead to the creation of an electric current depending on the shape and the electrical characteristics of the material. These currents are called eddy-currents and the heat generated within the conductive material is due to Joule effect.

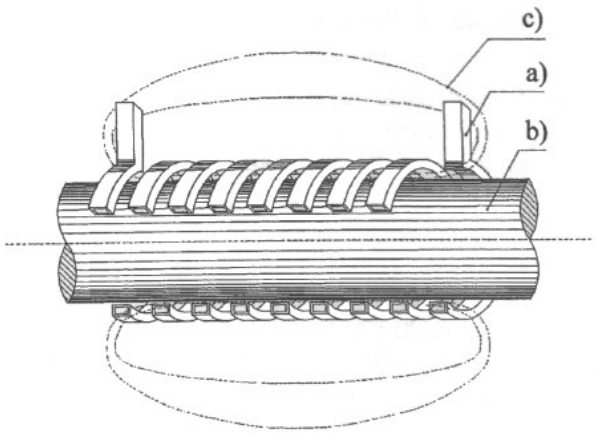

Figure 5.3 – Magnetic field in a solenoid coil used for induction heating of a metal rod. (a) Inductor, (b) Load, (c) Magnetic field isolines [29]

The basic components of an induction heating system are an induction coil, an alternating-current (AC) power supply, and the conductive load. The coil, which can be designed in different shapes depending on the required heating pattern, is connected to the power supply for allowing the generation of a magnetic field due to the current flow (see Figure 5.3). The magnitude of the

magnetic field depends upon the amplitude of the current and the number of turns in the coil. If an electrically conductive object is placed inside the magnetic field generated by the coil connected to the AC power supply, eddy currents are generated within the conductor material following the Faraday's law of electromagnetic induction:

$$e = -N\frac{\partial \phi}{\partial t}$$

The induced voltage e [V] is then dependent on the number of turns N and the time variation of the magnetic flux ϕ [A/m^2].

The induced currents also generate their own magnetic fields, which are in opposition to the field generated by the coil, preventing therefore the field from penetrating to the center of the object; the eddy currents are then more concentrated at the surface and decrease in strength toward the center of the object. This phenomenon is called skin effect.

The mathematic equations needed to explain the skin effect involve a differential equation that has solutions in the form of Bessel functions. These solutions demonstrate that the induced current in a large planar object in which its thickness is much higher than the expected eddy current penetration decreases exponentially from the surface into the electrical load. This allows the definition of the so-called “penetration depth”, which represent the distance from the piece surface at which the induced current drops by 1/e (or 37%) of the surface value.

The penetration depth δ [m] can be evaluated as:

$$\delta = \sqrt{\frac{2\rho}{\omega\mu\mu_0}} = \sqrt{\frac{\rho}{\pi\mu\mu_0 f}}$$

in which ρ is the resistivity of the conductive material [Ω/m], $\mu_0=4\pi\cdot10^{-7}$ H/m is the vacuum magnetic permeability, μ is the relative magnetic permeability of the load, ω is the pulsation [rad/s], and f is the frequency [Hz] of the alternating magnetic field generated by the coil.

Heat is generated within the conductive load for Joule effect caused by the eddy currents interacting with the resistivity of the material, and depends on the square of the eddy current value. The non-uniform distribution of the eddy current within the conductive material, complex inductor and load geometries and possible non-linearity for materials’ properties are the main reasons that

pushes the development and use of numerical models for the design and fine tuning of induction heating systems.

5.2.2 LAB-SCALE IDSS AT PADOVA UNIVERSITY

A lab scale iDSS furnace had been designed and developed at the Laboratory of Electroheat (LEP) at the Department of Industrial Engineering at Padova University in the framework of the "Polo di ricerca nel settore del fotovoltaico[3]" project. The furnace is a lab-scale version of the 450 kg G5 induction heating directional solidification furnace developed by an Italian company in collaboration with the Laboratory of Electroheat at Padova University [30].

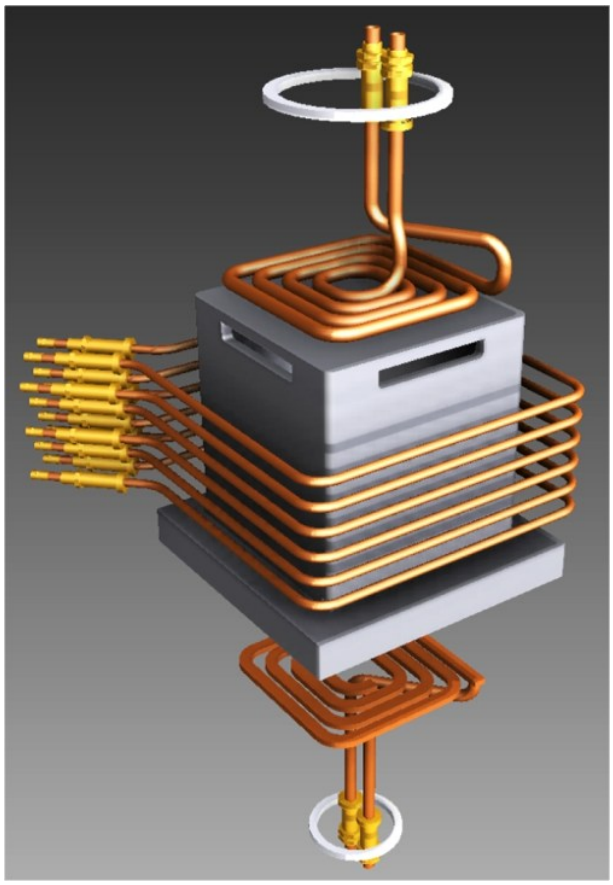

Figure 5.4 – 3D model of the induction heating system and hot zone of the iDSS furnace

The hot zone of the iDSS furnace had been designed to contain a (440 × 440 × 420) mm quartz crucible. These dimensions, bigger than common lab scale furnaces, allow to process up to 120 kg of silicon, making it possible to

[3] Progetto Regione Veneto, SMURP n. 4148, "Polo di ricerca nel settore del fotovoltaico", POR CRO parte FESR 2007 – 2013 Azione 1.1.1 a regia regionale, DGR 2286 del 28/09/2010.

conduct experimental tests which results could be easily scalable to full-size industrial systems.

The heating system is made of a graphite susceptor box that surrounds the crucible and is directly heated through induction heating. The use of induction heating allows to reduce the thermal losses of the system, thanks to the possibility to interpose a thermal insulator board between the susceptor and the inductors; it also allows to control the power distribution in the susceptor, and therefore close to the crucible, by dimming the power of each inductor.

5.2.2.1 INDUCTORS SYSTEM

The iDSS inductors system is composed by three separate inductors: one bottom, one lateral and one upper inductor (see Figure 5.4).

Each inductor is connected to a 6 kHz, 50 kW power generator. Tuning the power of each inductor during the process allow a complete control of the heat flow in the hot zone without the need of any moving parts inside the vacuum chamber.

The main features of each inductor are the following:

BOTTOM INDUCTOR

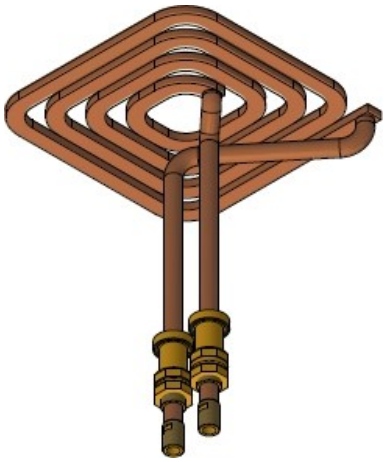

Figure 5.5 – 3D model of the bottom inductor of the iDSS furnace

The bottom inductor is a “pancake” water cooled inductor with rectangular cross-section (see Figure 5.5). It is used as an active inductor during the melting process for multi-crystalline silicon casting and, after switching off its power, as a cooler during the solidification process. This allows removing heat from the bottom of the melt, setting the thermal gradient necessary for columnar crystal growth and directional solidification. The rectangular cross section had been

chosen for maximizing the inductor surface, increasing therefore the irradiative thermal exchange phenomena.

UPPER INDUCTOR

The upper inductor had been designed with the same shape of the bottom inductor, but with circular cross section since it is arranged over an insulating board that reduces the thermal irradiation phenomena (see Figure 5.6). It is used for heat transfer to the top susceptor during both the melting and solidification process.

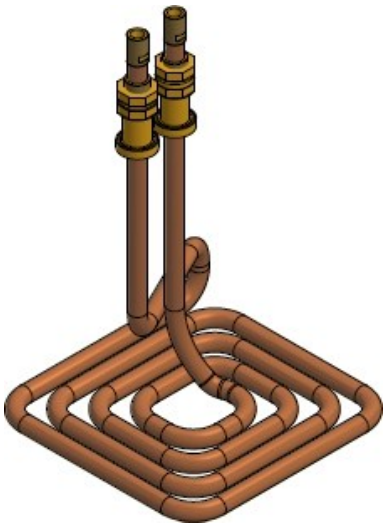

Figure 5.6 – 3D model of the bottom inductor of the iDSS furnace

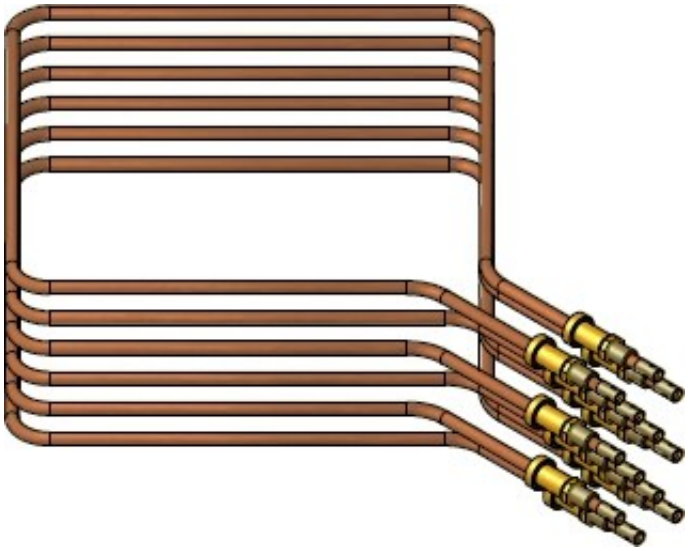

Figure 5.7 – 3D model of the lateral inductor of the iDSS furnace

LATERAL INDUCTOR

The lateral inductor is a multi-coil system with six separate coils (see Figure 5.7). It contributes to the heat transfer during the melting process, whereas it can also be used for better controlling the solid-liquid interface and directional crystal growth during the solidification process. The power supply system for the lateral inductor can be easily upgraded with a device that will allow to switch off each coil during the solidification process. The lateral inductor system will allow to better control the heat transfer, realizing an active insulation system. The coils could also be used for generating an electro-magnetic stirring effect in the melt for conducting experimental tests on the impact of this improvement on multi-crystalline silicon casting.

Figure 5.8 – Graphite susceptors in use in the 120 kg iDSS furnace built at University of Padova

5.2.2.2 ELECTRO-MAGNETIC SIMULATIONS AND DIMENSIONING

The iDSS furnace built at University of Padova is a complex lab-scale system with all the main features of an industrial scale furnace. Its design is then not only a scale-reduction of the full-scale system, but it requires the development of a dedicate project since the scale factors for each components are different and the operation in an university laboratory environment requires the design and development of dedicate electric and hydraulic systems that are usually

available on an industrial production site, but not on an university research laboratory.

The design of the system required, among other parallel activities, the design of the vacuum chamber, of the vacuum and argon flow control systems, the design of the hot zone (see Figure 5.8) and of the induction heating and power supply system, as well as the dimensioning of the insulator boards and of the water cooling system and hydraulic circuits. The result is a lab-scale system which, in spite of a capacity being one quarter of the full-scale one, covers an overall area of more than 30 m^2. A comparison of the overall dimensions of the full-scale system and of the lab-scale system built at Padova University can be done looking at Figure 5.9 representing the full-scale G5 furnace and Figure 5.10, representing the 3D rendering of the lab-scale one.

Figure 5.9 – 450 kg iDSS furnace

Whereas the dimensioning of the vacuum chamber and gas control system, of the power supply system and of the water cooling circuit and automation system had been conducted by specialized third parties following the technical requests and working in strict collaboration with the researchers working at the Laboratory of Electroheat, the hot zone and induction heating system design, as well as the process development, had been conducted entirely by the LEP research team.

The design and optimization of the inductors cannot be done using an analytical approach, since the geometry cannot be described by simple analytical models. It has therefore been chosen to study the optimization of the heating system, before its production, with Cedrat Flux, a 3D finite element software that allows conducting multi-physics parametric simulations.

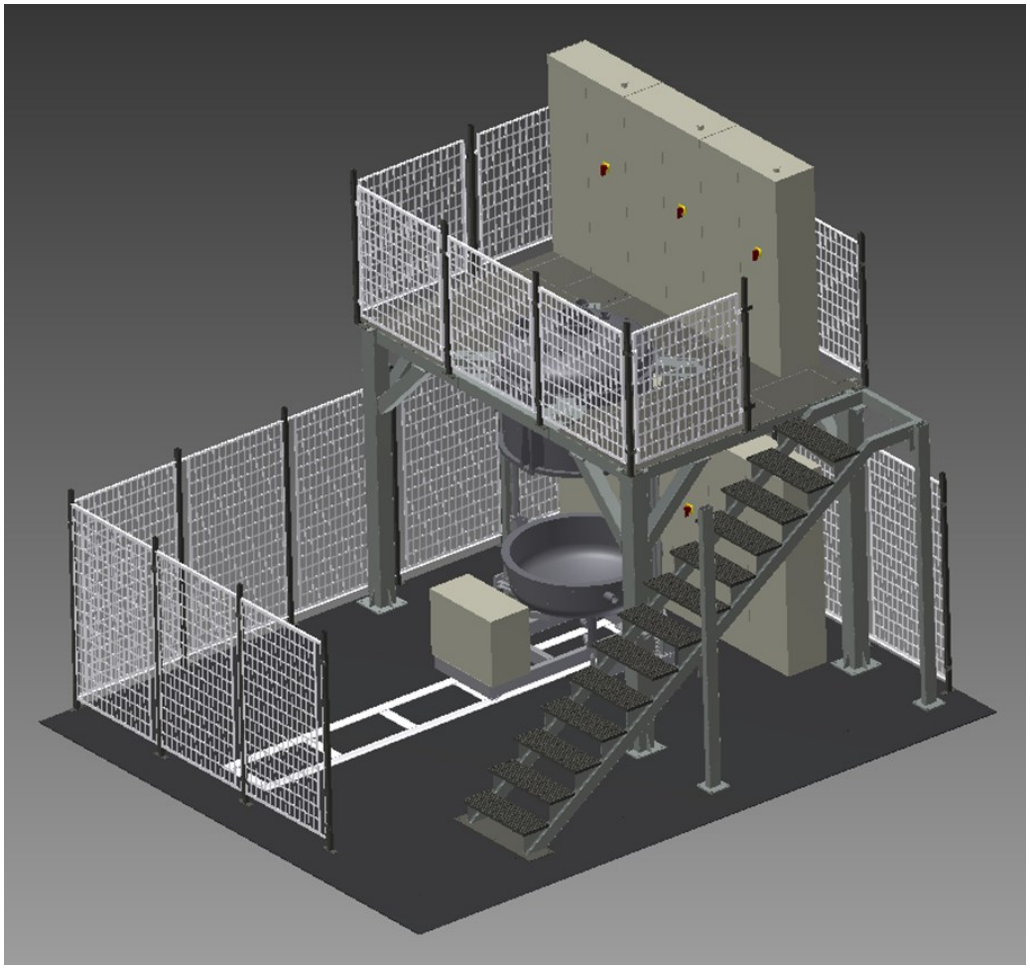

Figure 5.10 – 3D rendering of the 120 kg iDSS furnace developed and built at University of Padova

The knowledge acquired by researchers working at LEP, together with the data acquired during the first experimental tests conducted with the full scale 450 kg furnace [31] had been essential for defining the geometry of the system; further simulations had been necessary for scaling the system, since some critical parts couldn't be simply geometrically scaled for non-linear phenomena and practical obstacles to the construction of small dimension critical parts.

The insulator board thickness, for example, could not be reduced for the temperature of the hot zone being the same as in the full-scale system and the

inductors could not be geometrically scaled down for guarantee an adequate section for the cooling liquid flow inside the inductor themselves.

The geometry chosen for the heating system is therefore the one represented in Figure 5.4; a bottom pancake inductor with square cross section and four turns had been adopted for heating the bottom part of the hot zone and as a irradiative heat exchange system during the gradient and solidification process; a top pancake inductor with circular cross section and four turns with a geometrical configuration equivalent to the bottom one had been adopted for heating the top graphite susceptor; whereas six coils arranged along the sidewalls of the hot zone had been adopted for heating the lateral susceptor, reducing therefore the nucleation probability from the wall sides of the crucible, making also it possible to tune the power distribution between the different coils with the aim of differentially heating the silicon charge in the molten and solid phase. The lateral inductor system is also suitable for the development of an electromagnetic stirring system; the superimposition of a current with different frequency on the lateral inductor allows, in fact, the generation of a steady or time varying magnetic field inside the silicon melt, modifying therefore the fluid flows, making it possible to segregate impurities and obtain higher quality ingots.

The main geometrical differences between the full-scale industrial system and the lab-scale one are on the top and bottom inductor design. The full-scale 450 kg system, in fact, is based on the adoption of four pancake inductors for heating the bottom and top part of the susceptor box [32]; whereas this configuration allows to concentrate the heating power near the center of the crucible, the scaling down of the system is not possible for allowing the respect of turns distance for guarantee electrical insulation and for permitting an adequate fluid flow inside the inductors for their cooling.

It has therefore been chosen to adopt the pancake geometry for the top and bottom induction heating systems, but with only one inductor for each part. The electromagnetic design of the system and the check of the power induced distribution, together with a complete analysis of the system performance had then to be conducted.

Three finite element 3D parametric models had then been made for the design of the three inductors sets. The models had been made using Cedrat Flux and had been used for making electro-magnetic and thermal analysis. The principal results of the design process are presented in the following paragraphs.

BOTTOM INDUCTOR

The geometry of the 3D finite element model designed for the analysis of the performance of the bottom inductor is shown in Figure 5.11. The bottom 30×15 mm rectangular section inductor interacts with the bottom susceptor made of a 30 mm thick graphite plate placed over a 25 mm thick graphite cap which is intended for giving the induction system protection in case of silicon leakage. It is in fact important to prevent any possible contact between molten silicon and cooling water following a crucible failure event for avoiding the generation of hydrogen due to the interaction of silicon with water.

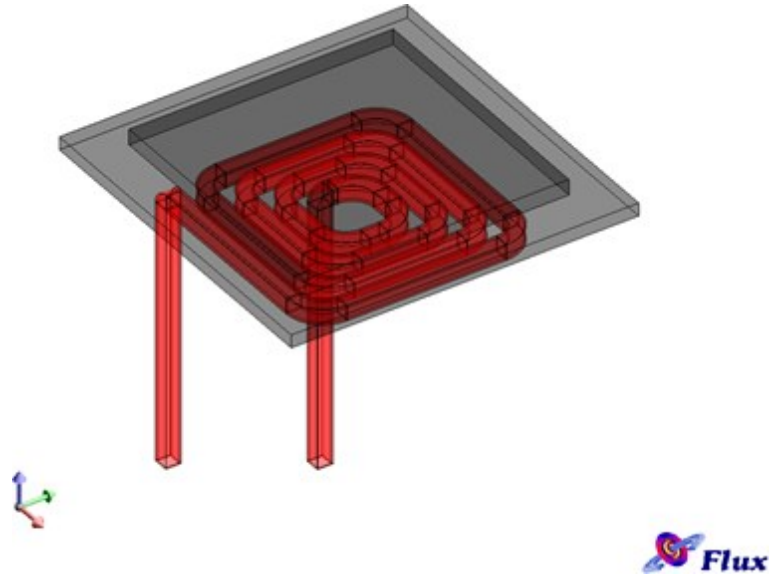

Figure 5.11 – Finite element 3D model for the bottom inductor and graphite susceptor of the lab-scale induction heating directional solidification system

The finite elements simulations allowed the definition of the system geometry and the heating efficiency had been evaluated in 60.6%. The power density distribution on the graphite susceptor is shown in Figure 5.12. The finite element analysis had also been conducted with different geometric configurations for the pancake inductors that didn't gave better results or had demonstrated not to be practically realizable. The adoption of a copper plate on top of the pancake inductor, for example, had been considered for increasing the irradiative thermal exchange; the accurate manufacturing of this component, though, would had led to a radical increasing of the inductor system cost, making the solution not practically feasible for lab-scale applications.

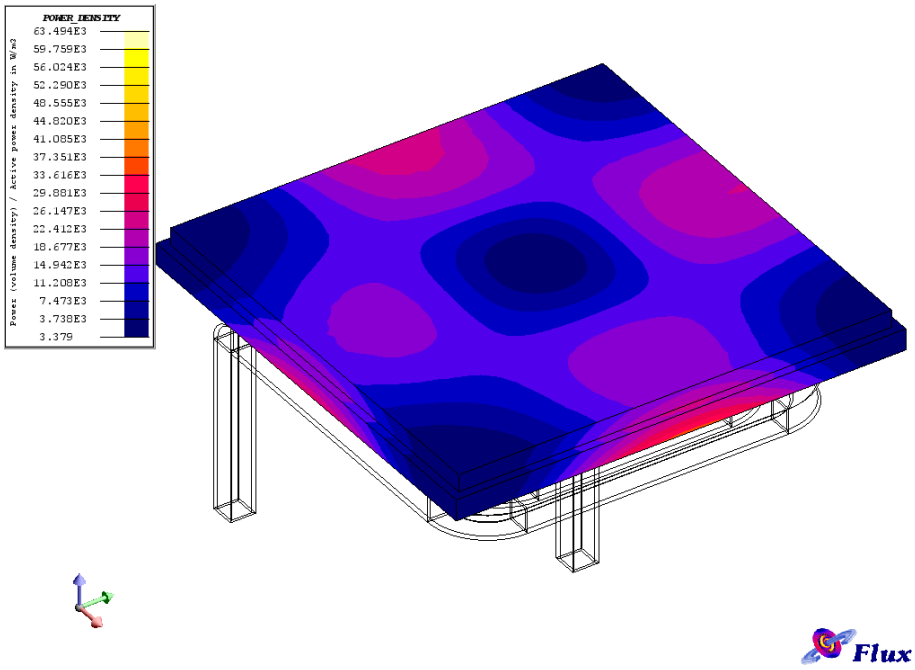

Figure 5.12 – Power density induced on the bottom susceptor of the lab-scale induction heating directional solidification furnace

TOP INDUCTOR

The top inductor dimensioning and design process had been similar to the one conducted for the bottom inductor. The main geometrical differences between the two models are the adoption of a cheaper and easier to manufacture circular cross section inductor in substitution to the square cross section one adopted on the bottom inductor, and the different distance between the inductor and the susceptor due to the necessity to put a thermal insulation layer between the susceptor and the inductor. The inductor adopted is ø30 mm, whereas the susceptor layer is characterized by a 25 mm thickness. The geometry of the 3D finite element model and the induced power distribution on the top graphite susceptor is shown in Figure 5.13 and Figure 5.14.

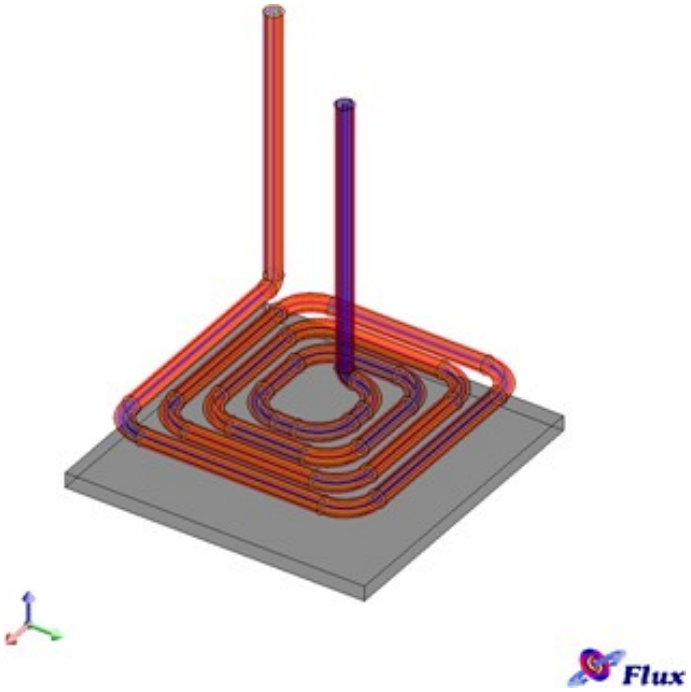

Figure 5.13 - Finite element 3D model for the top inductor and graphite susceptor of the lab scale induction heating directional solidification system

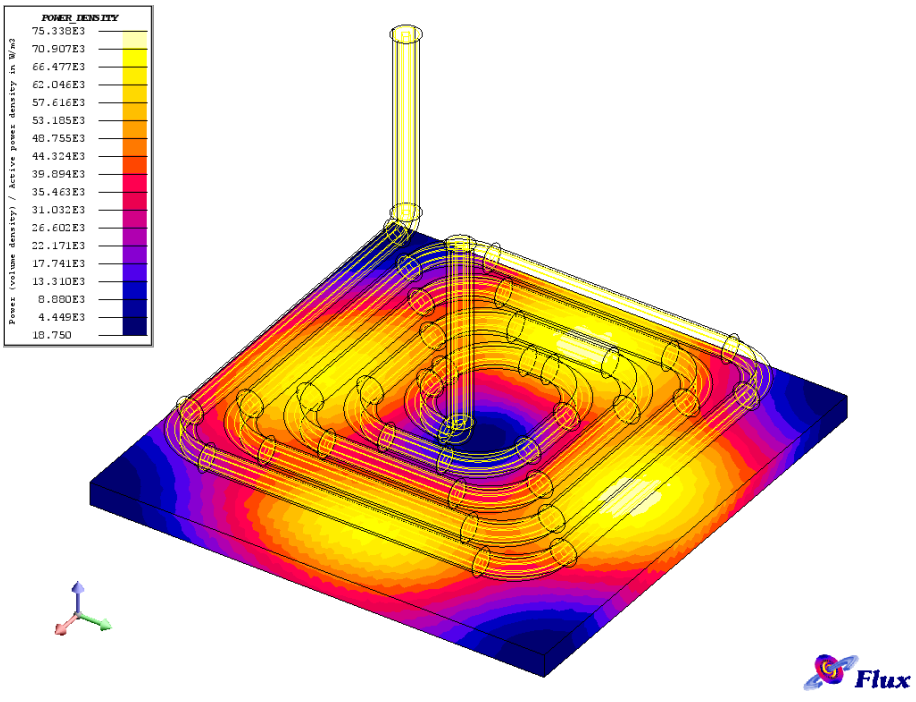

Figure 5.14 - Power density induced on the top susceptor of the lab scale induction heating directional solidification furnace

LATERAL INDUCTOR

The lateral inductor, as described in 5.2.2.1, has been designed as a multi-coil inductor made of circular cross section turns. Each coil can be powered separately, allowing the complete control of the power distribution on the lateral susceptor and the accurate definition of the thermal field.

The dimensioning of a multi-coil inductor system, heating a square shaped load, is quite simple; the particular application and geometric disposition of the inductor within the iDSS furnace, though, made the lateral inductor optimization process more challenging than expected.

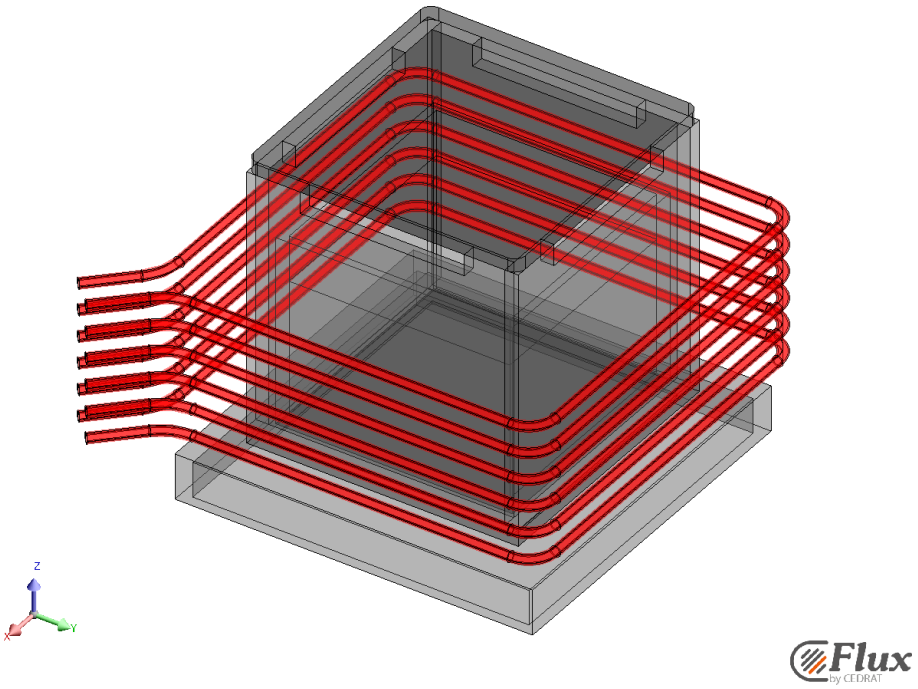

Figure 5.15 – Geometry of the 3D finite element model of the lateral multi-coil inductor and graphite susceptors

The lateral inductor, in fact, not only interacts with the lateral susceptor, actively transferring power to the load, but also transfers power to the graphite cap designed for the bottom inductor protection. Since the graphite bottom cap is not thermally insulated, the power transferred to its outer part can be considered wasted, since it doesn't contribute directly with heat transfer to the load. It had therefore been necessary to conduct a series of parametric analysis for assessing the optimal disposition of the lateral inductor for obtaining the highest possible efficiency.

A finite element 3D model has been built for the lateral inductor, considering 6 turns made of ø20 mm copper tubes, with a distance of 55 mm between each turn. The model, unlike the models built for the top and bottom inductors,

considered the lateral susceptor, as well as the bottom susceptor and the real geometrical configuration of the bottom cap. A 3D representation of the geometry of the model is represented in Figure 5.15.

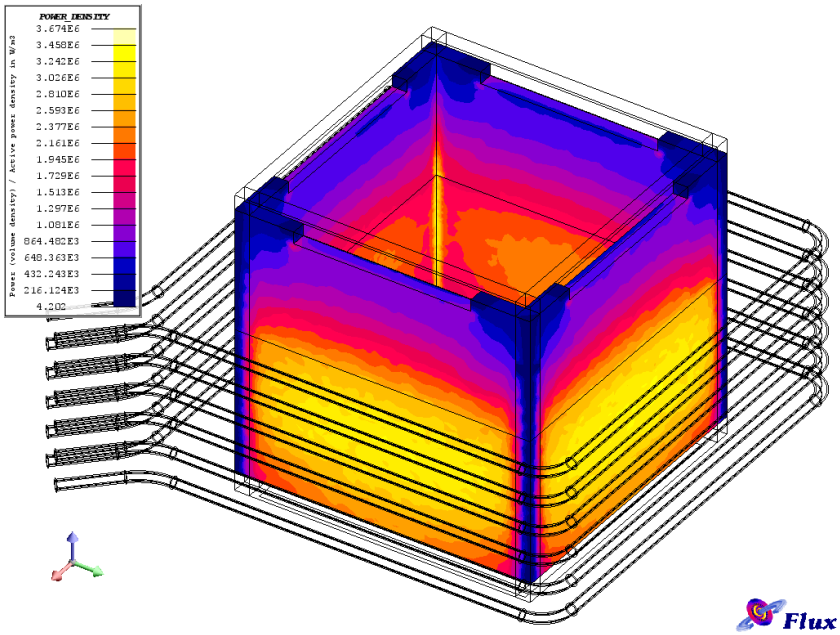

Figure 5.16 - Power density induced on the lateral susceptor of the lab scale induction heating directional solidification furnace. Base scenario.

The first analysis had been conducted for assessing the impact of the distance between the susceptor and the lateral coil inductor on the power transfer efficiency. The model didn't take into account the effect of the presence of the bottom cap; the efficiency values obtained after the analysis of the simulation's results are therefore representative of an ideal situation and were considered as reference values for the dimensioning of the insulator boards thickness. The distance between the inductor and the susceptor had then been chosen in 100 mm. The power density induced on the lateral susceptor during a step of the parametric analysis is shown in Figure 5.16, whereas the graphs showing the lateral induction system efficiency vs. coil-susceptor distance is shown in Figure 5.17. The observation of the power distribution on the lateral inductor represented in Figure 5.16, highlighting the concentration of power on the bottom part of the lateral inductor, had been essential for understanding the necessity to consider the effect of the presence of the bottom susceptor and protection cap for a correct evaluation of the overall efficiency.

After the definition of the optimal distance between the susceptor and the lateral inductor that guarantee the installation of an insulation layer of adequate thickness without a strong impact on the efficiency, the effect of the bottom

graphite cap on the lateral induction heating system efficiency had been evaluated. The model geometry had been improved and the full graphite susceptor box had been designed (see Figure 5.15). Considering the base scenario, the "lateral efficiency" has been defined as the ratio between the power transferred to the lateral susceptor and the power required by the system, whose active part is the lateral inductor; the power transferred to the bottom susceptor is therefore considered as lost and an efficiency drop of 22% due to the presence of the bottom cap had been recorded. The power losses in the bottom susceptor and cap due to the interaction with the lateral inductor are shown in Figure 5.18.

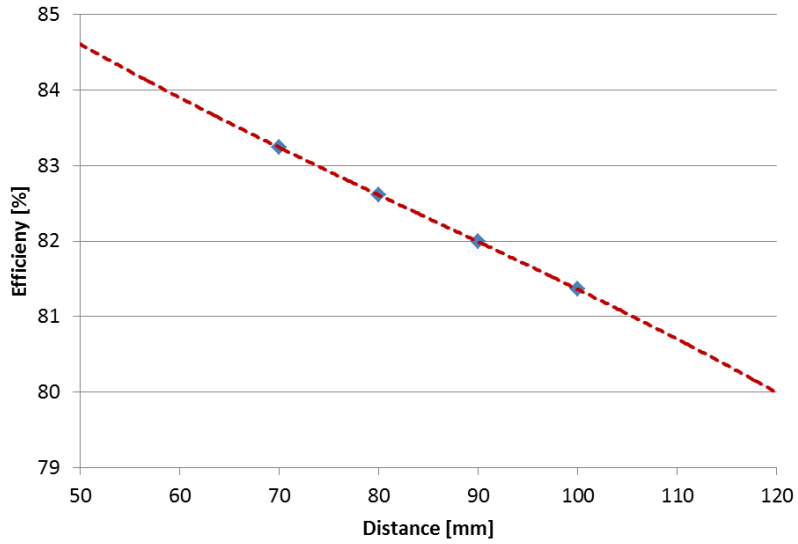

Figure 5.17 – Efficiency of the lateral inductor system varying the distance between inductor and susceptor

The undesired heating phenomena on the bottom cap that reduce the overall energy efficiency of the system had been reduced acting on the inductor height; increasing the distance between the bottom susceptor and the bottom coil of the lateral inductor allowed to increase the efficiency from 60% to an acceptable 74% by increasing the lateral inductor height of 60 mm (see Figure 5.20). Further increasing the inductors height would have led to the heating of the lateral susceptor above the crucible height with no beneficial effect on the casting process. The power density distribution on the bottom and lateral susceptor at the maximum lateral inductor height is shown in Figure 5.21 and Figure 5.22. Comparing them to Figure 5.19, representing the power density induced in the lateral susceptor in the base case scenario, it is possible to see the different distribution of the power density on the lateral susceptor.

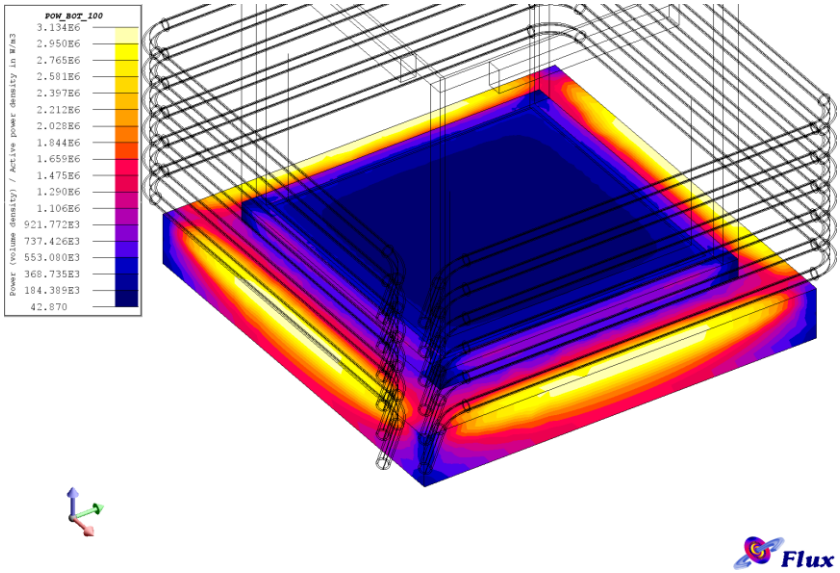

Figure 5.18 - Power density induced (lost) on the bottom susceptor cap of the lab scale induction heating directional solidification furnace due to the effect of the lateral inductor. Base scenario.

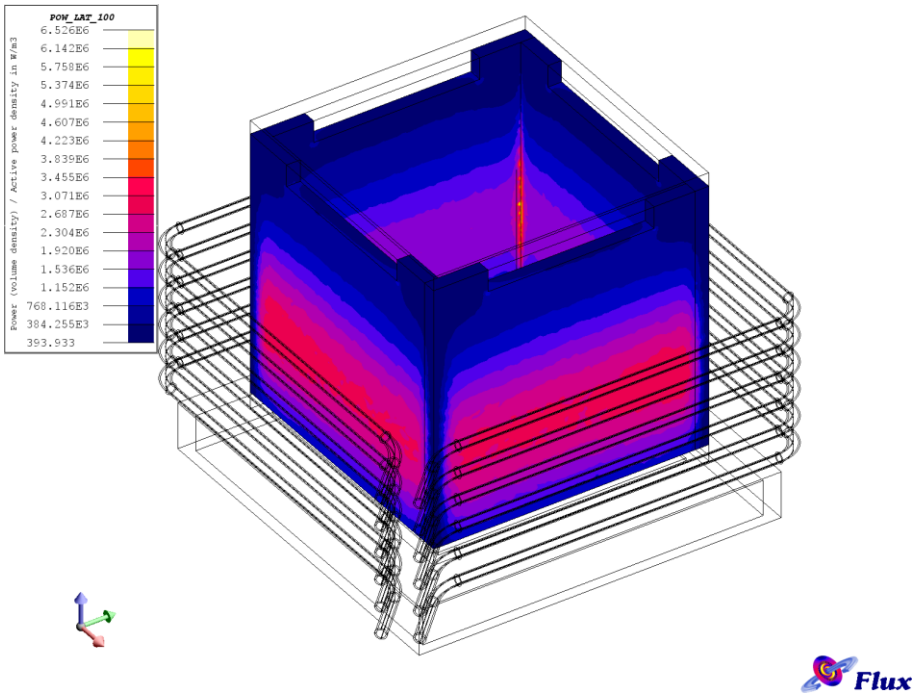

Figure 5.19 - Power density induced on the lateral susceptor of the lab scale induction heating directional solidification furnace due to the effect of the lateral inductor. Base scenario.

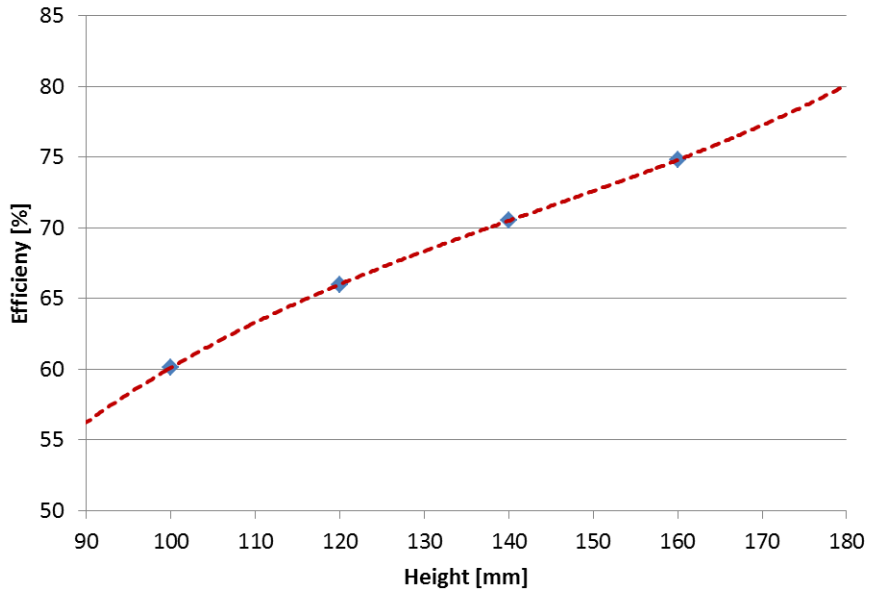

Figure 5.20 - Efficiency of the lateral inductor system varying the height from the bottom susceptor

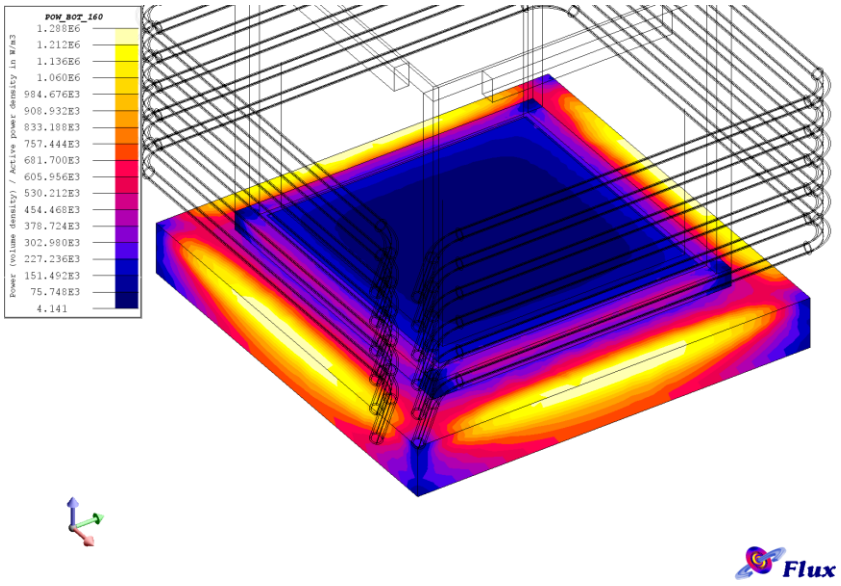

Figure 5.21 - Power density induced (lost) on the bottom susceptor cap of the lab scale induction heating directional solidification furnace due to the effect of the lateral inductor. Increased height scenario.

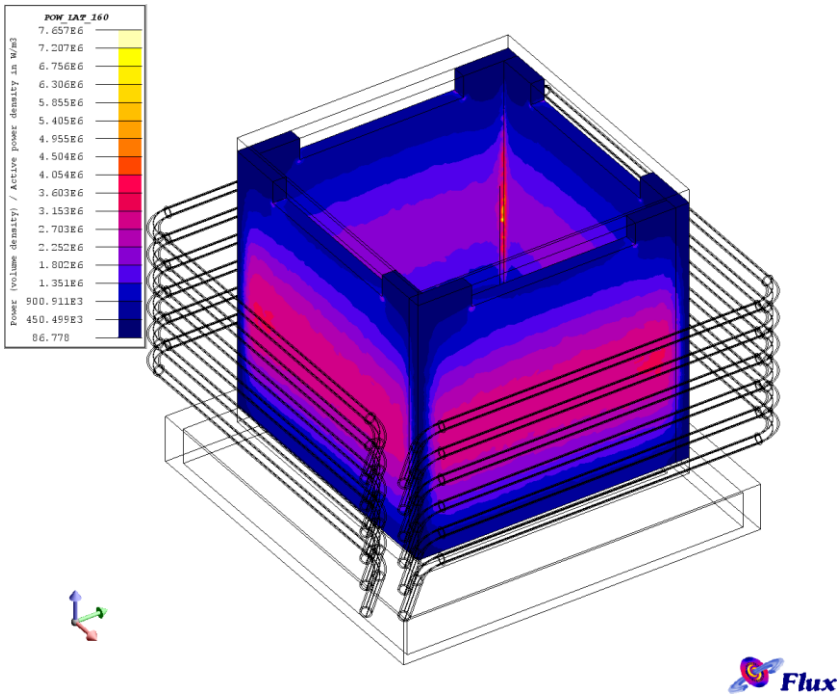

Figure 5.22 - Power density induced on the lateral susceptor of the lab scale induction heating directional solidification furnace due to the effect of the lateral inductor. Increased height scenario.

FULL GEOMETRY MODEL

For completely describing and understanding the effects of the interaction of the three inductors systems with the susceptor box, a 3D model describing the full geometry had been designed. The model is a simplified model based on a quarter section of the geometry, considering the symmetry effects. The parametric model has been designed considering the real dimensions of the components in the hot zone and can be easily modified following possible dimensions variations thanks to its parametric design. The geometry of the model is represented in Figure 5.23. Considering the silicon charge inside the crucible could be useful for understanding the effect of a superimposed current in the lateral inductor on the generation of a magnetic field inside the melt with possible stirring effect.

The model had not yet been solved for its high computational cost and a temporary lack of computation resources at the moment of designing the inductors; it will though be useful for making post-process analysis after the first experimental tests in the lab-scale furnace.

The furnace design had then being followed by finite element simulations using CGSim for understanding the crystallization processes and setting the process parameter. An example of the results obtainable using the crystal

growth simulation software will be shown in 5.3.5 analyzing the possibility to use the iDSS furnace for casting high efficiency mono-crystalline silicon ingots.

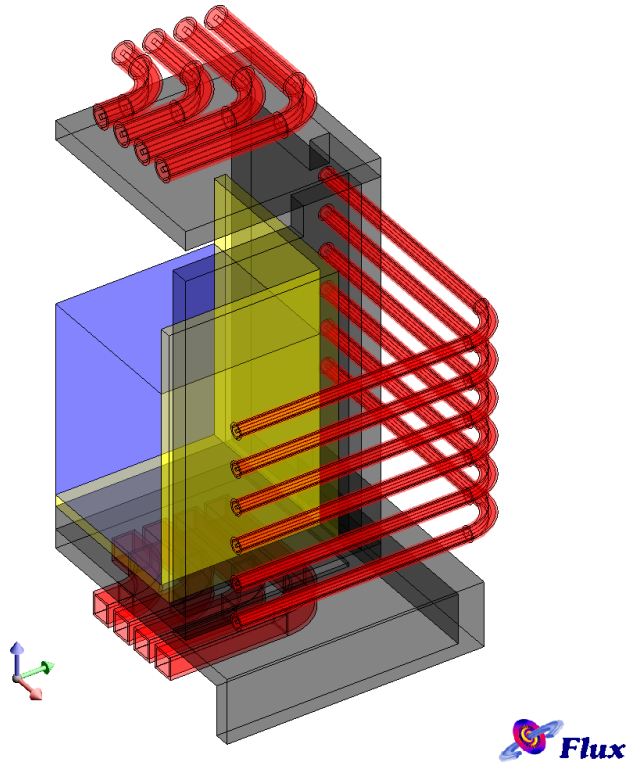

Figure 5.23 – 3D finite element model of the induction heating lab scale furnace. Main components: inductors (red), susceptors (gray), crucible (yellow), silicon (blue).

5.2.3 FURNACE INSTALLATION AND EXPERIMENTAL TESTS

The research conducted at the Laboratory of Electroheat at University of Padova and the design process described in 5.2.2 led to the realization of a lab scale induction heating furnace installed in the department of Industrial Engineering at University of Padova and completed at the end of 2012. The furnace installation took one year from the delivery of the first component to the final connection to the hydraulic and electric systems and the furnace (Figure 5.24) is now ready to be tested.

The first tests will be conducted by the third parties that installed the systems; in particular the vacuum test and the inductor coupling tests need to be conducting before the first experimental tests. Once the furnace will be ready for operation the first no load tests will be conducted for controlling the process parameters and for writing the recipes and the control software; the first casting processes will then follow, starting from multi-crystalline silicon casting processes, to seeded growth and quasi-mono crystalline silicon casting

processes. Some studies on the possibility to use the vacuum chamber for making experimental tests on the crystallization of different materials using different sets of inductors are currently underway. In Table 5.1 the main characteristics of the iDSS furnace designed and built at University of Padova are synthesized.

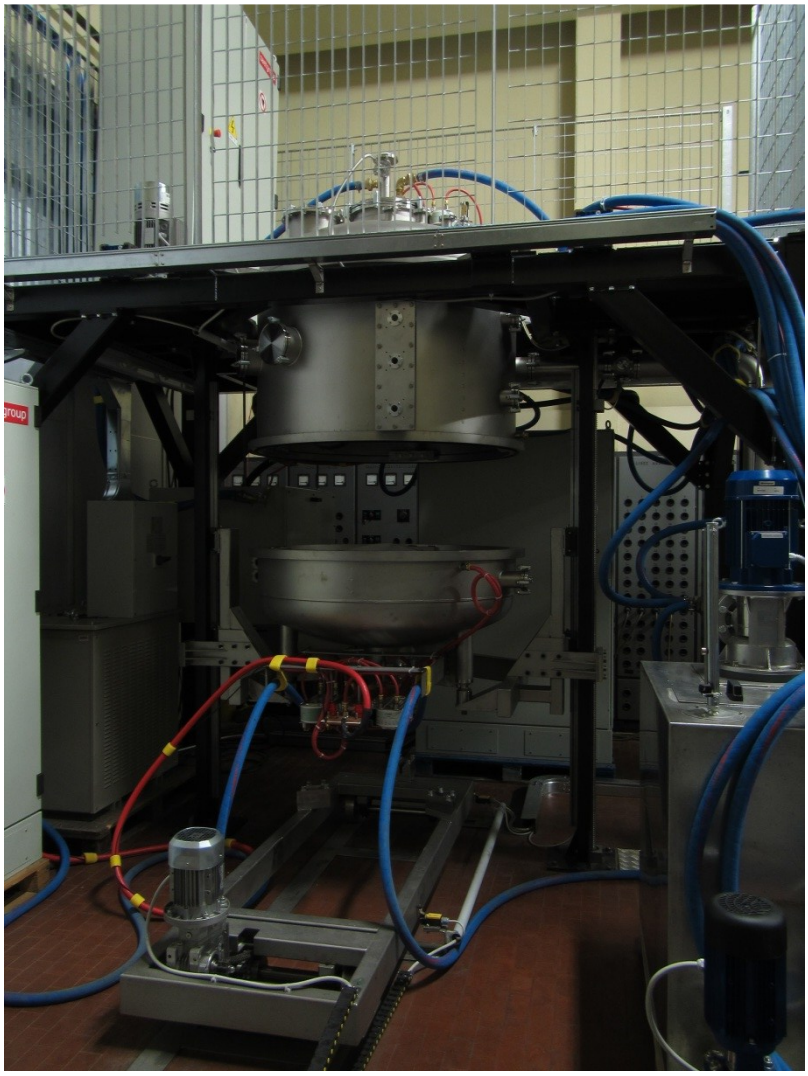

Figure 5.24 – Lab-scale iDSS furnace built at the Laboratory of Electroheat at Padova University

Before the final assembly of the lab-scale furnace some experimental tests had been conducted using the 450 kg G5 furnace, which 3D model is shown in Figure 5.2, built by an Italian company in collaboration with the University of Padova Spin-off Inova Lab and the Laboratory of Electroheat of University of Padova; the experimental tests results showed the possibility to obtained high efficiency multi-crystalline silicon ingots thanks to the thermal control obtainable using the induction heating system. Detailed results cannot be

disclosed, but the picture of one of the 450 kg ingots obtained using the G5 iDSS furnace, of a silicon wafer cut from one of the bricks, and the minority carrier lifetime map of two bricks obtained from the ingot are showed in Figure 5.25, Figure 5.27, and Figure 5.28.

Table 5.1 – Main characteristics of the lab scale iDSS system

Heating system	
Top heater	Pancake geometry, water cooled
Bottom heater	Pancake geometry, water cooled
Lateral heater	Multi-coil geometry, water cooled
Power supply	
Generators power (IGBT)	3×50 kW
Frequency	6 kHz
Vacuum system	
Vacuum chamber	Stainless steel, water cooled
Technical gas	Argon
Cooling system	
Cooling power	2×41 kW
Water flow	400 l/min
Hot zone	
Susceptor material	Graphite
Susceptor thickness	30-55 mm
Crucible material	Quartz
Crucible dimensions	440×440×420 mm
Feedstock maximum capacity	120 kg

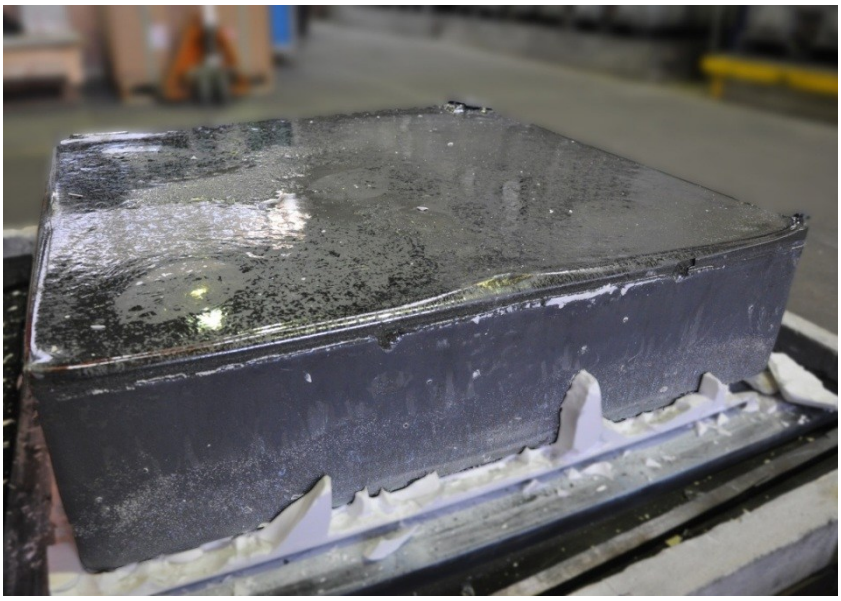

Figure 5.25 - 450 kg multi-crystalline silicon ingot obtained using thee 450 kg iDSS furnace

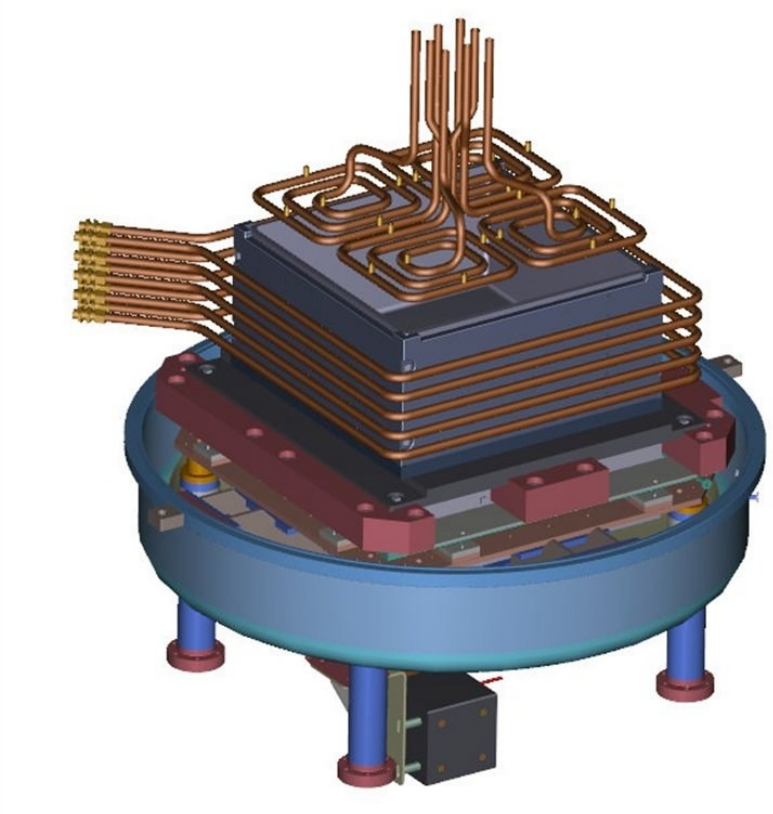

Figure 5.26 – 3D rendering of the heating system and hot zone of the 450 kg induction heating directional solidification furnace

Figure 5.27 – Multi-crystalline silicon wafer obtained using the 450 kg iDSS furnace

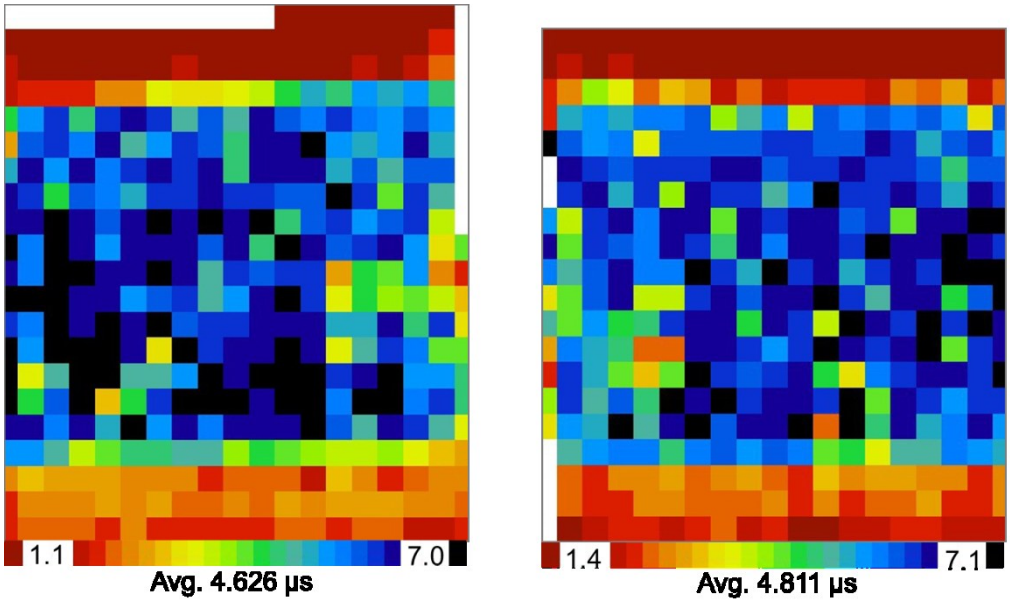

Figure 5.28 – Minority carrier lifetime for bricks obtaining using the 450 kg iDSS furnace. The average lifetime guarantees a performance increase of +0.3% in comparison with standard multi-crystalline silicon.

5.3 iDSS FOR MONO-LIKE CASTING

The iDSS heating system is well suited not only for growing multi-crystalline silicon ingots, but, the possibility to easily control the thermal field inside the hot zone of the system and the possibility to fine tune the power transferred in different parts of the graphite susceptors made it a good appliance for conducting experimental tests on casting quasi-mono silicon ingots.

In the following paragraphs the theory of nucleation from a seed that are fundamental for understanding the seed-casting process will be presented.

5.3.1 SEED GROWTH THEORY

Considering a single phase system in equilibrium at a certain temperature and pressure, the possibility to generate a second phase is due to the change of external conditions; during a phase transition the analysis of the thermodynamic and cinematic aspect is essential for understanding the phase transition phenomena. During near-equilibrium processes transition phenomena are driven by its thermodynamics, whereas in presence of

transformations far from the equilibrium phase the transition is driven by the cinematic aspect and metastable phases could generate.

The Gibbs free energy ΔG can be used for evaluating the thermodynamic stability of a phase α in relation to another phase β. If at defined external conditions $G_\beta < G_\alpha$ phase β is more stable than phase α; it may happen, though, that changing the external conditions can lead to a situation in which $G_\alpha < G_\beta$ and the β phase start to transform into phase α as described by the following:

- $T=T_c$ $G_\beta=G_\alpha$ equilibrium,
- $T<T_c$ $G_\beta>G_\alpha$ α is more stable,
- $T=T_c$ $G_\beta=G_\alpha$ β is more stable.

Figure 5.29, representing the Gibbs energy, shows the equilibrium temperature T_c at the intersection of the curves representing the Gibbs energy for each phase.

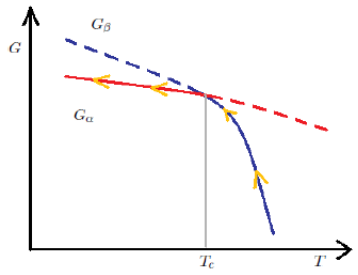

Figure 5.29 – Gibbs energy vs. temperature

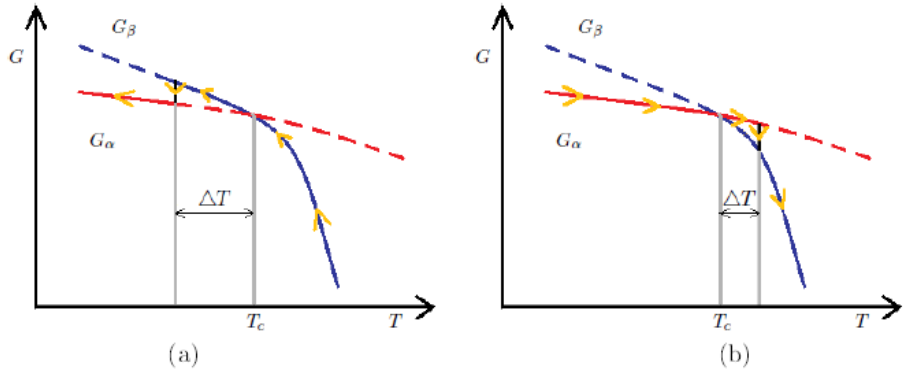

Figure 5.30 – Gibbs energy during cooling (a) and heating (b) process.

Considering a cooling process, it can be seen that a slow thermodynamically driven quasi-equilibrium transformation lead to the transformation of phase β into phase α. In the real case undercooling is necessary to allow the starting of the transformation process, since at $T=T_c$ the driving force that makes the transformation possible is null. Conversely, during a heating process with transformation of phase α into phase β overheating is needed as shown in Figure 5.30.

The thermodynamic driving force can be evaluated, considering small ΔT with the following:

$$\Delta G(T) = \Delta H(T) - T\Delta S(T)$$

In which:

- *ΔH(T)* is the enthalpy variation,
- *ΔS(T)* is the entropy variation.

Considering a phase transition in the proximity of the equilibrium temperature T_c, it is possible to consider H and S temperature independent, obtaining the following simplified equation:

$$\Delta G(T) = \Delta H - T\Delta S$$

Within the above mentioned hypothesis of quasi equilibrium conditions at temperature T_c, it is possible to assume the enthalpy variation equal to the transformation latent heat $\Delta H = -L$; it is also $\Delta S = L/L_c$, obtaining:

$$\Delta G(T) = \Delta H - T\Delta S = L - T\frac{L}{T_c} = \frac{L}{T_c}(T_c - T) = \frac{L}{T_c}\Delta T$$

The Gibbs energy variation is then proportional to the undercooling ΔT; conversely considering the heating process an overheating $\Delta T = T - T_c$ is necessary and, since the transformation cinematic is faster at higher temperature, the following is always verified:

$$\Delta T_{(\alpha\rightarrow\beta)} < \Delta T_{(\beta\rightarrow\alpha)}$$

For silicon the transformation latent heat is 1800 kJ/kg, or 50.55 kJ/mol.

5.3.1.1 HOMOGENEOUS NUCLEATION

Considering a homogeneous phase β, following an undercooling process ΔT, it can be seen that small particles of phase α starts to nucleate within the β

phase. This case represents the realistic case of solidification of a pure molten element. The Gibbs energy related to the particle nucleation of α inside a β phase melt is, under the hypothesis of nucleation of spherical particles:

$$\Delta G(T) = \frac{L}{T_c}\Delta T$$

Or, considering the volumetric energy:

$$\Delta G_v(T) = \frac{1}{V_m}\frac{L}{T_c}\Delta T$$

Being r the radius of the spherical particle, the Gibbs energy related to the transformation of the entire particle is described by the following and is monotonically decreasing (see Figure 5.31):

$$\Delta G_{Vol} = \frac{4}{3}\pi r^3 \Delta G_v = \frac{4}{3}\pi r^3 \frac{1}{V_m}\frac{L}{T_c}\Delta T$$

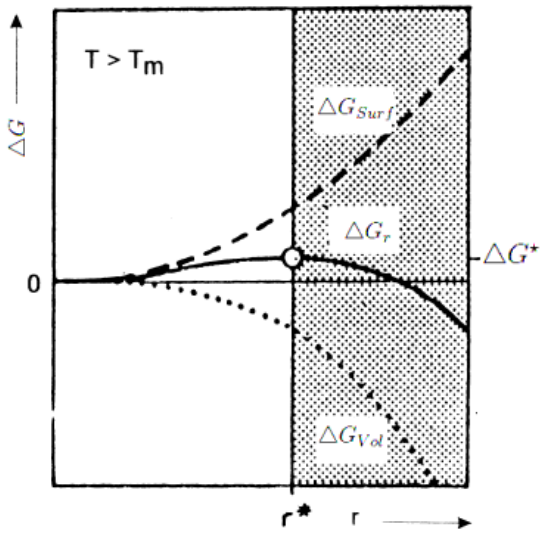

Figure 5.31 – Gibbs energy vs. particle radius

The relations considered so far don't consider the effect of the phase interface; the separation interface effect, in fact, needs to be added to the Gibbs energy and is dependent on the superficial free energy γ:

$$\Delta G_{Surf} = 4\pi r^2 \gamma$$

Another contribution to the free energy is due to the different density of each phase that makes the different phases occupy different volumes, leading to compression or dilatation of the nucleus structure; the free energy related to the compression or dilatation strain is:

$$\Delta G_{strain} = \frac{4}{3}\pi r^3 \varepsilon$$

And the total free energy needed for the nucleation of a spherical particle, considering ΔG_{strain} negligible for silicon solidification, is therefore:

$$\Delta G_r = \Delta G_{Vol} + \Delta G_{Surf} = \frac{4}{3}\pi r^3 \Delta G_v + 4\pi r^2 \gamma$$

It is therefore possible to plot ΔG_r versus the particle radius finding the value of the critical radius r_c for which the value of the Gibbs energy is the highest; particles which dimension is lower than r_c are called embryos and they are characterized by a reduced lifetime; otherwise particles with $r>r_c$ will keep growing during the transition process, since ΔG_r for the growing process is negative. The value ΔG^* is defined as the Gibbs energy relative to the critical radius and represents the energy activation barrier to the nucleation of the new phase.

It is possible to analytically evaluate the value of r_c and ΔG^* considering that in $r=r_c$ the derivative of ΔG_r is zero:

$$\frac{d[\Delta G_r]}{dr} = 4\pi r^2 \Delta G_v + 8\pi r\gamma = 0$$

Obtaining the following expressions for r_c and ΔG^*:

$$r_c = \frac{-2\gamma}{\Delta G_v}; \quad \Delta G^* = \frac{16}{3}\frac{\pi\gamma^3}{\Delta G_v^2}$$

Which values are temperature dependent:

$$r_c \propto \frac{c_1}{\Delta T}; \quad \Delta G^* \propto \frac{c_2}{\Delta T^2}$$

The above described equations shows that without the undercooling of the liquid phase the nucleation process is not possible since $\Delta G^* \to \infty$; increasing the undercooling, otherwise, reduce both the critical radius and the energy barrier, enabling the start of the nucleation process.

The description of the nucleation phenomena using the simplified equations presented above is not fully representative of the real case; in fact the

precipitates are not always spherical, since, depending on the interface structure, it is possible to obtain anisotropic precipitates, changing therefore the equations describing the interface energy. The thermodynamic equilibrium is also a dynamic event that macroscopically describe local microscopic situation of non-equilibrium.

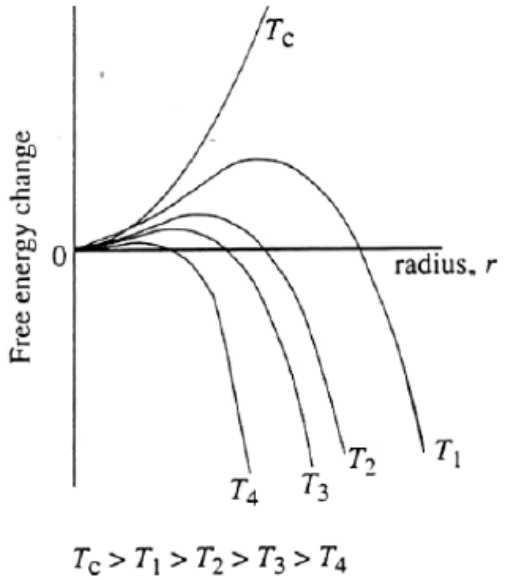

Figure 5.32 – Gibbs energy vs. particle radius and temperature

Even situations of a single homogeneous phase cannot be described by analytical equations, since there will always be fluctuations and local microscopic events that require a statistical analysis for understanding the idea of thermodynamic equilibrium. The probability of growing a new phase is never zero and increases with the reduction of the temperature gap to the critical temperature (see Figure 5.32). The precipitates formation velocity can be described as:

$$v = Cexp\left(-\frac{\Delta G}{k_B T}\right)$$

With C constant, dependent on the solidification statistic and k_B the Boltzmann constant.

5.3.1.2 HETEROGENEOUS NUCLEATION

The case described in the previous paragraph about homogeneous nucleation processes within a single liquid phase is not entirely representative of the real case. In fact, even if from a theoretical analysis of the nucleation process it could be possible to achieve highly undercooled liquid phases, in the real case the presence of vacancies, dislocations, stacking-faults, impurities, grain boundaries and solid parts in contact with the liquid phase activate other nucleation processes called heterogeneous nucleation processes, which reduce the nucleation activation energy.

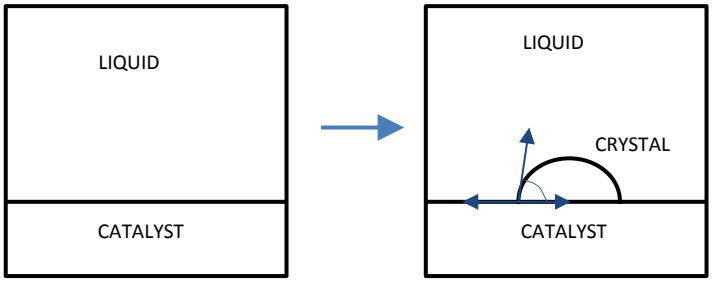

Figure 5.33 – Heterogeneous nucleation on a solid-liquid interface

The heterogeneous nucleation process is hereby described considering the nucleation of a β phase on a planar grain boundary, with a lenticular shaped nucleus (see Figure 5.33). Considering the balance of the interfacial stresses, being θ the contact angle between the lenticular nucleus and the planar grain boundary, the equilibrium condition is represented by:

$$\gamma_{\alpha\alpha} = 2\gamma_{\alpha\beta}\cos\theta$$

The Gibbs energy variation due to the formation of the nucleus characterized by its curvature radius r, considering the strain term negligible, can be written as:

$$\Delta G_r^{het} = \Delta G_{Vol} + \Delta G_{Surf} = V\Delta G_v + A_{\alpha\beta}\gamma_{\alpha\beta} + A_{\alpha\alpha}\gamma_{\alpha\alpha}$$

In which:

V is the volume of the lenticular nucleus,

$A_{\alpha\beta}$ is the area of the new $\alpha\beta$ interface,

$A_{\alpha\alpha}$ the area of the covered $\alpha\alpha$ interface.

It is possible to make an analytical comparison between the Gibbs energy for homogeneous and heterogeneous nucleation, obtaining the following equations that show the dependence of the heterogeneous nucleation Gibbs energy on the contact angle θ and the so-called shape factor $S(\theta)$:

$$\Delta G_r^{het} = \Delta G_r^{hom} \cdot S(\theta)$$

$$S(\theta) = \frac{(2 + \cos\theta)(1 - \cos\theta)^2}{2}$$

Being the shape factor dependent only on the value of the contact angle θ, the critical radius doesn't change between homogenous and heterogeneous nucleation; the activation energy, though, varies proportionally to the shape factor $S(\theta)$ and a schematic representation of the phenomena can be seen in Figure 5.34:

$$r_c = \frac{-2\gamma_{\alpha\beta}}{\Delta G_v}$$

$$\Delta G_{het}^* = \frac{16}{3}\frac{\pi\gamma^3}{\Delta G_v^2} \cdot S(\theta) = \Delta G_{hom}^* \cdot S(\theta)$$

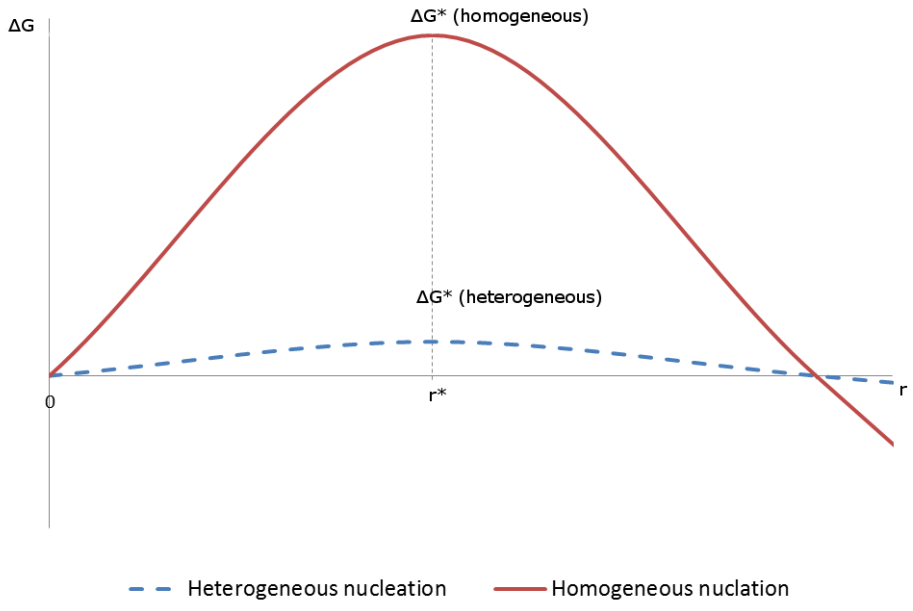

Figure 5.34 – Gibbs energy for homogeneous and heterogeneous nucleation

Typical values for the shape factor $S(\theta)$ for nucleation on a planar grain boundary are shown in Table 3.1; the lower the contact angle is the lower is the shape factor and consequently the Gibbs activation energy. The critical radius is independent from the localization of the nucleation, but the activation energy is lower with lower nucleus volumes. Multiple grain boundaries will then be favorable spots for starting the nucleation process.

Table 5.2 – Shape factor for heterogeneous nucleation. ϑ_{Si}=11°

ϑ	$S(\vartheta)$
90°	1
60°	0.32
30°	$2.6 \cdot 10^{-2}$
11°	$5.03 \cdot 10^{-4}$
10°	$1.4 \cdot 10^{-5}$

5.3.1.3 NUCLEATION AND GROWING KINETIC

The transformation of a stable phase of a component into another stable phase (e.g. from liquid to solid phase decreasing the component temperature) I due to homogenous or heterogeneous nucleation processes described in the previous paragraph that depends on the activation energy that is dependent on the temperature, nucleus radius and presence of impurities or dislocations that make the starting of nucleation favorable.

Through the analysis of the kinetic of the transformation process it is possible to divide the solidification process into two phases: nucleus formation and nucleus growing. For each transformation it is possible to define a transformation velocity. During the first phase of the transformation process, the transformation velocity is related to the probability of existence of nucleus and, as it had been described in 5.3.1.1, the lower is the undercooling temperature, the higher is the probability to form new critical dimension nucleus.

Analyzing the following equations describing the nucleation phenomena it is possible to see that the nucleation velocity v_1 has a maximum in correspondence to T=T_c/3:

$$v_1 = Cexp\left(-\frac{\Delta G}{k_B T}\right); \quad \Delta G^* \propto \frac{c_2}{\Delta T^2}$$

$$v_1 \propto exp\left(-\frac{C'}{(T_c - T)k_B T}\right)$$

After the nucleation phase has been completed, the new phase can grow with a growing velocity dependent on the number of atoms that can join the new phase surface. The migration of atoms to the new phase's surface and consequent phase change is dependent on the mobility within the medium (nucleus in gas, liquid or solid materials). The process is temperature dependent and high temperature increase the process velocity; in fact, the diffusion coefficient of atoms can be described through the Arrhenius law:

$$D = D_0 exp\left(-\frac{E_D}{k_B T}\right)$$

and the velocity of the second phase of the transition process is therefore:

$$v_2 = C'' exp\left(-\frac{E_D}{k_B T}\right)$$

The transformation velocity, then, decreases exponentially with the reduction of the temperature.

The total transformation velocity can then be described by the following:

$$V = v_1 v_2 = C''' exp\left(-\frac{E_D}{k_B T}\right) exp\left(-\frac{\Delta G}{k_B T}\right)$$

and the maximum transformation velocity is at a temperature low enough to guarantee high nucleation velocity value; the temperature, though, should not be too low, limiting the atoms diffusion and consequent growth of the new phase (see Figure 5.35).

Due to the presence of a maximum for the transformation velocity it will be possible to obtain a specific transformation with different temperature, but with the same velocity; the result, though, will be different with big grains obtained at high transformation temperature and small grains at lower temperature due to high nucleation velocity and low growing velocity.

Macroscopic crystals can then be obtained from a liquid phase through a slow process with relatively low undercooling temperature; this will allow to let the nucleus growing into big crystals; conversely, operating at high transformation velocity will lead to the formation of an amorphous solid with no ordinated orientation.

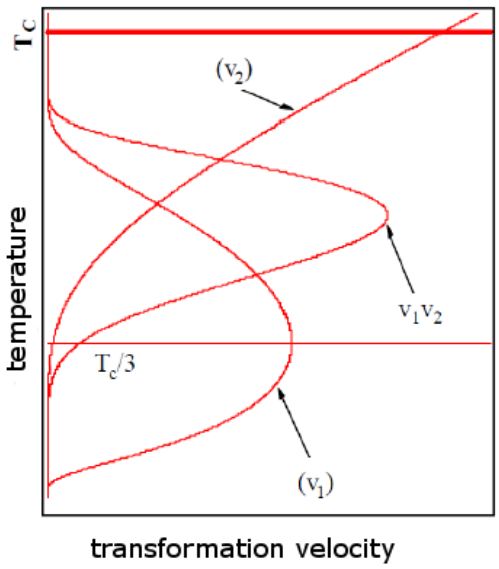

Figure 5.35 – Influence of temperature on phase transformation velocity. (v_1) nucleation velocity, (v_2) growing velocity

5.3.2 SEED CASTING

One of the challenges faced by the crystal growers' community working for the PV industry has been for years the development of a silicon growing technique that would tie the advantages of seed growing processes like CZ and FZ, with the advantages of bulk crystalline growing process. The idea that the PV industry wanted to develop after the polysilicon shortage era had been the realization of a furnace and method for growing mono-crystalline silicon ingots in big square crucibles.

An upgrade of the directional solidification process for growing multi-crystalline silicon ingots with controlled crystalline structure have been developed and is based on growing silicon ingots starting from a mono-crystalline silicon seed placed on the bottom of the crucible.

The mono-crystalline seed is made of a series of thick mono-crystalline wafers, called tiles, which cover the bottom part of the crucible. The tiles are usually produces through CZ or FZ technique and needs to be defect and dislocation free. The dimension of a typical tile is similar to the one of standard wafers (156×156) mm, or (125×125) mm, with a thickness ranging from 5 to 50 mm, depending on the process characteristics.

For allowing the tiles to form the seed and to make it easier to arrange them on the bottom of the crucible, the single tiles are arranged with the same crystallographic orientation on a flat surface, they are then soldered together using a laser technique or electric arc soldering, or connected through a thin amorphous silicon layer obtained through epitaxial growing. The seed is then polished and etched in a NaOH bath for removing the silicon oxide layer from its surface.

After the deposition of the seed on the bottom of a quartz crucible, similar to the ones used for multi-crystalline silicon casting processes, the crucible is filled with the silicon feedstock. Usually slightly high purity feedstock is required for seed-growth in comparison to multi-crystalline silicon ingots; this is due to the necessity of avoiding the generation of local defects that could deteriorate the overall quality of the ingot.

The process phases for casting seeded crystalline silicon ingots are similar to the ones described in 5.1 for growing multi-crystalline silicon ingots using a directional solidification furnace; the process parameters, though, needs to be finely controlled during the process. It is necessary, in particular, to pay attention to the melting step. In fact, not only the solidification process needs to be directional, but also a directional melting process needs to be achieved; the melting process, in fact, have to start from the top of the feedstock and the solid-liquid interface needs to be as planar as possible even during the melting process and to be controlled until it reaches the seed arranged on the bottom of the crucible. The melting process needs to be very slow when the solid-liquid interface is near the seed, and, for avoiding the melting of the seed, the bottom of the crucible needs to be cooled down. The process needs to operate in a near-equilibrium phase with heating velocity in the order of 0.5°C/min, or even lower.

The seed needs to be partially melted and, after the starting of the nucleation processes on the seed surface, the solidification process can start and can be controlled through the creation of the thermal gradient in the melt and through the control of the undercooling temperature. This will limit the probability of nucleation from the side of the crucible, while making it possible to obtain big vertically oriented mono-crystals. Strongly reducing the transformation velocity make it possible to obtain vertically oriented crystals with same dimensions of the tiles; the crystals dimensions, though, is limited by the tiles junctions that are favorable spots for heterogeneous nucleation of non-oriented silicon crystals.

5.3.3 MONO-LIKE CASTING

The terms “mono-like” or “quasi-single” crystalline are used by crystal growers and by the PV community for describing ingots obtained with a seeded casting process in which a big portion of the bulk, up to 95% [33], has a mono-crystalline structure, whereas the remaining part has multi-crystalline, possibly vertically oriented, structure.

For growing big quasi-single crystalline silicon ingots with a high percentage of the mono-crystalline part, using a seeded growth method in a directional solidification process, a special monolithic mono-crystalline seed should be used from a theoretical point of view. The seed should be big enough to cover the bottom part of any industrial size crucibles and therefore its dimension should be as big as 880 mm for a G5 furnace; considering that the Czochralski method allows the growth of mono-crystalline silicon rods with a maximum diameter of 400 mm, it is clear that producing mono-crystalline silicon seeds for producing quasi-mono crystalline silicon ingots is a big hurdle to the development of the mono-like casting technique applied to the photovoltaic industry.

The realization of the mono-crystalline silicon seed, though, is possible using a modified directional solidification furnace. The growing process is based on a seeded growth method in which the seed is placed on the bottom of the crucible and covered by the silicon feedstock; the feedstock is directionally melted and the controlled solidification is triggered by the presence of the CZ mono-crystalline tile. The modified furnace impose a thermal gradient that is not vertically oriented like in the multi-crystalline casting process, but a horizontal component of the thermal gradient is imposed for letting the mono-crystalline part of the bulk expand towards the crucible sidewalls.

This process, schematically descripted in Figure 5.36 [34], allows to obtain a few mono-crystalline seeds, depending on the ingot height, that could be cut from the ingot and which dimension is comparable to the dimension of the crucible sides. After the mono-crystalline silicon seed have been produced the process can be conducted in a similar way in comparison to the tile-seed growing process.

The heating process for quasi-mono crystalline casting is not different from the one described for multi-crystalline silicon ingot casting, with the main difference that the melting process needs to be “directional”. The feedstock charge, in fact, needs to be melted starting from the top of the crucible, while the bottom of the crucible needs to be cooled down to avoid the melting of the

mono-crystalline silicon seed. The heating step will then be longer than the one used for obtaining multi-crystalline silicon ingots, since the last part of this step needs to follow a heating ramp of less than 0.5°C/min for allowing working in a near-equilibrium phase.

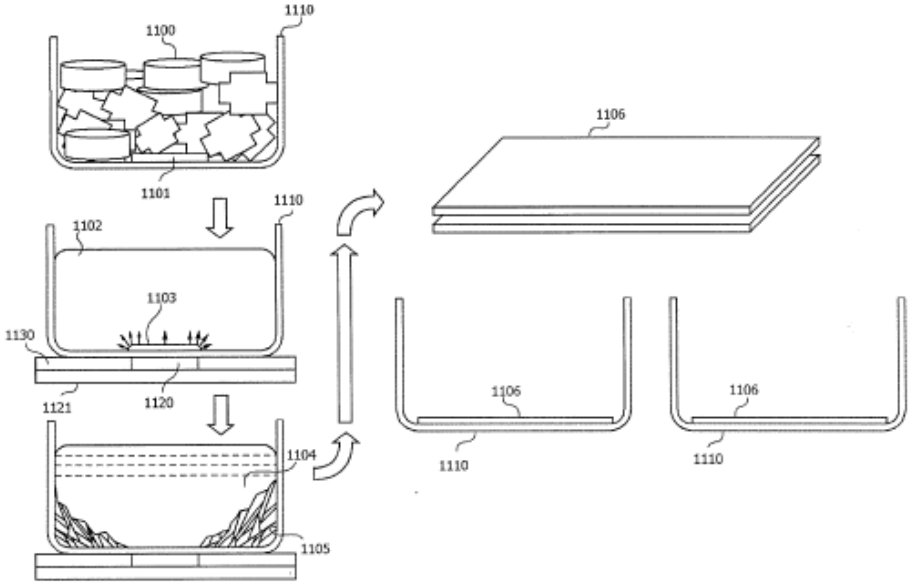

Figure 5.36 – Process for manufacturing large area, dislocation free mono-crystalline layers for use as silicon seeds [34]

The homogenization step that normally follows the melting step in a multi-crystalline silicon ingot casting process is very critical in the quasi-mono crystalline silicon ingots casting process. In fact, the homogenization step is useful for improving the quality of the casted ingot, since the thermal driven fluid flows allow to avoid the concentration of impurities. The need of maintaining the liquid phase in equilibrium with the solid seed without melting it requires the application of a thermal gradient that generates thermal energy losses caused by the necessity to transfer heat to the upper part of the system, while cooling down the bottom part.

The low thermal gradient during the melting step of the quasi-mono crystalline silicon ingot casting process in comparison to multi-crystalline, reduce the thermal-driven fluid flows inside the melt, reducing therefore the melt homogenization. An electromagnetic stirring effect could be used for increase the fluid flows; in industrial applications, though, the homogenization process is not conducted for reducing the complexity of the process.

The directional solidification process is then conducted with solidification velocity ranging from 14 to 21 mm/h, with the mono-crystalline percentage of the ingot increasing with the reduction of the solidification velocity. The solidification velocity is chosen as a compromise between ingot quality and process time and related energy consumption. The solid liquid interface needs to be as planar as possible for guarantee vertical orientation for the mono crystal; a slightly convex interface near the crucible walls allows the reduction of nucleation of multi-crystalline phases from the sides.

Finally, once the ingot is completely solidificate, an annealing phase and a thermally controlled cooling phase are needed before natural cooling at room temperature.

The ingot is then cut into bricks and wafers and wafers need to be sorted depending on their mono-crystalline percentage. Some studies [35] had been conducted on the possibility of recycling the seeds; the growing of the dislocation density following the thermal stresses, though, reduces drastically the quality of the seed after each use. In the real case quasi-mono crystalline silicon ingots are often produced starting from a tiled seed. This process allows an important cost reduction, while making it possible to obtain crystalline ingots with a relevant share of mono-crystalline silicon; the dislocation density multiplication starting from seed boundaries, though, limits the overall efficiency of quasi-mono crystalline silicon solar cells.

All the steps for the production of a quasi-mono crystalline silicon ingot using a directional solidification furnace are shown in Figure 5.38 and can be compared to the ones needed for the production of multi-crystalline silicon ingots, using the same furnace, described schematically in Figure 5.37.

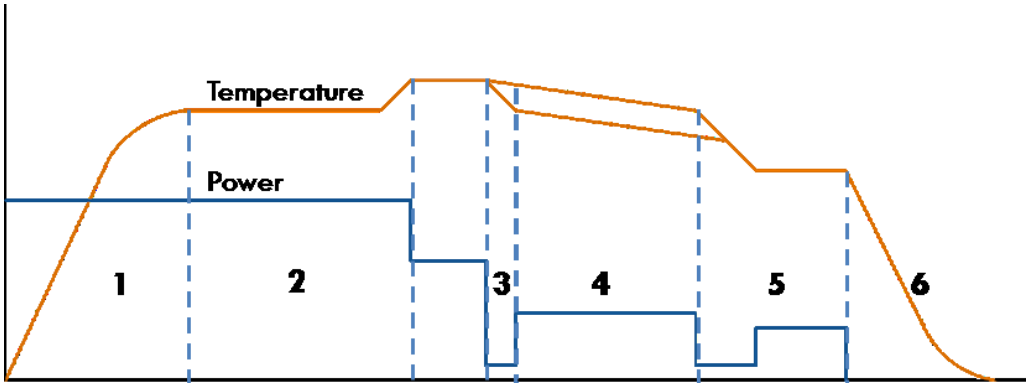

Figure 5.37 – Process parameters for a multi-crystalline silicon ingot casting process using a directional solidification furnace. (1) Heating, (2) Melting, (3) Vertical gradient and homogenization, (4) Directional solidifications, (5) Controlled cooling and annealing, (6) Free cooling.

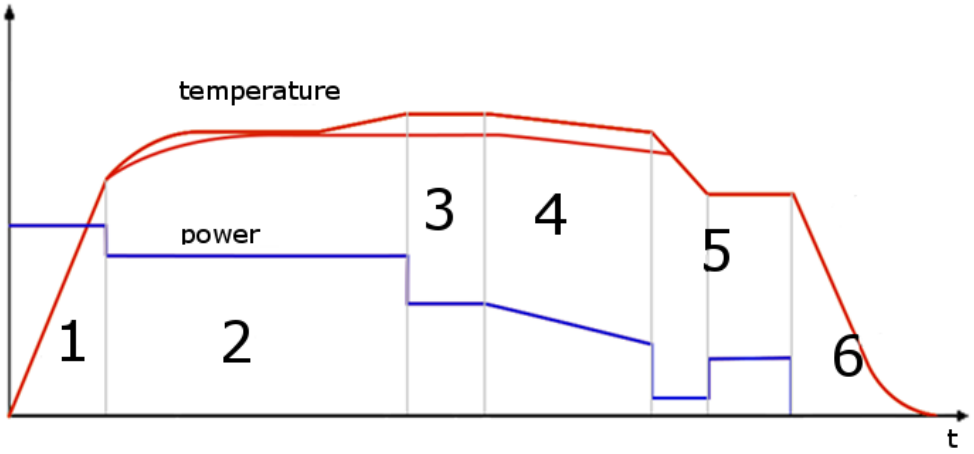

Figure 5.38 – Process parameters for a quasi-mono crystalline silicon ingot casting process using a directional solidification furnace. (1) Heating, (2) Directional melting, (3) Homogenization, (4) Directional solidification, (5) Controlled cooling and annealing, (6) Free cooling.

5.3.4 MONO-LIKE CASTING: INDUSTRIAL PRODUCTION

The interest of the PV industry on following a roadmap for cost reduction and efficiency increase has pushed many companies to invest on the development of industrial processes for the production of quasi-mono crystalline ingots and therefore solar cells with an efficiency closer to the one of mono-crystalline ones, but with scale economies and less energy intensive production processes characteristic of multi-crystalline solar cells production.

The firm that pushed the development of the quasi-mono crystalline silicon market had been BP Solar, the company that developed and patented the mono-like casting process [34], [33], [35], [36], [37]. Nowadays the technology developed by BP solar had been acquired by the furnace manufacturer AMG and had been integrated into AMG's engineering system division ALD vacuum technology; ALD Mono^2 and quasi-mono cells are now available in the PV market.

Ingots with mono-crystalline share of up to 95% have been reported [33] and cell efficiencies of up to 19% had been recorded for quasi-mono crystalline silicon wafers. An example of a quasi-mono (Mono^2) G6 crystalline silicon ingot casted by ALD using their upgraded directional solidification furnace is shown in Figure 5.39; the mono-crystalline part can be clearly seen in the 16 central bricks.

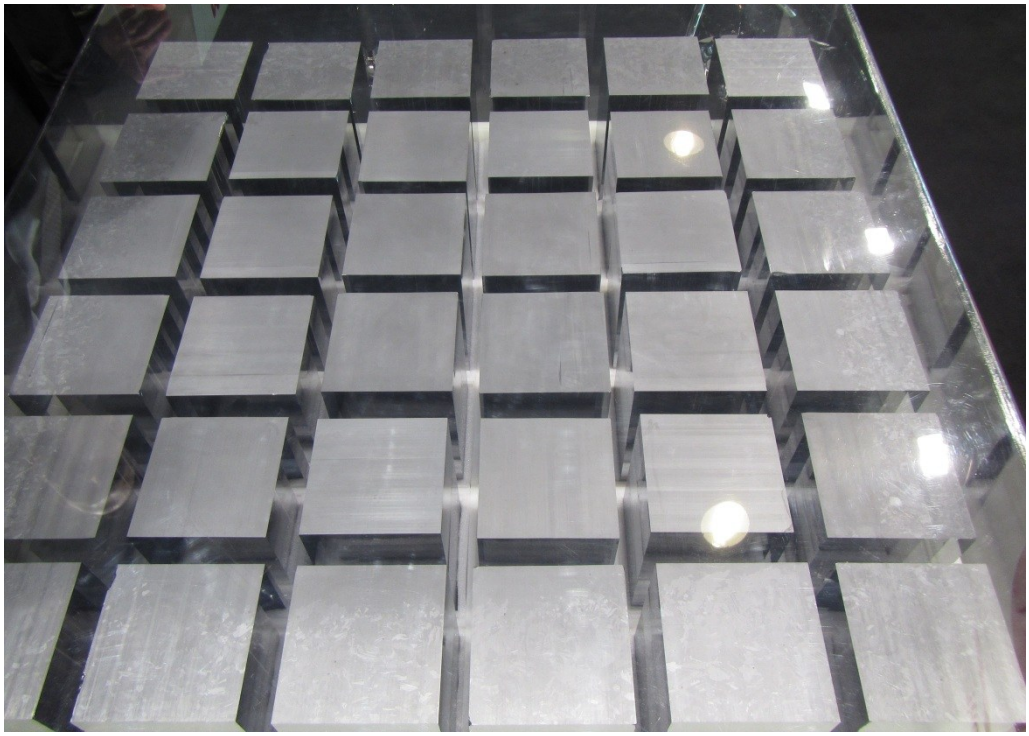

Figure 5.39 – Mono^2 silicon bricks obtained using an ALD G6 directional solidification furnace.

Quasi-mono crystalline silicon ingots are usually obtained using a tiled seed composed by square mono-crystalline seeds. Whereas the seeds used to be recycled for 3 to 5 cycles, nowadays it is considered preferable to use new seed materials for each solidification process for obtaining better quality products, even if at higher cost. Silicon ingots of up to 600 kg can be grown using resistive heating furnaces; the adoption of an inductive heating system like the one developed at the Laboratory of Electroheat at Padova University could easily improve the process, since the thermal control within the melt using the three heaters system is more accurate and the thermal inertia of the system is lower.

5.3.5 QUASI-MONO CASTING PROCESS USING THE IDSS FURNACE

The lab-scale iDSS furnace developed at the Laboratory of Electroheat at Padova University and described in **Errore. L'origine riferimento non è stata trovata.**, for its heating system configuration and for the possibility of adopting a system for the control of travelling magnetic field in the melt, is well suited for conducting experimental tests on seed casting processes for the development of a method for producing quasi-single crystalline silicon ingots.

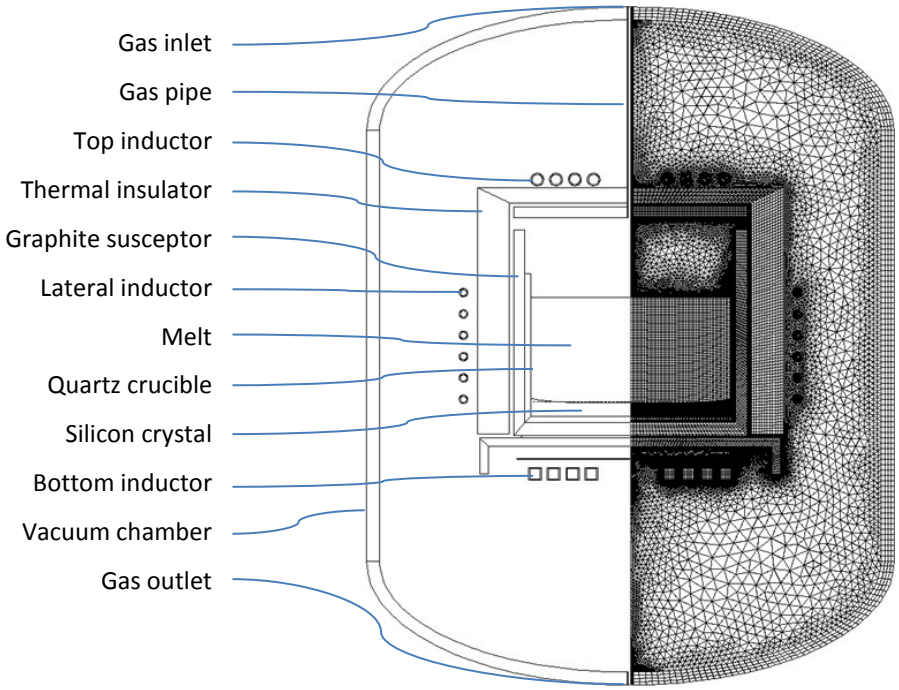

Figure 5.40 – 2D axisymmetric model of the iDSS furnace with components description and computational finite element mesh

One of the most important challenges faced during the design and optimization of the casting process is the control of the radial thermal instabilities and consequently of the buoyancy driven flows in the melt. The induction system allows a fine control of these phenomena, more accurate than the one achievable with traditional resistor heating technologies. These phenomena are related to heat and mass transfer during the solidification process and are important for controlling both the solid/liquid interface shape and the impurities distribution in the ingot [38].

2D axisymmetric thermal and electromagnetic calculations have been carried out using CGSim, a commercial software which makes use of finite elements modeling. The model geometry includes the silicon feedstock, the mono-crystalline seed, the thermal insulation and the chamber, and is shown in Figure 5.40.

The first problem in the implementation of seed-assisted Mono-Like-Casting is the preservation of the seed during all the phases of the process. It is therefore essential to carry out directional melting to avoid the seed melting and to permit its surface activation. The control of the process must be very precise for this phase being very critical, especially when the solid/liquid interface reaches seed surface. The melting velocity can be high at the beginning

of the process, but must be slowed down to reach a quasi-equilibrium state when molten silicon are in contact with the seed surface. The equilibrium stage is the beginning of the solidification phase; in Figure 5.41 the thermal map and the map of fluid velocity (also represented by vectors) are shown; the shape of the solidification front is also show and its concavity can be sees.

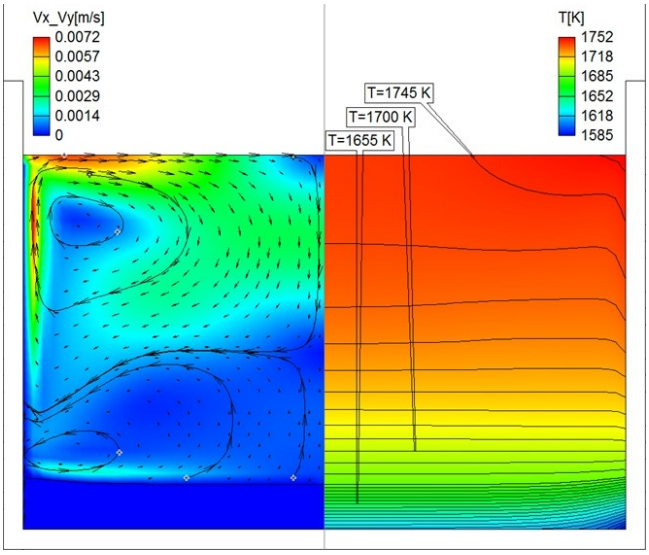

Figure 5.41 – Velocity and temperature map at the near equilibrium state at the end of the directional solidification

At the beginning of the solidification stage there are two convection cells, with the most important being the one closest to the seed; this cell moves the melt from the side towards the center near the solidification front. This situation has a great influence on the carbon distribution.

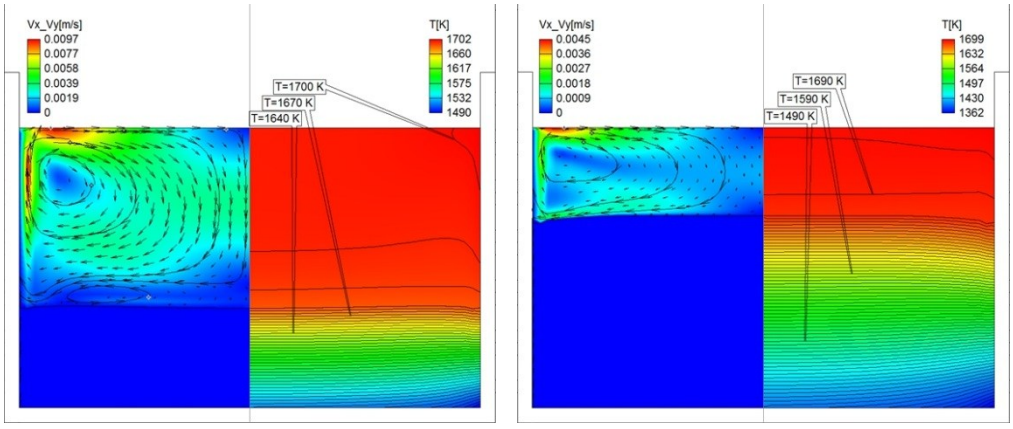

Figure 5.42 – Velocity and temperature map at 30% and 70% of the solidification process. The change of the solid liquid interface shape can be seen.

Figure 5.42 shows the change of the solid/liquid interface from concave to convex; in other words, the horizontal component of the temperature gradient

changes gradually. This aspect has beneficial effects on the final ingot quality limiting the expansion of new grains growing from the crucible side walls due to heterogeneous nucleation.

The fluid flow inside the melt is determined by natural convection and Marangoni effect; after the establishment of the concave shape on the interface, the direction of the flow changes near the front. This feature is very important for the distribution of impurities in the ingot, in fact the scrambling motions have a dominant effect compared to the diffusion mechanism.

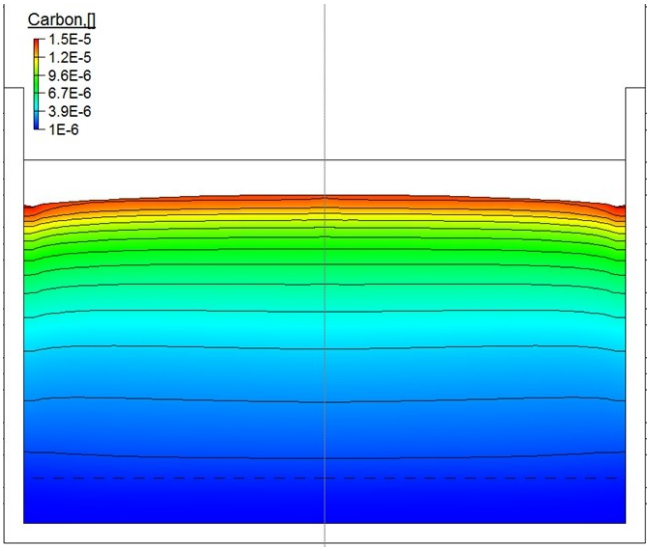

Figure 5.43 – Carbon distribution on the solidified part after 90% of the solidification process

In Figure 5.43 the carbon distribution map is shown, the starting data are: 1 ppm carbon concentration in the homogeneous crystal, 25 ppm in the melt, $D_{C,melt}=3\cdot10^{-8}$ m^2/s, $D_{C,solid}=3\cdot10^{-14}$ m^2/s. The model has been designed as a closed system with only one exchange surface, that is the solidification front, setting the segregation coefficient of carbon k_o equal to 0.07 [39].

The impurity density, at same height, is more concentrated in the lateral zone than in the center; considering that usually in a bulk process the material closer to the crucible is discarded, this lead to a major purification of the useful ingot.

Numerical simulation results show the suitability of the iDSS furnace for the directional melting process for mono-like casting applications and the possibility to finely control the thermal fields and fluid flows within the melt, with the aim of obtaining a bigger mono-crystalline part characterized by better material properties.

6 TECHNOLOGIES FOR PV RECYCLING

The use of photovoltaic systems for the production of electrical energy has drastically grown in the last years due to technological and economical improvements of this renewable energy technology and thanks to the still increasing public awareness over the environmental impact of energy production and possible climate changes related to human activities.

Many PV systems, ranging from small residential rooftop installations to multi-megawatt solar power plants have been installed during the last years but, while many technological improvements have been done along the whole production chain for making the PV technology competitive in the electrical energy sector and for the reduction of its environmental impact, developing solutions for treating end-of-life solar modules has often been considered secondary. The PV industry, though, needs to invest on research for the development of economical viable and environmental friendly solutions for recycling end-of-life solar panels, with the aim of creating a closed-loop cycle for raw materials used in solar panels.

6.1 PV RECYCLING: MARKET VOLUMES AND REGULATIONS

The development of recycling technologies for recovering raw materials from end-of-life PV panels should be one of the main tasks for researchers working with the PV industry. While in the mid of the last decade the interest on the development of recycling systems for crystalline silicon solar panels grew rapidly due to the shortage of polysilicon feedstock for the production of solar wafers that made it profitable to recovery silicon and wafers from end-of-life solar modules, even with energy intensive or costly methods, the drop of the cost of polysilicon feedstock related to the realization of a polysilicon supply chain dedicated to PV, made most of the recycling processes still developed not economically viable.

Nowadays PV recycling is not considered an economic opportunity by the PV sector due to the relatively low value of the recovered materials in comparison

to raw materials costs; the still increasing installation volumes, though, requires the PV industry to think about recycling with the aim of reducing the impact of the PV sector in terms of intensive use of raw materials and environmental impact for their extraction.

The reasons for the development of PV recycling systems, as well as the technological challenges that the researchers have to face for recovering raw materials from end-of-life PV panels are analyzed in details in the following paragraphs.

6.1.1 PV MARKET VOLUMES AND PV RECYCLING

The analysis of the PV installation volumes during the last years can be useful for making educated estimates on the volumes of end-of-life solar panels, originating from dismantled PV power plants, which will need to be treated as "waste" in the next years.

Some estimates of the yearly volumes of PV wastes until 2040 have been done starting from the analysis of the historical installation data in Europe and in the World given by the European Photovoltaic Industry Association (EPIA) [1].

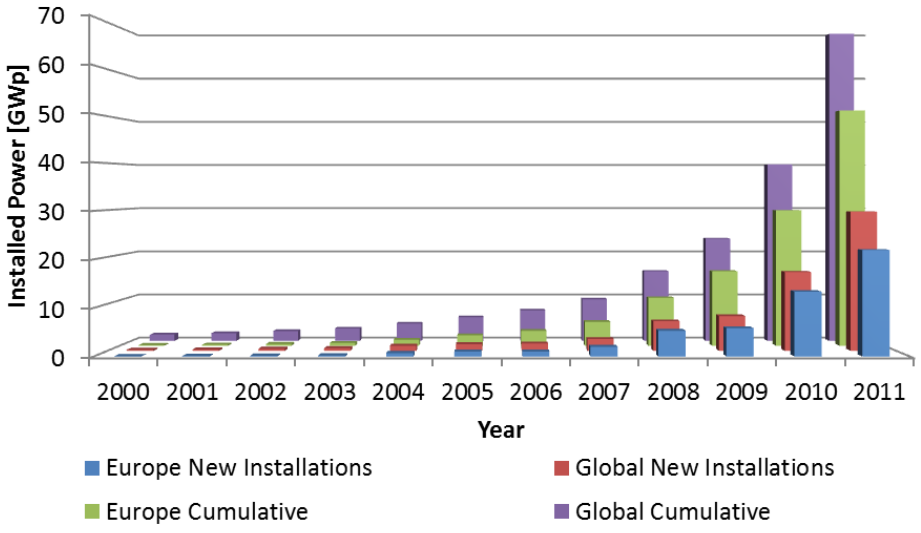

Figure 6.1 – European and global cumulative and annual PV installations (source: EPIA)

During the last ten years the global and European PV cumulative installed capacity, as well as the annual installations, have grown exponentially and at the end of 2011 almost 70 GW of PV have been installed and are in operation

worldwide, with more than 50 GW (~74%) installed in Europe (Figure 6.1). Considering the annual installation volumes it can be seen that during the last year the growth rate at both global and European level is almost 74%, with almost 22 GW of PV installed in 2011 in Europe.

Considering these data, together with some technical assumptions related to the mean weight of the installed PV panels and their expected lifetime, it is possible to make some analysis on the future volumes of PV wastes.

Through the analysis of technical data-sheets for commercial PV modules it is possible to determine the mean weight/power ratio for PV panels currently available in the market. Considering the different technologies and PV panels structures a value of 80 g/Wp has been considered realistically representative of the current PV market.

Considering also a lifetime for PV panels of 30 years, some estimates on PV waste volumes can be drawn and the estimated PV waste volumes generated per year in Europe up to 2041 can be seen in Figure 6.2.

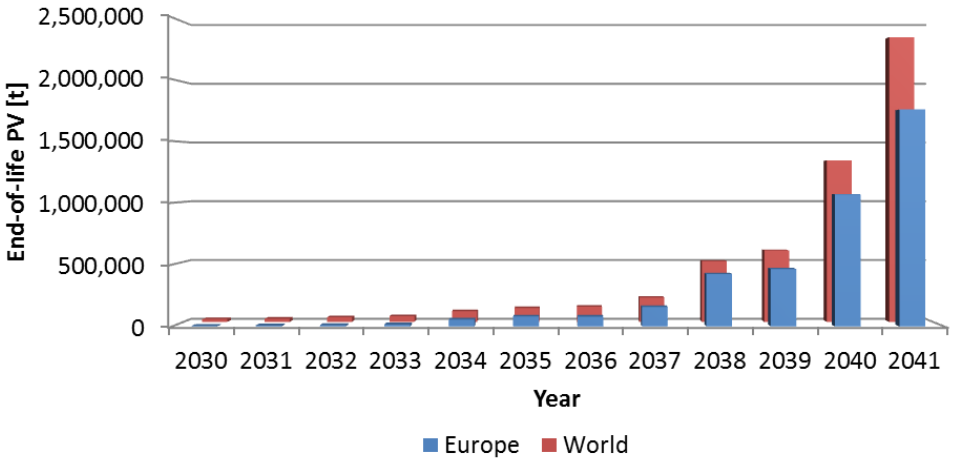

Figure 6.2 – PV "waste" volumes estimates up to 2041

Analyzing these results it can be seen that starting from 2040 a relevant amount of PV waste, greater than 1 000 000 t will be generated per year in Europe, making it necessary to develop some industrial systems for efficiently treating and recycling end-of-life PV panels. The total amount of PV installed in Europe to date (2011) can be estimated in 4 160 000 t.

These data are only rough estimates since they consider a constant weight/power ratio along a 10 years' time span. A more complex analysis could

be done considering the technologies improvements during the years. In fact the improvement of the cell conversion efficiency, the reduction of the raw material use, or the adoption of PV modules without frame, lead to the reduction of the weight/power ratio with time, reducing the relative increase of PV waste volumes during the years.

It is also possible that PV modules installed today will be substituted before their expected lifetime of 30 years not for technological reasons, but for economic reasons that could make it convenient to invest on the installation of new PV modules with better performance and higher return of investment. The growing of a substitution market could lead to waste volumes bigger than the ones expected from the estimates drawn from the current market situation.

6.1.2 REGULATIONS AND LAWS ON PV RECYCLING

The reasons that push the PV industry to develop recycling systems for end-of-life PV modules are not only technological or economical. Although PV wastes are non-toxic and could be easily treated as normal solid wastes, the growing interest of the public opinion concerning possible health and safety issues related to the installation, use and decommissioning of PV modules has pushed many government to investigate the opportunity of regulating the decommissioning and end-of-life treatment and recycling of PV wastes.

In Italy the first regulatory action for the treatment of end-of-life PV modules has not been a law regulating the recycling of PV, but a part of the feed-in-tariff support scheme. In fact, the Italian Law "Quarto Conto Energia" [4] required the installer to produce a certification stating that the PV modules installed have been manufactured by a producer that is part of a consortium for the recycling of end-of-life PV modules and that the recycling activities is pre-funded using a quota of the modules' price.

Although this law didn't build any direct barrier to the installation of products without the guarantee of recycling, it made less convenient for final users to buy and install modules non certified for recycling that make it not possible to take part in the feed-in-tariff support scheme.

The Italian Law "Quarto Conto Energia" had been enforced, for the part regarding the recycling of PV on June 30th, 2012. It has, though, been substituted

[4] D.M. 5 maggio 2011

by the "Quinto Conto Energia"[5], with similar requirement for installers and producers on August 27th, 2012.

Whereas in Italy the recycling of PV modules have been regulated in a non-direct way acting on economic interests of installers, producers and end users, the European Community, following the requests of the State Members for the regulation of the activity of treatment, disposal and recycling of PV wastes, investigated the opportunity to treat PV waste in the same way of waste of electric and electronic equipment (WEEE).

After a long re-casting process, started on December 2008 for the definition of the new WEEE directive that regulates the treatment, recycling and disposal of wastes of electric and electronic equipment, considered hazardous for the use of toxic material such as, for example, lead; and after long discussions during the legislative process, regarding the opportunity to consider PV as WEEE waste, on July 24th, 2012, the new WEEE directive have been published[6] and PV is now considered WEEE waste.

The new WEEE directive needs to be adopted by every Member State through local laws before February 14th, 2014. Meanwhile, during the transitional period, the directive is still operative for some categories of EEE wastes, including PV waste.

In particular the directive, with the objective to "*preserve, protect and improve the quality of the environment, to protect human health and to utilise natural resources prudently and rationally"*, considers PV as category 4 waste: "*Consumer equipment and photovoltaic panels"*; the directive, though, shall not be applied to "*large-scale fixed installations, except any equipment which is not specifically designed and installed as part of those installations*".

The directive defines the collection rate for EEE waste that needs to be reached by each Member State. The collection rate is evaluated every three years as a weight/weight percentage between WEEE collected and EEE introduced in the market in the previous three years in each Member State. It is useful to highlight that due to the growing of the PV market in the last years and due to the long-life of PV panels, reaching the WEEE collection rates in the first years of application will be particularly challenging if PV wastes would have been considered separately. The directive, though, calculate the collection rate as a whole for all the EEE wastes collected, allowing growing markets not to be penalized by the Directive itself.

[5] D.M. 5 luglio 2012

[6] WEEE directive (2012/19/EU) published on European Official Journal L197

The directive, unlike the first Italian Law "Quarto conto energia", also define the recovery and recycling rate as a weight percentage of the collected WEEE for each category. The recovery and recycling rates for PV panels, as defined in Annex V of the Directive, are the following.

From August 13th, 2012, until August 14th, 2015:

- 75% shall be recovered,
- 65% shall be recycled.

From August 15th, 2015, until August 14th, 2018:

- 80% shall be recovered,
- 70% shall be prepared for re-use and recycled.

From August 15th, 2018:

- 85% shall be recovered,
- 80% shall be prepared for re-use and recycled.

It's worth noting that the Italian Law "Quinto Conto Energia", written after the publication of the WEEE Directive, is based on the same recovery and recycling rates as the WEEE Directive and requires the PV recycling consortia to fulfill all the requirement imposed by the WEEE Directive.

6.2 PV RECYCLING: TECHNOLOGICAL CHALLENGES

Whereas the reasons that have to push the PV industry to invest on the development of affordable, clean and industrially optimized recycling processes for treating end-of-life PV modules have been showed in the previous paragraph, the analysis of the structure of PV modules can show which are the main technological issues that need to be solved for making it possible to recovery and recycle the vastest amount of raw materials using as less energy as possible and with the lowest environmental impact.

The majority of PV modules installed to date is based on c-Si wafers and PV modules are made of a laminate of glass, silicon solar wafers and polymeric materials. Other technologies, such as thin films, are available in the PV market, but, even if their market share is not negligible, the analysis of recycling systems for non-crystalline silicon PV modules will not be conducted in this study for the possibility to easily recycle them with well-established industrial methods. The

CdTe case is representative of this fact: the vast majority of PV modules based on CdTe have been manufactured by First Solar, one of the biggest PV companies in the world in term of production capacity. First Solar, with the aim of making its product as clean as possible, before the introduction of laws on the reduction of use of the toxic element Cadmium and on the mandatory recycling of components using this element, established its own recycling process for avoiding the disposal in landfill of CdTe solar panels and for the recycling of the non-toxic compound CdTe [40]. The realization of a worldwide pre-funded collecting and recycling system allows the recovery of valuable and rare elements, such as for example Tellurium, while realizing a closed-loop cycle for Cadmium, a byproduct of the extraction, smelting and refining of copper, zinc and lead ores, that otherwise should need to be treated as hazardous and toxic waste.

The First Solar process is an example of a well-established industrial scale recycling process for PV that could be considered as a benchmark for the development of recycling processes for c-Si PV modules.

6.2.1 CHALLENGES FOR THE DEVELOPMENT OF C-SI RECYCLING PROCESSES

Whereas the technologies for recycling the materials used in crystalline silicon solar modules are well-established at industrial level and they don't need big research efforts for their improvement, the main hurdle for the industry working for the recycling of end-of-life PV panels is the separation of the different materials used for the manufacturing of the PV module itself.

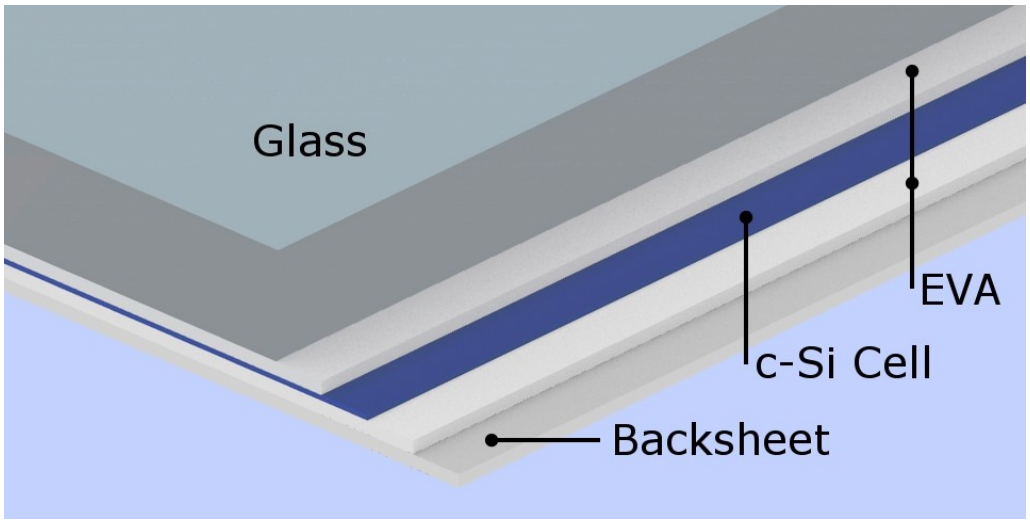

Figure 6.3 – Cross section of a c-Si PV module showing the different material layers

Crystalline silicon PV modules are usually made by a stack of layers of different materials with different physical and electrical properties that are essential for guarantee the long-term efficiency and reliability of the system.

Crystalline silicon PV modules have been introduced in the market in different configurations, but the two most diffused configurations have been the glass-EVA-glass structure and the glass-EVA-polymer structure, with the first nowadays almost completely disappeared in large scale PV production.

In Figure 6.3 a simplified cross section of a c-Si PV panel based on the glass-EVA-polymer structure is shown. The PV panel can be considered made by five layers stacked one upon each other.

The first layer starting from the bottom of the panel is a non-transparent polymeric layer called "backsheet". The backsheet layer is essential for guarantee electrical insulation of the system, mechanical protection for the solar cells and has to be made by a material that is resistant to humidity, corrosion, heat and light exposure. Usually a DuPont™ Tedlar® film; a polymeric material made of (PVF) had been used widely for the backsheet layer of crystalline silicon solar panels. Nowadays the majority of c-Si PV modules are manufactured using backsheet made of Polyethylene (PE), Polyester (PET) and PVF or, most often, by a sheet made of a sandwich of the described materials for giving the product the best electrical and mechanical characteristics. The thickness of the backsheet layer usually range between 250 and 350 μm and the discharge voltage is always higher than 1 kV for guarantee the electrical insulation of the system.

Above the backsheet layer a second polymeric layer is deposited. This layer is made of Ethyl Vinyl Acetate (EVA), a transparent polymeric material used as encapsulant.

The third layer of the c-Si solar panel is made by crystalline silicon solar wafers (which thickness range from 210 to 150 μm) interconnected through printed silver paste grids and soldered conductive ribbons. This is the active part of the solar panels and these electrical parts needs to be protected from humidity and from exposure to external agents.

The forth layer is made of EVA and has the same characteristics of the second layer. While EVA could also be not transparent in the second layer, it is essential that the fourth layer is transparent and doesn't degrade with sun exposure for guarantee the best performance of the solar cells during the whole lifetime of the system. EVA layers are used for the polymer peculiar properties: it is used in 300 to 800 μm thick sheets that can be thermally cured with a lamination

process that allows to melt the EVA that undergoes a cross-linking process, encapsulating therefore the solar cells into a polymeric material that not only protect the cells from the environmental exposure, but also act as a strong adhesive material between each layer of the solar panels.

The upper layer of the laminate is a 3 to 5 mm (usually 3.2 mm) thick soda-lime textured glass. The glass gives the panel mechanical strength, protects the EVA from aggressive atmosphere exposure and guarantee optimal optical properties during the whole lifetime of the solar panel.

While this structure is essential for giving the PV module adequate protection during the exposure to sunlight and to adverse environmental conditions, making it possible to guarantee the reliability and energy production for many years, the high adhesive strength of EVA after the curing process is the main hurdle to the development of recycling systems for end-of-life c-Si PV panels, since it make not possible to easily separate the different materials used in c-Si solar panels for their reuse as recycled raw materials.

6.3 STATE OF ART FOR C-SI PV RECYCLING

The interest on recovering valuable materials from end-of-life or damaged PV modules increased until the end of the polysilicon shortage in 2009. In fact, the high cost of the polysilicon feedstock made it profitable to recycle wafers and silicon from end-of-life solar modules.

The rapid reduction of the polysilicon cost, starting in 2010 when a production chain dedicated to PV had been established, made the recycling activities less economically viable and the interest of the PV industry on this topic dropped sharply.

Nowadays the interest for PV recycling has grown due to changes in the legislative framework and thanks to the increased awareness of the public opinion on the impact of electricity generation from raw materials to decommissioning.

The researchers working for the PV industry on the development of new low-impact recycling systems for end-of-life PV modules have now to fill the gap left between the studies conducted at the start of the PV era and the new requirement for a fully sustainable PV industry.

In the following paragraphs two of the industrial processes developed for the recovery of raw materials from end-of-life c-Si PV modules are presented. The analysis of the strengths and weaknesses of each process is useful for developing novel processes with higher yield and much lower environmental impact. Other processes, developed only at lab-scale, either based on thermal or chemical treatment, will not be analyzed in details in this chapter [41], [42].

6.3.1 SOLAR CELLS INCORPORATED RECYCLING PROCESS

In the second half of the 90's Solar Cells Inc., an American company working on crystalline silicon solar cells, that will convert its core business in the following decade on the production of CdTe thin film modules with the new name First Solar, developed a recycling process for the recovery of solar cells from end-of-life crystalline silicon PV modules [43].

The process, developed at lab scale, was aimed at the recovery of unbroken solar wafers and electric connections for their high value at the time. The recovered solar cells would have been re-used in newly laminated PV modules without any other treatment, while clean glass would have been sent to recycling.

The process starts with the manual removal of a TPT (Tedlar®-polyester-Tedlar®) backsheet after slowly heating the PV module; afterward the core of the separation process was based on inert gas pyrolysis of the EVA encapsulant for allowing the manual separation of solar cells and glass.

The chose to operate in inert gas (nitrogen) was due to the requirement to obtain clean cells and glass that wouldn't need to be furthermore treated. In fact the pyrolysis in inert gas without oxygen allows preventing any sign of undesirable combustion of EVA. The process, experimentally tested on cell-size samples (approx. 10 × 10 cm) required the treatment of the sample at temperature of 520°C for the complete decomposition of EVA in 60 minutes.

The process didn't reach the industrial maturity due to problems related to the production of gas that would need to be treated before emission into atmosphere, making the process not only not economically feasible, but also with non-negligible environmental impact. The exhaust gas, in fact, should need an after burn process for avoiding the emission of gas phase organics. It's worth noting, though, that the afterburning process will still produce carbon dioxide that would be emitted into the atmosphere.

The high process temperature could also enhance the diffusion of phosphorous and boron in the solar cells, reducing therefore their efficiency. Whereas the authors of the study described the effect to be negligible on solar cell efficiency, they also underline that the possible diffusion of silver from the front and back contacts could lead to performance degradation that could make the process not feasible.

6.3.2 DEUTSCHE SOLAR RECYCLING PROCESS

The process developed by the German company Deutsche Solar (now Solarworld) is the first case of industrial pilot-scale process for the treatment and recycling of end-of-life PV modules. The process had been in operation since 2003 and had been adopted by the European consortium for voluntary take-back and recycle of end-of-life PV modules PVCycle since the start of the take-back and recycling activities. Nowadays the process and the pilot-scale line built in Freiburg are not in use.

The process [44], [45] was based on thermal treatment of end-of-life crystalline silicon PV modules for the separation of glass and solar cells from the laminate. The process was divided in two steps: thermal process for the removal of the plastic material, and chemical etching for the recovery of solar cells.

After the manual removal of the junction box and aluminum frame the solar modules are thermally processed at 600°C. This temperature cause the combustion of the plastic and polymeric parts of the modules, allowing the manual separation of glass and metal that are fed into dedicated recycling systems and intact solar cells that will be sent to the second step of the recovery process.

The second step consists on a series of acid etching for the chemical removal of the electric contacts, the anti-reflective coating and the doping. The cells are then surface treated for their re-use in newly made PV modules.

Whereas this process allowed the recovery of intact solar wafer, the reduction of their mean thickness caused a strong reduction of the process yield making it not economically feasible. The process is also affected by other weaknesses: the thermal process of PV modules in incinerating ovens doesn't allow the building of an in-line high throughput process and the exposure of solar wafers at high temperature can cause the diffusion of unwanted elements in the solar wafers causing the degradation of the cell's performance. This recycling method also requires a complex system for treating the exhaust fumes

produced by the combustion, increasing therefore the recycling costs and posing some questions on the environmental impact of this recycling activity.

6.4 RADIO-FREQUENCY DE-LAMINATION PROCESS FOR C-SI PV RECYCLING

All the industrial, lab-scale or pilot line processes developed so far for the treatment of end-of-life PV panels for silicon recycling are based on high-temperature thermal or chemical processes. Whereas these processes allow the separation of glass, metals and silicon from end-of-life solar modules, their environmental impact is high and could not justify the application of these recycling processes.

In fact, from an economical point of view, it is convenient to develop a recycling system only when the cost of recycling is lower than the cost of extraction and refining of raw materials. On the other hand, from an energy use point of view, it is worth developing a recycling system only if the energy consumption related to the recycling activities is lower than the energy consumption due to raw materials extraction activities.

For a complete analysis of the convenience of recycling in comparison to raw materials extraction, a complete life cycle analysis (LCA) should be conducted for every recycling process. Conducting a full LCA on an industrial process, though, is a very complex task that requires access to every details of each step of the industrial process, including data that are usually not disclosed like, for example, energy consumption or relevant proprietary data. Without a full LCA it is not easy to compare the economic and environmental impact of different industrial processes, but some simple consideration can however be done.

Considering the two high-temperature processes for treating end-of-life PV modules described in the previous paragraph, it is easy to understand how their indirect costs are high, even without conducting a full LCA; in fact, the use of pyrolysis or combustion for removing the polymeric materials used for the encapsulation of the solar cells, making it possible to manually separate the silicon wafers, produces harmful and hazardous fumes that needs to be treated before their emission into atmosphere, highly increasing the energy and economic costs and posing some questions on the real environmental impact of those recycling processes.

The objective of researchers working for the development of novel recycling processes for treating end-of-life PV modules is then to study methods for the

separation of the laminated materials without combustion and reducing the use of chemical products.

A method for treating end-of-life c-Si PV modules for their de-lamination for the separation of recyclable materials without combustion, based on radio-frequency (RF) heating have been developed at the Laboratory of Electroheat in the Department of Industrial Engineering at University of Padova. This electrothermal process, working at temperature lower than the decomposition temperature of EVA and backsheet, strongly reduce the environmental impact of PV decommissioning and recycling.

The electrothermal RF heating process and the method developed are described in the following paragraphs. The method had been presented for patent application in 2012 by University of Padova[7].

6.4.1 RADIO FREQUENCY DIELECTRIC HEATING

Dielectric losses heating is based on the thermal effect of an alternating magnetic field on a dielectric material. This is due to polarization effects related to microscopic displacements of bounded charges and to conduction currents due to free charges, moving for the effect of the electric field in macroscopic scale.

Dielectric materials are usually characterized by a low electric conductivity, making them unsuitable for other electrothermal processes, like direct conduction heating. Thermally processing them in ovens will also be not feasible because they are often bad thermal conductors and they will therefore be heated only superficially or, if the process time is long enough to reach the process temperature in the center of the volume, the temperature distribution will not be uniformly distributed.

The parameters that completely define a dielectric material under the effect of a sinusoidal high frequency electric field are the real part of the permittivity ε' and the total loss tangent $\tan\delta$.

The total power density p [W/m3] transformed into heat in a dielectric material subjected to the application of a high frequency electric field is:

$$p = \omega E^2 \varepsilon_0 \varepsilon' \tan\delta$$

[7] F. Dughiero, A. Doni and M. Bullo, "Metodo per la separazione di componenti di moduli fotovoltaici laminati". Italy Patent VR2012A000103 - Patent Pending, 19 05 2012.

In which,

ω [rad/s] is the electric field angular frequency,

E [V/m] is the applied electric field,

ε_0=8.85419·10^{-12} [F/m] is the vacuum permittivity,

ε' and tanδ as defined previously.

The system acts as a capacitor and the heat generated in dielectric materials is due to dielectric power losses caused by the polarization of the materials and to conduction currents.

The main advantage of this process, in comparison with other thermal processes, is the possibility to uniformly heat the dielectric material; the heat is directly generated within the mass of the materials and a core heating on non-conducting materials is therefore possible.

The values of ε' and tanδ for the materials used in c-Si solar panels are shown in Table 6.1, together with the frequency at which these values had been found in commercial datasheet. Non zero values for ε' and tanδ highlight the possibility to apply a dielectric radiofrequency heating process for power transfer and heat generation within these materials.

Table 6.1 – Dielectric Characteristic for c-Si PV Modules' Dielectric Materials

Material	Frequency	ε_r	Loss Factor
Backsheet	1 MHz	6-10	0-0.165
EVA	10 kHz	2-4	0.05-0.06
Tempered glass	10 kHz	3-10	-

It must be highlighted that these parameters are heavily frequency dependent since losses phenomena are different at different frequencies. In Figure 6.4 a qualitative graph describing the typical behavior of the total loss factor $\varepsilon_e''=\varepsilon'tan\delta$ at typical industrial frequencies is shown. It can be noted that at lower frequencies the conduction currents play a more important role in the heating process in comparison with the polarization and relaxation phenomena.

Looking at these parameters it can be noted that dielectric heating allows to heat selectively the EVA layers. As it will be described in details in the following paragraph, the selective heating of EVA is essential for the de-lamination process developed at University of Padova. Silicon, being a semiconductor, contributes to the heat generation due to conduction currents. This effect

enhance the process velocity since the silicon wafer is encapsulated between two EVA layers and, therefore, all the heat generated inside the silicon wafer due to conduction currents is transferred to the EVA layers that need to be heated during the de lamination process, contributing to the heating process.

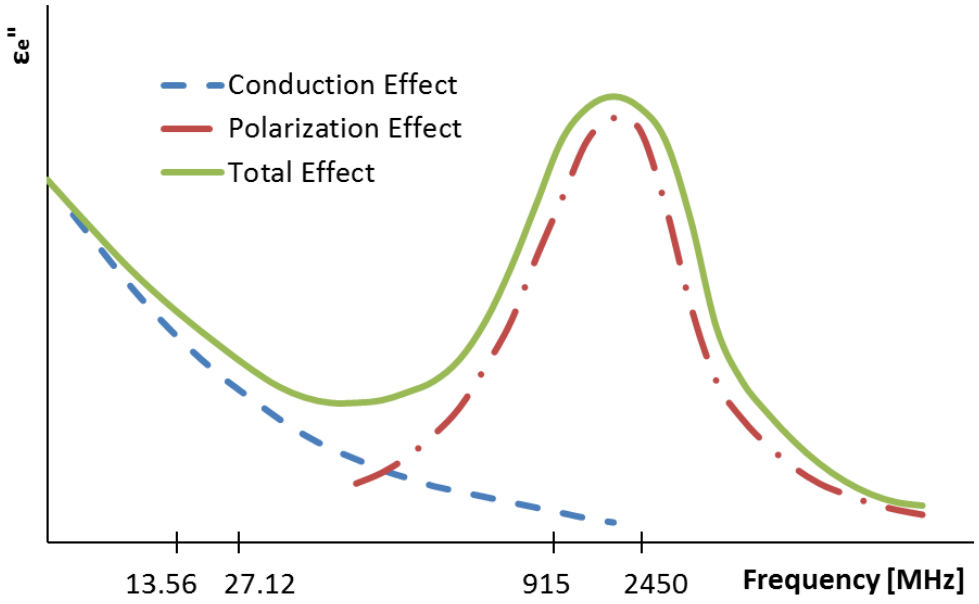

Figure 6.4 - Qualitative description of the typical behavior of ε_e" in the range of industrial frequencies used for dielectric heating.

6.4.2 RADIO FREQUENCY DE-LAMINATION PROCESS

The research activities for the development of the RF de-lamination process for the recycling of end-of-life PV panels had been divided into three parts: analysis of the possibility of building a finite element electro-thermal model for simulating the EVA heating process using dielectric heating, conduction of small scale experimental tests for assessing the possibility to heat directly the EVA layers through dielectric heating, and de-lamination experimental tests for the separation of recyclable materials from the laminates.

The first step of the research activity has been the building of a finite element model for analyzing the thermal effect of the application of a RF electric field to a PV panel, before starting the experimental tests. The software chosen for the simulations is Cedrat Flux; it allows building 2D and 3D models for solving multi-physics finite element simulations.

A 2D planar model for a part of a PV panel with the dimensions of one solar cell has been built and two planar ideal electrodes have been considered for

simulating the RF electric field. The accurate definition of materials' physical characteristics is essential for obtaining accurate results from a finite element simulation. Dielectric properties (e.g. permittivity and loss factor), as well as electrical and thermal properties (e.g. thermal conductivity and thermal capacity) needs to be defined for each material.

The values of these parameters are temperature dependent and dielectric properties are also dependent on frequency. While thermal characteristics for every material have easily been found in datasheets, no data for dielectric properties at radiofrequency had been found. Conducting a set of experimental tests for characterizing the dielectric properties of these materials at temperature ranging from 20°C to 200°C and at the operative frequency (13.56 MHz) would have been too expensive and the obtained results could have been different from the reality since, for example, it wouldn't have been possible to test cured EVA in sheets, but only non-cured EVA in blocks. It has been chosen, therefore, to use the simulation tools only for conducting electric simulations aimed at the definition of the electric limits of the system to avoid discharges and to have an idea of the heat flows inside the PV panels during the heating process.

The second step of the research activities consisted on the set-up of the experimental tests for assessing whether it would be possible to heat directly the EVA layers through dielectric heating.

The design of the first experimental system built in the Laboratory of Electroheat at University of Padova (LEP) has been done considering the equipment still owned at the moment of starting these research activities, and adapting them to this research field. The RF power generator and matchbox used for the experimental tests are characterized by a nominal RF frequency of 13.56 MHz, maximum RF power of 3 kW and maximum output voltage of 3 kV. The MS Windows® based graphic user interface allows the operator to control important process parameters such as injected RF power, reflected RF power and load transferred power. These parameters are essential for understanding whether the system is tuned or the power is just reflected to the generator by a non-tuned system, making the process uncontrollable and inefficient. The tuning of the system is done firstly manually by the operator, and afterwards, when the stability of the power transfer had been reached, automatically via software control. The tuning of the system can be reached changing the value of the capacity of two motorized variable capacitors in the matchbox.

The RF voltage can also be remotely controlled, allowing the operator to check that it is always lower than the dielectric strength of the materials,

avoiding discharges and possible damages to the RF generator. During the experimental tests the applied voltage have always been limited to 1 kV; the dielectric strength of the backsheet layer for avoiding discharge effects.

The RF generator parameters have shown to be suitable for building the first prototype of RF heater for PV panels. In particular the system had been designed to handle samples, cut from end of life or damaged solar panels, of the size of approximately one crystalline solar cell (156 × 156 mm).

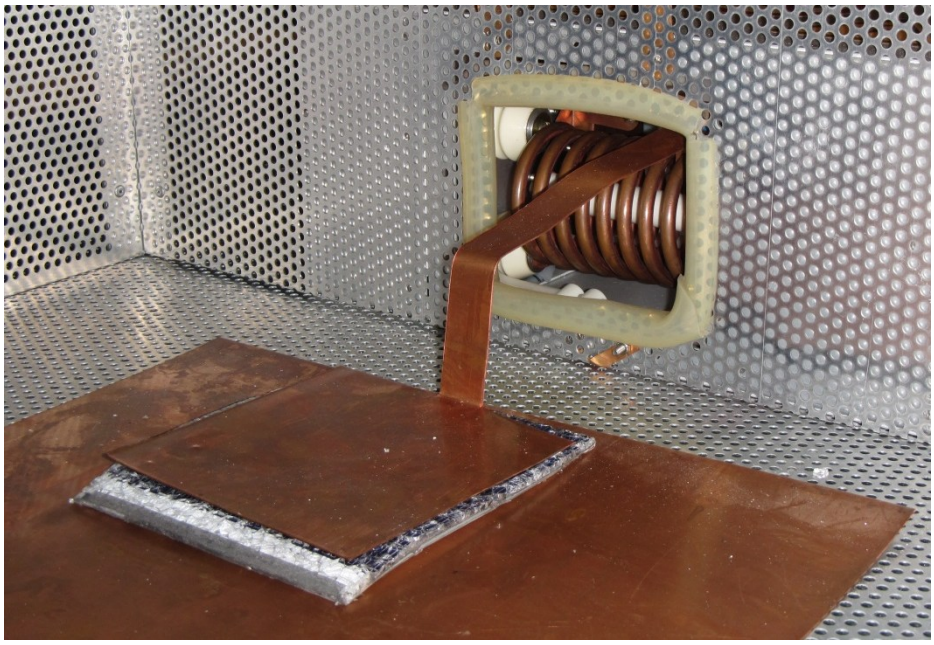

Figure 6.5 – Picture of the prototype of RF heater for PV modules de-lamination

Two simple non-magnetic flat electrodes have been designed and cut from a copper sheet, as to produce a uniform transverse RF electric field investing the sampe. The lower electrode is grounded, whereas the upper one is connected to the RF voltage supply.

The solar panel samples are therefore inserted between the two electrodes and pressure is applied to the upper electrode during the heating process. This allows transmitting the optimal RF power to the samples, while keeping the applied voltage lower than the value needed in presence of an air gap. An air gap will be necessary for further tests aimed at the development of an in line system. The voltage related problems can be easily solved with a modification of the electrodes' geometry. For electromagnetic compatibility and protection of the operators, a grounded non-magnetic faraday cage has been built to accommodate the experimental apparatus. A picture of the RF heating system built for conducting the thermal and de-lamination tests is shown in Figure 6.5.

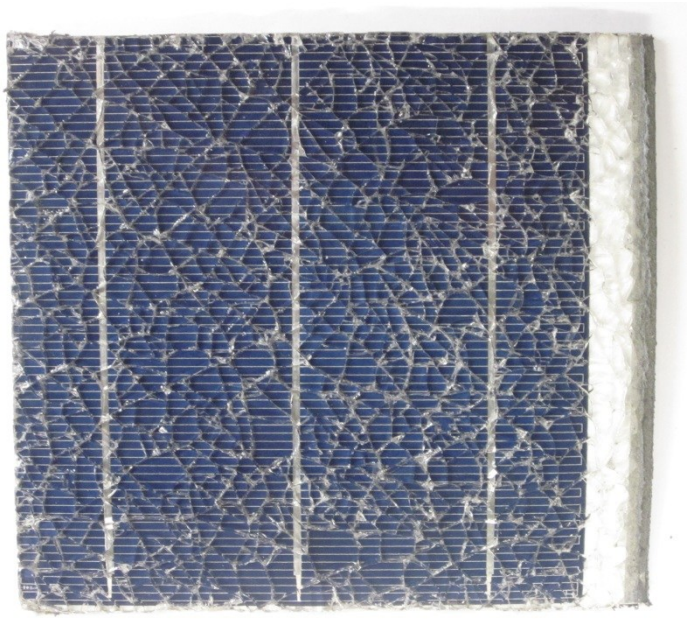

Figure 6.6 – Cell-size sample with broken glass used for RF heating and de-lamination tests

The first round of experimental tests had been conducted on samples taken from a damaged PV panel with broken glass. The samples where cut in squares of the dimension of a single silicon wafer (156 × 156 mm); a picture of one of the samples used for the experimental tests is shown in Figure 6.6.

The first step of the experimental tests has been the tuning of the generator with the load. This required the application of a small amount of RF power, insufficient for heating the laminate, to the system. The analysis of the influence of each generator's variable parameter on the ratio between reflected power and injected power allowed to correctly tune the system to the load and to carry on with heating tests. In Figure 6.7 it is possible to see the electric parameters during the test: the non-tuning of the system can be seen from the difference from the injected power and the load power; a big part of the injected power is reflected to the generator making it not possible to transfer the power to the load, and therefore to start the heating process.

After completing the tuning of the system, the first thermal tests have been conducted with the aim of assessing whether it would be possible to heat directly the core of the PV panels with the application of an RF electric field. The load transferred power has been increased with small steps up to 400 W and the temperature in different parts of the PV panel samples and the electrodes have been measured after 10 minutes of power application. For measuring the

temperature of the wafer inside the PV panel, the backsheet have been partially detached from one of the samples (see Figure 6.8).

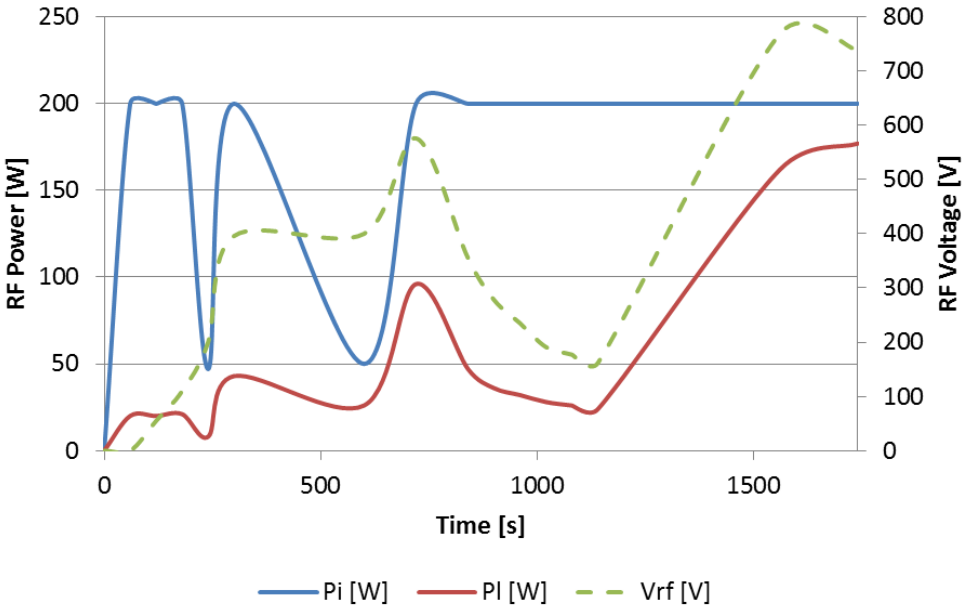

Figure 6.7 – Electrical parameters during a non-tuned test; load coupling is within reach at the end of the process

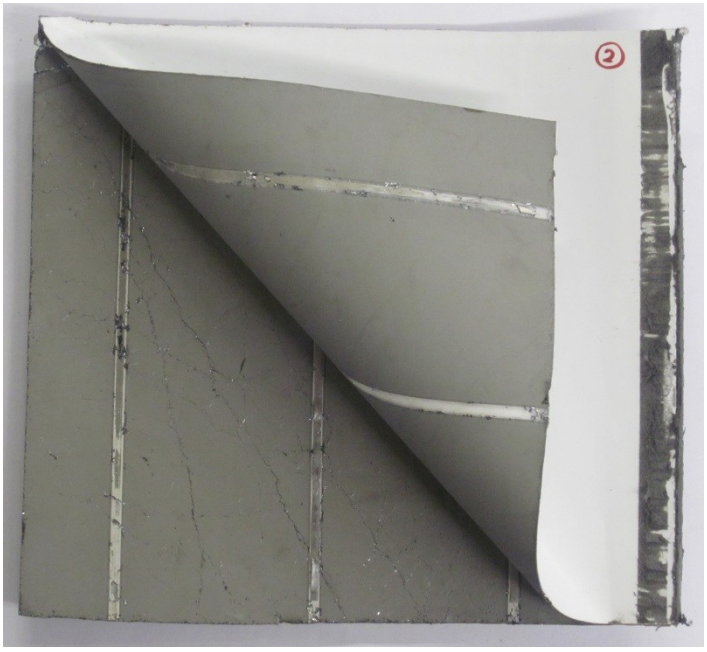

Figure 6.8 – Sample for partially removed backsheet for temperature measurement

It has been noted that during the first 2 to 5 minutes it is necessary to manually regulate the matchbox parameters for keeping the reflected power lower than 10%; after minimizing the reflected power, the matchbox operation

could have been switched to automatic, letting the generator's software control the fine tuning of the system. The need of changing the generator's parameter on a wide range during the first part of the heating process is a consequence of the variations of the dielectric characteristic of the materials with the temperature. The temperature reached in different parts of one of the samples processed with 300 W for 10 minutes are shown in Table 6.2. The repeatability of the test's results has been checked repeating the test on the same sample and conducting the test on different samples; the thermal results of three of the thermal tests conducted are presented in Figure 6.9.

Table 6.2 – Temperature distribution after a 300 W, 10 min thermal test. Temperature measured with thermocouple

Measurement position	Temperature
Upper electrode	69°C
Glass surface	60°C
Internal temperature	72°C
Backsheet back side	54°C
Lower electrode	45°C
Room temperature	22°C

The important result obtained from these tests is the demonstration of the possibility of heating directly the core of the PV panel. Since the upper electrode operates at high temperature, the measurement of the cell temperature has been necessary to assess whether the core of the samples is heated with dielectric heating or is simply heated by the power dissipated on the upper electrode, through conduction heat transfer. The internal temperature has shown to be always higher than the sample's superficial temperature (see Figure 6.9), demonstrating that heat is effectively generated inside the PV laminate during the application of the RF electric field.

In Figure 6.10 the process electrical parameter are shown. It's worth noting the good coupling between the load and the matchbox that allows the power transmission from the generator to the EVA layer through the application of the RF electric field.

After experimentally demonstrating the suitability of RF heating for direct heating the EVA layers, and developing a thermal process for treating end of life PV panels, the following step of the research activity have been aimed at the test of the possibility of de-laminate the PV panels after the thermal treatment. Further thermal tests have been conducted with the objective of checking the

possibility of de-laminate the panels after the thermal treatment, thanks to the change of the materials' physical properties during the heating process.

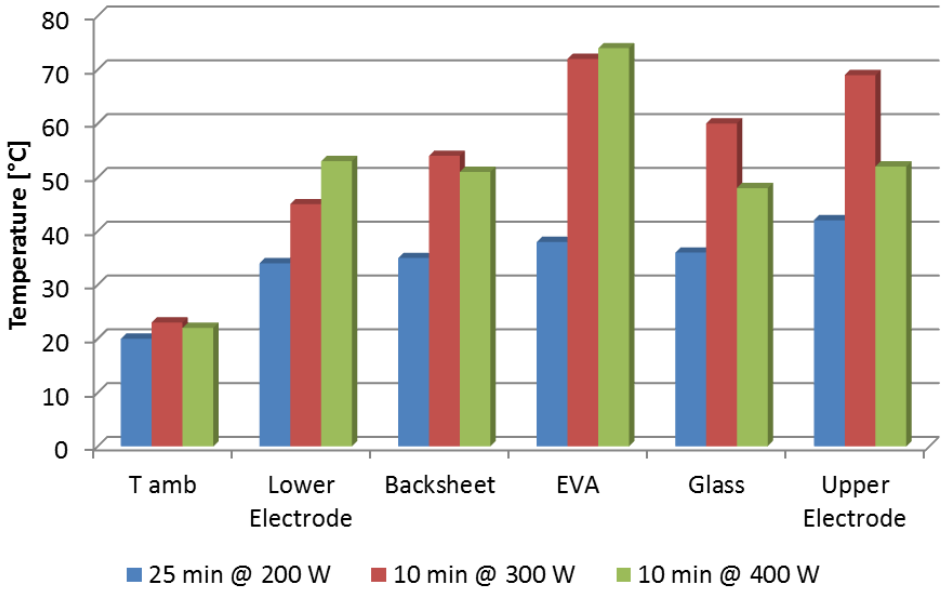

Figure 6.9 – PV modules temperature after different thermal tests

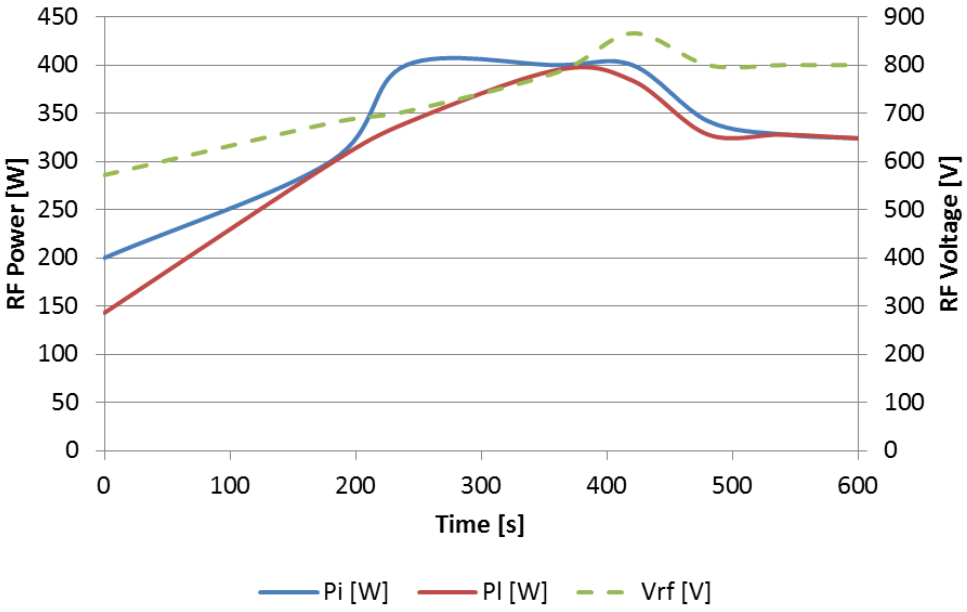

Figure 6.10 – RF generator electrical parameters during the heating process

A sample has been heated with the application of 400 W and the temperature has been controlled every 10 minutes. The physical properties have also qualitatively been controlled manually. In particular the flexibility of the sample

has been tested and the adhesive strength of EVA in contact with glass has been tested as well.

After the application of 400 W for a total time of 10 minutes, the detachment of small glass fragments from the laminate has been noted while bending the sample. The process has been repeated and, as a result, a big portion of glass fragments have been manually peeled off from the PV sample, using no tools but manually rubbing the glass surface with a glove, after 15 minutes of treatment.

The process has been repeated on several samples and the result of the experimental tests is the demonstration of the possibility of easily removing the broken glass from the PV panels through the application of the RF electrothermal process developed. A picture of one of the samples after the application of the RF heating process and mechanical glass removal can be seen in Figure 6.11.

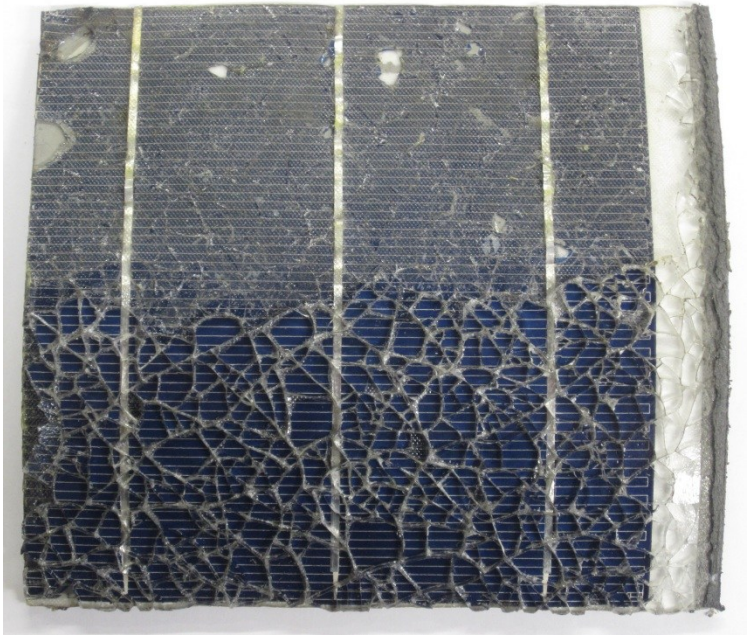

Figure 6.11 – Sample after the de-lamination process. Glass has been removed from the top part of the sample

In every test part of the glass have been kept on the sample due to technical reasons related to the design of the simple electrodes used in these tests; the parts of glass still attached to the samples allow the geometry of the system to be kept constant and therefore an easier regulation of the tuning parameters of the generator during the heating process. A few pieces of glass detached from the samples with a small fragment of silicon wafer attached to them. Those were the one which dimensions was bigger and they detached when the samples

were cooling down. Keeping the process temperature slightly higher, or preferably working with an in-line system, will help to remove those pieces from the PV laminate without removing parts of the solar cell.

After assessing the possibility to heat directly the EVA layers using an RF heating process, and after achieving the removal of clean glass from cell-size samples, some experimental tests have been conducted on full scale 60 cells multi-crystalline silicon PV modules with the aim of scaling the technology to full-size industrial systems and for designing an in-line process.

The first tests conducted using a 200 kW, 27.12 MHz power generator, with electrodes not in physical contact with the module, showed the possibility to easily heat the EVA layers through RF heating, while keeping the backsheet layer at low temperature. The connection grids, though, interfere with the electric field distribution, creating some high field zones and related hot spots that can lead to backsheet discharge. The demonstration of the possibility to work on the scale-up of the system, though, allow to work on the optimization of the electrodes configurations for reducing the hot spots phenomena, making it possible to realize an in line fully automated process for the reduction of handling time and costs.

Considering the new regulations imposed by the WEEE directive described in 6.1.2 and the recovery and recycling rate imposed thereof, considering that the glass part of a c-Si solar panel accounts for almost 75% of the total weight and the aluminum frame for 15%, it is easy to understand that the method proposed allow to reach the objective imposed not only for 2012, but also for 2018. It is also worth noting that the sandwich composed by backsheet, EVA, solar cell and EVA could be further more treated, either with a thermal or chemical process, allowing to recovery the metals and semiconductors of the solar panels, making it possible to reach even higher recovery and recycling rate.

7 CONCLUSIONS

In this work the analysis of the processes and technologies for the production of multi-crystalline and quasi-mono-crystalline silicon for photovoltaic applications has been conducted and the development of innovative electrothermal processes for improving the current technologies has been carried out.

In particular a technical-economical comparison had been carried out for assessing the cost of different PV technologies in terms of cost of energy. This analysis made it possible to compare different technologies for which a simple price based comparison would not be sufficiently realistic. The study highlighted the strong leadership of crystalline silicon technologies in the PV market not only for technological reasons, but also for economic reasons.

After the analysis of the PV market and the study of the production processes for PV modules, especially for multi-crystalline silicon modules, an application of induction heating electro-thermal process had been developed for realizing an innovative furnace for casting multi-crystalline silicon ingots. The innovative induction heating furnace design allows to improve the multi-crystalline silicon casting process, making it possible to obtain high quality products at lower cost in comparison to traditional resistive heating furnaces. The development of the furnace had been carried out designing 3D finite element models for the electro-thermal analysis of the system and the study resulted in the design and construction of a lab-scale 120 kg induction heating directional solidification furnace that will be an important instrument that will allow to conduct experimental tests aimed at the improvement of the casting process, which results can be easily scalable at industrial level.

The final part of the work consisted on the development of a treatment system for end-of-life PV modules with the aim of raw materials recovery and recycling. A radio-frequency de-lamination process for the separation of the glass from end-of-life PV modules had been developed and patented at the Laboratory of Electroheat and the tests conducted on the custom made prototype showed a great recovery potential and the possibility to integrate the system in more complete recovery and recycling systems.

The innovative electrothermal heating processes developed within this research activity can thus be considered a technological breakthrough that could raise the competitiveness of PV thanks to high added value process innovation and optimization.

REFERENCES

[1] G. Masson, M. Latour and D. Biancardi, "Global market outlook for photovoltaics until 2016," EPIA - Europan Photovoltaic Industry Association, Brussels, may 2012.

[2] M. Rekinger, I.-T. Theologitis, G. Masson, M. Latour, D. Biancardi, A. Roesch, G. Concas and P. Basso, "Connecting the sun: solar photovoltaics on the road to large-scale grid integration," Craig Winneker, Brussels, 2012.

[3] M. Šúri, T. Huld, E. Dunlop and H. Ossenbrink, "Potential od solar electricity generation in the European Union member states candidate countries," *Solar Energy,* vol. 81, pp. 1295-1305, 2007.

[4] T. Huld, R. Müller and A. Gambardella, "A new solar radiation database for estimating PV performance in Europe and Africa," *Solar Energy,* vol. 86, pp. 1803-1815, 2012.

[5] Ministero dello Sviluppo Economico, *DM 5 luglio 2012,* 2012.

[6] GSE, "Risultati incentivazione GSE," 31 12 2012. [Online]. Available: http://www.gse.it/it/Conto Energia/GSE_Documenti/Fotovoltaico/05 Risultati incentivazione/TOTALE_DEI_RISULTATI_DEL_CONTO_ENERGIA.pdf. [Accessed 10 01 2013].

[7] Terna, "Rapporto mensile sul sistema elettrico - Consuntivo al 31 dicembre 2012," 31 12 2012. [Online]. Available: http://www.terna.it/LinkClick.aspx?fileticket=TaTsJCKRG5E%3d&tabid=379&mid=3013. [Accessed 10 01 2013].

[8] Fraunhofer ISE, "Fraunhofer institute for solar energy systems ISE - Photovoltaics report," Fraunhofer ISE, Freiburg, 2012.

[9] P. Moskowitz and V. Fthenakis, "Toxic materials released from photovoltaic modules during fires: health risks," *Solar cells,* vol. 29, pp. 63-71, 1990.

[10] A. Luque, Handbook of photovoltaic science and engineering edited by Antonio Luque and Steven Hegedus, Chichester: Wiley, 2011.

[11] Energy & Strategy Group, "Solar Energy Report 2008".

[12] J. P. V. Arkhipov, Thin film solar cells fabrication, characterization and applications, Hoboken: Wiley, 2006, pp. 435-439.

[13] K. Zweibel, "Issues in thin film PV manufacturing cost reduction," *Solar Energy Materials and Solar Cells,* vol. 59, no. 1-2, pp. 1-18, 1999.

[14] K. Zweibel, "Thin film PV manufacturing: Materials costs and their optimization," *Solar Energy Materials and Solar Cells,* vol. 63, no. 41, pp. 375-386, 2000.

[15] H. C. K. V. M. Fthenakis, "CdTe photovoltaics: Life cycle environmental profile and comparisons," *Thin solid films,* vol. 515, no. 15, pp. 5961-5963, 2007.

[16] A. G. Aberle, "Thin-film solar cells," *Thin film solid films,* vol. 517, no. 17, pp. 4706-4710, 2009.

[17] European Commission Joint Research Center, "Photovoltaic Geographical Information System (PVGIS)," [Online]. Available: http://re.jrc.ec.europa.eu/pvgis/. [Accessed 10 gennaio 2010].

[18] H. J. Scheel and T. Fukuda, Crystal growth technology, Chichester: Wiley, 2004.

[19] M. de Wild-Scholten, "Environmental profile of PV mass production: globalization," in *26th European Photovoltaic Solar Energy Conference*, Hamburg, 2011.

[20] J. O. Odden, G. Halvorsen, H. Rong and R. Gløckner, "Comparison of the energy comparison in different production processes for solar grade silicon," in *Silicon for the chemical and solar industry IX*, Oslo, 2008.

[21] V. Hoffman, K. Petter, J. Djordjevic-Reiss, E. Enebakk, J. T. Håkedal, R. Tronstad, T. Tronstad, I. Tronstad, S. Tronstad and M. Bauer, "First results on industrialization of Elkem solar silicon at Pillar JSC and Q-Cells," in *23rd European Photovoltaic Solar Energy Conference*, Valencia, 2008.

[22] P. Preis, P. Diaz-Perez, D. Rudolph, K. Peter and A. K. Søiland, "High Efficiency potential of Cz Silicon Solar Cells from Metallurgical Process Route," in *27th European Photovoltaic Solar Energy Conference*, Frankfurt, 2012.

[23] A. K. Søiland, J. O. Odden, B. Sandberg, K. Friestad, J. Håkedal, E. Enebakk and S. Braathen, "Solar Silicon from a metallurgical route by Elkem Solar – a viable alternative to virgin polysilicon," in *6th International workshop on Crystalline Silicon Solar Cells*, Aix Les Bains, 2012.

[24] M. Meyers, "(Over-)supply and demand – challenges for silicon manufacturers," in *PHOTON's 10th Solar Silicon Conference*, Berlin, 2012.

[25] J. Vedde, T. Clausen and L. Jensen, "Float-zone silicon for high volume production of solar cells," in *3rd World conference on photovoltaic energy conversion*, Osaka, 2003.

[26] P. Rudolph, M. Czupalla, B. Lux, F. Kirscht, C. Frank-Rotsch, W. Miller and M. Albrecht, "The use of heater-magnet module for Czochralski growth of PV silicon crystals with quadratic cross section," *Journal of Crystal Growth,* vol. 318, no. 1, pp. 249-254, 2011.

[27] W. Scott Radeker and W. Cunningham, "A hierarchy of slurry reprocessing options," in *TMS Annual meeting and Exhibition*, Seattle, 2010.

[28] J. Dupuis, E. Saint-Sernin, O. Nichiporuk, P. Lefillastre, D. Bussery and R. Einhaus, "NICE module technology - from the concept to mass production: a 10 years review," in *38th IEEE Photovoltaic Specialists Conference*, Austin, 2012.

[29] S. Lupi, *Appunti di elettrotermia.*

[30] F. Dughiero, M. Forzan and D. Ciscato, "A new DSS furnace for energy saving in the production of multi-crystalline silicon," in *35th IEEE Photovoltaic Specialists Conference*, Honolulu, 2010.

[31] F. Dughiero, M. Forzan, D. Ciscato and F. Giusto, "Multi-crystalline silicon ingots growth with an innovative induction heating directional solidification furnace," in *37th IEEE Photovoltaic Specialists Conference*, Seattle, 2011.

[32] F. Dughiero, M. Forzan, D. Ciscato, M. Cesano, F. Crivello and R. Bechini, " Device for obtaining a multicrystalline semiconductor material, in particular silicon, and method for controlling the temperature therein". PCT Patent WO 2011/048474 A1, 28 04 2011.

[33] E. Pihan, G. Fortin, D. Camel, N. Plassat, D. Chavrier, J. Champliaud, S. Bailly, N. Enjalbert and A. Jouini, "Recent developments on seeded growth in pilot and industrial furnaces," in *6th International workshop on Crystalline Silicon Solar Cells (CSSC)*, Aix Les Bains, 2012.

[34] N. G. Stoddard, "Methods and apparatuses formanufacturing cast silicon from seed crystals". PCT Patent WO 2009/014957 A2, 29 01 2009.

[35] I. Guerrero, V. Parra, T. Carballo, M. Miranda, B. Moralejo, O. Martínez, J. Jiménez, A. Piñeiro, E. Diéguez, J. F. Lelièvre and C. del Cañizo, "Mono-crystalline silicon wafers manufactured by casting methods: Optoelectronic, structural and solar cell study," in *5th International workshop on Crystalline Silicon Solar Cells (CSSC)*, Boston, 2011.

[36] N. G. Stoddard, "Methods and apparatuses for manufacturing monocrystalline cast silicon and monocrystalline cast silicon bodies for photovoltaics". PCT Patent WO 2007/084934 A2, 26 07 2007.

[37] N. G. Stoddard, B. Wu, R. F. Clark and J. A. Cliber, "Methods and apparatuses for manufacturing cast silicon from seed crystals". PCT Patent WO 2009/014961 A1, 29 01 2009.

[38] N. G. Stoddard, "Methods for manufacturing monocrystalline or near-monocrystalline materials". PCT Patent WO 2009/015167 A1, 29 01 2009.

[39] N. G. Stoddard, "Seed layers and process of manufacturing seed layers". PCT Patent WO 2010/088046 A1, 05 08 2010.

[40] D. Vizman, J. Friederich and G. Mueller, "3D time-dependent numerical study of the influence of the melt flow on the interface shape in silicon ingot casting," *Journal of crystal growth,* vol. 303, no. 1, pp. 231-235, 2007.

[41] Y.-Y. Teng, J.-C. Chen, C.-W. Lu and C.-Y. Chen, "The carbon distribution in multicrystalline silicon ingots grown using the directional solidification process," *Journal of crystal growth,* vol. 312, no. 8, pp. 1282-1290, 2010.

[42] V. M. Fthenakis, "End-of-life management and recycling of PV modules," *Energy Policy,* vol. 28, no. 14, pp. 1051-1058, 2000.

[43] L. Frisson, K. Lieten, T. Bruton, K. Declercq, J. Szlufcik, H. De Moor, M. Goris, A. Benali and O. Aceves, "Recent improvements in industrial PV module recycling," in *16th European Photovoltaic Solar Energy Conference*, Glasgow, 2000.

[44] T. Doi, I. Tsuda, H. Unagida, A. Murata, K. Sakuta and K. Kurokawa, "Experimental study on PV module recycling with organic solvent method," *Solar Energy Materials & Solar Cells,* vol. 67, no. 1-4, pp. 397-403, 2001.

[45] J. R. Bohland and I. I. Anisimov, "Possibility of recycling silicon PV modules," in *26th IEEE Photovoltaic Specialists Conference*, Anaheim, 1997.

[46] K. Wambach, "Recycling of solar cells and photovoltaic modules," in *19th European PV Solar Energy Conference*, Paris, 2004.

[47] A. Müller, K. Wambach and E. Alsema, "Life cycle analysis of a solar module recycling process," in *20th European Photovoltaic Solar Energy Conference*, Barcelona, 2005.